MODELING ENERGY SAVINGS OF GLAZED AND UNGLAZED COLLECTORS USED FOR SPACE HEATING, WATER HEATING, AND SPACE COOLING

A Thesis
by
BRADLEY RICHARD PAINTING

Submitted to the Graduate School
at Appalachian State University
in partial fulfillment of the requirements for the degree of
MS in TECHNOLOGY

December 2015
Department of Sustainable Technology and the Built Environment

MODELING ENERGY SAVINGS OF GLAZED AND UNGLAZED COLLECTORS USED FOR SPACE HEATING, WATER HEATING, AND SPACE COOLING

A Thesis
by
BRADLEY RICHARD PAINTING
December 2015

APPROVED BY:

Jeffrey S. Tiller
Chairperson, Thesis Committee

Brian W. Raichle
Member, Thesis Committee

Marie C. Hoepfl
Member, Thesis Committee

R. Chadwick Everhart
Chairperson, Department of Sustainable Technology and the Built Environment

Max C. Poole, Ph.D.
Dean, Cratis D. Williams School of Graduate Studies

Abstract

MODELING ENERGY SAVINGS OF GLAZED AND UNGLAZED COLLECTORS FOR SPACE HEATING, WATER HEATING, AND SPACE COOLING

Brad Painting
B.S., Ohio University
M.S., Appalachian State University

Chairperson: Jeffrey Tiller

Glazed and unglazed solar thermal collectors were compared in TRNSYS simulations for a multi-use application of space heating, water heating, and space cooling. The solar thermal system added or removed heat from two separate storage tanks that provided hot or cold water to a slab-on-grade radiant floor system within an 1800 ft^2 house. The system collected heat using traditional solar absorption and removed heat using night-sky radiative cooling. The overall solar fraction achieved by two (7.6 m^2) of the glazed collectors was similar to the solar fraction achieved by six (22.8 m^2) of the unglazed collectors in the climates of Raleigh, NC, Jacksonville, FL, and Albuquerque, NM. However, the unglazed collectors produced less energy cost savings at these sizes because a greater proportion of their energy was provided as cooling, which was supplied more efficiently by auxiliary equipment. For each type of collector, the greatest solar fraction of space heating and water heating were achieved in Jacksonville, and the greatest solar fraction of space cooling was achieved in Albuquerque. The climate of Raleigh generally produced heating and cooling performances that were in the middle of the range produced by collectors in the three

geographic regions. For glazed and unglazed arrays of equal size in Raleigh (15.2 m^2), the ratio of the unglazed solar fraction to the glazed solar fraction was 0.26 for space heating, 0.73 for water heating, and 2.71 for space cooling.

Acknowledgments

This study would not have been possible without the guidance, feedback, and support from the members of my thesis committee: Jeffrey Tiller, Marie Hoepfl, and Brian Raichle. They have all invested extensive time into a topic entirely of my choosing. A special thanks to Professor Tiller who met with me weekly over the course of the study to offer help and direction in response to its challenges. Dr. Hoepfl generously reviewed many iterations of research proposals before the study even began, and Dr. Raichle provided invaluable instruction and problem-solving skills in TRNSYS. Susan Doll also deserves a thank you for offering me flexible hours of employment and encouragement throughout the process, and for giving me a wake-up call about finishing on a realistic timeline.

Finally, thanks to my parents who raised me lovingly and supported me during this process, and to my sister who encourages me as an older sibling and as a friend.

Table of Contents

Chapter One: Introduction

There are a variety of systems that can use solar energy to heat or cool buildings. One of the major types used for heating is the solar thermal collector. Collectors designed for the medium-temperature range typically have a glass or polycarbonate cover (or "glazing") intended to trap heat. Unglazed collectors, without said cover, are typically used for low-temperature applications such as pool-heating at a lower financial cost. According to Burch, Salasovich, and Hillman (2005), unglazed collectors typically cost one-fifth the price of equally sized glazed collectors, but collect only about one half to two-thirds as much heat annually when used for domestic hot water (DHW) heating at an array size of 40 ft^2 (3.72 m^2). However, the absence of glazing allows the collectors to also cool a working fluid if operated at night by means of night-sky radiative cooling, expanding their potential utility.

The combined functions of heating and cooling have been underexplored as a viable economic investment in renewable energy. Burch, Christensen, Salasovich, and Thornton (2004) performed a simulation for three different climate zones for combined heating and cooling of a 185 m^2 home using unglazed collectors to power a hydronic forced air system. In Albuquerque, NM, the collectors saved 56% of the energy that would have been required without any collectors present.

Forced air systems represent just one method of utilizing the combined heating and cooling potential of unglazed collectors. Radiant floors, ceilings, or wall panels may be more compatible with the fluid temperatures achieved within solar collectors than forced-air systems. This is especially true in systems that actively store energy within the thermal mass of the building (often called thermo-active building systems [TABS]). For example, Olesen (2012) presented a review of TABS which demonstrated that a supply water temperature of only 18° C circulating through such a system can offset 38 W/m^2 of heat gain to a space. He also noted that TABS should allow solar collectors to operate more efficiently.

A system model was created and analyzed using TRNSYS. The purpose of the simulation was to compare the performance of glazed and unglazed thermal collectors in a radiant space heating system. The design utilizes a thermally active floor consisting of cross-linked polyethylene tubing (PEX) running through a slab-on-grade foundation. Two separate storage tanks, consisting of hot or cold water charged by the solar collectors, service the radiant floor as it is used for heating or cooling. A heat pump in series with the tanks, located immediately prior to the inlet of the radiant floor loop, supplies auxiliary heating and cooling energy. See Chapter Three for further details on the model.

Statement of Problem

Few studies have been performed on the use of solar thermal collectors for the combined functions of heating and night-sky radiative cooling. Burch et al. (2004) investigated the energy savings from using unglazed collectors for space heating, space cooling, and domestic hot water heating. They established that unglazed collectors can make significant contributions to both heating and cooling needs, but it remains to be established whether the total energy cost savings can justify switching from the more traditional choice of using glazed collectors for domestic hot water and/or space heating. Moreover, their method of conditioning the house (i.e., with forced air systems) is not an ideal fit for solar thermal collectors because it demands higher fluid temperatures for heating and lower fluid temperatures for cooling than well-designed radiant systems (see Siegenthaler, 2013). The comparison is further complicated by the substantially lower cost of unglazed collectors, noted by Burch et al. (2005) to be about 20% of the cost of glazed collectors per unit area. There is a need for a study that compares the performance of both types of collectors within the context of both heating and cooling in order to inform an economic analysis.

Significance of Study

The advancement of solar thermal technology is widely researched for its potential financial and environmental benefits. Solar thermal systems may make buildings more affordable by decreasing energy costs needed to meet heating needs (and in some cases, cooling needs). As building envelopes become better sealed and insulated, they have greater cooling needs relative to heating

needs. This creates a strong argument for increased focus on energy-efficient methods of space cooling. The resulting decrease in traditional energy consumption also decreases the environmental impacts.

Unglazed collectors are a cheaper, simpler, technology than glazed collectors. If the energy savings from unglazed collectors employed for both heating and cooling is favorable to the savings from glazed collectors, it may encourage greater adoption of solar thermal technology and further research into unglazed collector functions.

Purpose of Study

This study used TRNSYS models to compare the performance of unglazed collectors used for the dual functions of heating and cooling to glazed collectors, which have superior heating performance but inferior ability to radiate heat for cooling. A cost savings analysis was then performed for each type. Energy and cost savings were investigated specifically for residential buildings with cooling loads in regions that could likely utilize slab-on-grade radiant floor systems, represented by Jacksonville, FL, Albuquerque, NM, and Raleigh, NC.

Research Goals

The goal of this research was to compare the energy and cost savings potential of using glazed collectors to unglazed collectors in residential buildings that require space heating, space cooling, and domestic hot water heating. This investigation was applied to the following questions within the context of three different climates in the U.S.:

1) How much energy is saved in space heating for each type of collector (i.e., glazed and unglazed) when compared to a radiant floor system with no solar assistance?
2) How much energy is saved in domestic water heating for each type of collector (i.e., glazed and unglazed) compared to a tankless water heater with no solar assistance?
3) How much energy is saved in space cooling for each type of collector (i.e., glazed and unglazed) when compared to a radiant floor system with no solar assistance?

4) What are the comparative savings on energy bills of unglazed and glazed thermal collector systems?

Limitations of the Study

The performance of the HVAC system will change when used with different buildings or in different climates. The results are sensitive to the properties of the building such as wall and ceiling R-Values, glazing properties, shading characteristics, and internal gains. The performance of the unglazed collectors may vary more between climates than is typically expected for glazed collectors due to their greater sensitivity to wind speed and ambient temperature. There are also likely differences between system costs that use glazed collectors and system costs that use unglazed collectors, and their comparative energy cost savings do not necessarily reflect the total comparative economic return.

The collector models available in the distributed package all had limitations. Each unglazed collector model had an issue with processing either wind speed or sky temperature. However, a reasonable workaround was developed for the collector model that contained no wind speed input. There was also a lack of glazed collector models that are able to model night-sky radiative cooling over the full range of possible temperatures, but a reasonable workaround was also developed for this. Details on these solutions are provided in the Methodology section.

Assumptions Made

A number of assumptions had to be made throughout the study in order to eventually analyze energy cost savings. Various assumptions were made about the occupants in terms of their schedules, thermal comfort needs, and hot water consumption in order to calculate energy requirements. Various assumptions were made about the building and solar thermal system parameters to help create a complete design. An electrical rate was assumed to calculate cost savings. Assumptions were also made about weather properties; for example, that the diffuse sky radiation is isotropic (see Definition of Terms), and that wind speed in residential areas is 50% of the wind speed measured in TMY2 files.

In rare cases, it may be possible for solar collectors to replace a system entirely when the output is high enough in comparison to the demand. It was assumed that this would not occur because solar thermal collectors generally operate least efficiently when the demand is the highest, as seen from the analysis by Burch et al. (2004). In other words, on the coldest winter days, collectors will produce little heat.

Definition of Terms

Absorptance – The fraction of incident radiation that is absorbed by a surface (rather than being reflected or transmitted).

ACH – An abbreviation for "air changes per hour" that describes the rate at which the air in a house is replaced with fresh air.

Aperture Area – Area of the collector face excluding the frame; the area through which solar radiation can actually enter the collector.

Azimuth angle – The angle between due south and the projection on a horizontal plane of the line between the sun and the receiving surface of its beam radiation.

Beam Radiation – irradiance that has not been scattered by the earth's atmosphere (traveling in a roughly straight line from the sun to the source).

Diffuse Radiation – irradiance that has been scattered by the earth's atmosphere (as is received behind a shaded surface).

Dry Bulb Temperature – The air temperature measured by a thermometer when there is a net-zero radiative flux between the thermometer and surrounding surfaces.

Emissivity – The fraction of thermal radiation that an object will emit at a given temperature in comparison to how much it would emit if it had perfect emissivity.

Gross Area – Area of the collector face, including the frame.

Heat Removal Factor – The effectiveness of the collector as a heat exchanger, defined as the ratio of the actual heat transfer to the potential heat transfer if the entire collector were at the inlet fluid temperature.

Isotropic – refers to diffuse radiation that is evenly distributed among all orientations.

Mean Radiant Temperature – the temperature perceived by an object based solely on its incident radiation, excluding air temperature effects.

Operative Temperature – A measure of thermal comfort that combines the influence of air dry bulb temperature and mean radiant temperature.

R-Value – the thermal resistance for a given thickness of material.

Solar Heat Gain Coefficient – the fraction of solar radiation that will pass through a window.

Thermal Capacity – The amount of energy required to raise a unit mass of a material by one unit of temperature measurement. Also known as specific heat.

TMY2 and TMY3 – refers to Typical Meteorological Year data representing compiled empirical weather data that characterizes weather patterns for a given location. Commonly used in building and renewable energy modeling situations.

Transmittance – the proportion of radiation that passes through a surface (without being absorbed by it).

U-Value – the thermal conductivity for a given thickness of material; the inverse of R-Value.

View Factor – The proportion of radiation emitted by a first surface that strikes a second surface.

Units of Measurement

The units of measurement appearing in the literature are mixed between the International System (SI) and the US Customary system (IP). Unit labels are frequently omitted from R-Value and U-Value when working within a single system, but because the literature is from various sources it is important to list the units of each system and the conversion factors between them.

Heat-related conversions:

$1\ kWh = 3412.14\ Btu \quad (Energy)$

$1\ W = 3.412 \frac{Btu}{hr} \quad (Power)$

$$1\frac{W}{mK} = 0.578\frac{Btu}{hr.ft°F} \quad (Conductivity)$$

$$1\frac{W}{m^2K} = 0.176\ \frac{Btu}{hr.ft^2°F} \quad (U-Value)$$

$$1\frac{m^2K}{W} = 5.678\ \frac{hr.ft^2°F}{Btu} \quad (R-value)$$

Dimension conversions:

$$1\ m = 3.28\ f$$

$$1\ m^2 = 10.76\ ft^2$$

Flow conversions:

$$1\frac{kg}{s} = 2.20\frac{lbm}{s}$$

$$1\frac{kg}{s} = 15.87\ gpm \quad (for\ water\ only)$$

Chapter Two: Review of Literature

Collectors

History

According to the Florida Solar Energy Center (FSEC) (2006), the first solar water heaters appeared in the 1800s as unglazed collectors in the form of bare metal tanks, painted black and tilted towards the sun. Ragheb (2014) described another application developed in 1885 by the French engineer Charles Tellier, who developed an unglazed collector that heated ammonia to run a turbine used to drive a pump. Its form was somewhat similar to modern unglazed collectors used to heat water, consisting of a watertight seal between iron sheets that served as a channel for the heated fluid.

Approximately four years later, he added glass glazing and insulation to improve its efficiency. The FSEC (2006) described the invention of traditional glazed collectors as a separate endeavor by Clarence Kemp in 1891. Kemp evolved the traditional bare metal tanks into a commercially-available glazed collector marketed as the "Climax," which utilized black galvanized iron tanks placed inside a glass-covered box. The storage tanks were first separated from the collectors in 1909 by inventor William Bailey, giving rise to the modern flat-plate collector, which exists today in both glazed and unglazed forms. Currently, unglazed collectors are most commonly used for pool heating while glazed collectors are more commonly used for DHW heating and space heating.

Current Applications in Space Conditioning

Energie Solaire, based in Switzerland, distributes a product called the Solar Roof, which is an unglazed collector that integrates into the roof structure, marketed for low-temperature applications, for example, providing heat to the evaporator of a heat pump to improve its efficiency (Energy

Solaire, 2015). There are also transpired collectors (i.e., air-based collectors) on the market used for heating and cooling fresh air drawn into buildings (Conserval Engineering, Inc., 2015).

Radiative Cooling

Anderson, Duke, and Carson (2013) developed a theoretical model for the cooling capacity of unglazed collectors on a per-unit-area basis and tested it against experimental results. The collector was integrated into a troughed sheet metal roof having an emissivity of 0.95 and absorber conductivity of 50 W/m-K. They verified the experimental model by measuring collector parameters such as temperature and flow rate coupled with environmental parameters such as irradiance, wind speed, ambient temperature, and cloud cover. They continuously circulated water through the collector from a 60-liter storage tank over 24 hours to compare the ambient temperature to the tank temperature. Unsurprisingly, the tank became much warmer than the ambient temperature during the day. However, during nighttime hours, the tank temperature dropped (by about 3 ºC) below ambient temperature. This corresponds to a cooling output of 50 W/m^2 during late night hours. Their theoretical model predicted typical nighttime stagnation temperatures of 5 ºC to 10 ºC below air temperature in several Australian cities. Because their experimental setup consisted of a single tank exposed to both heating and cooling conditions over a 24 hour period, it may not represent the maximum cooling potential of the collectors.

Sima, Sikula, Kosutova, and Plasek (2013) investigated night sky radiative cooling in the Czech Republic using roof-mounted radiating panels connected to concrete ceiling panels. They simply assumed cloudy sky conditions rather than using the dynamic parameter of sky cover from a TMY2 or TMY3 weather file. Rather than coupling the collectors directly to an Active Layer representing the chilled ceiling in TRNSYS, they created a new thermal zone to represent the chilled ceiling and used results from seven different steady-state simulations of the collectors in the software package, Fluent, to modify the temperature of the imaginary thermal zone representing concrete ceiling panels. The frequencies of operative temperatures and thermal comfort were compared to a simulation of a building without any form of cooling. Over the course of three summer months, the

operative temperature without any cooling ranged from approximately 30 °C to 40 °C. With radiative cooling, it ranged from approximately 19 °C to 30 °C. These temperature ranges were used to inform their thermal comfort model, which estimated that less than 15% of people would be dissatisfied during 70% of the working time when all cooling was produced by the radiating panels.

Eicker and Dalibard (2011) simulated and measured the performance of unglazed photovoltaic-thermal (PVT) panels used for night-sky radiative cooling. The panels were used to remove heat from either a phase change material (PCM) in the ceiling, a thermally massive floor, or a heat sink (storage tank), depending on the prioritization. The simulation was performed in both Madrid and Shanghai representing low and high humidity climates, respectively. Humidity had a large effect on the cooling capacity of the panels; annually they were able to remove 9.7 kWh/m^2 from the PCM in Madrid with an average cooling power of 30.7 W/m^2, but only 3.5 kWh/m^2 in Shanghai with an average cooling power of 22.5 W/m^2.

Domestic Water Heating

Burch et al. (2005) compared the energy cost savings of unglazed collectors to glazed collectors for use in domestic water heating using TRNSYS simulations. They found that for a 40 ft^2 (3.72 m^2) collector area, the glazed collectors with selective coating performed at an average efficiency of about 38% ± 1% over one year while the unglazed collectors performed at an average 21% ± 1% annual efficiency. Efficiencies were found to be "reasonably constant" (p. 3) across the United States as long as the load volume and system size were consistent. The unglazed collectors produced most of their useful heat at combinations of higher ambient temperature and irradiance compared to glazed collectors. Specifically, unglazed collectors harvested the most energy over the course of a year at a $(T_i - T_{amb})/I_{sun}$ of approximately 0.2 °C.m^2/W while glazed collectors harvested the most energy at approximately 0.4 °C.m^2/W, where T_i is the inlet water temperature, T_{amb} is the ambient temperature, and I_{sun} is the intensity of solar irradiance. It is possible that the annual efficiency of collectors could improve if used for low-temperature space heating in addition to medium-temperature water heating.

Combined DHW Heating and Space Heating

Bonhôte (2009) simulated the performance of unglazed thermal collectors integrated into an office building facade for space heating and domestic water heating. The simulation was performed using weather data from Zurich, Switzerland; Stockholm, Sweden; and Carpentras, France. Various collector parameters such as absorptance, emissivity, and orientation were varied to investigate heat output under different design conditions. Space heating and DHW heating were simulated separately and then in combination. The space heating system consisted of a boiler that supplied water at a maximum temperature of 38 °C to a heat exchanger connected to separate radiators in the north and south zones of the building. The boiler also serviced the DHW tank through a heat exchanger in the DHW simulation, in which the boiler set point was 80 °C. The simulations showed that the collectors saved 100 to 300 kWh/m^2-year when used for domestic water heating but only 20 to 100 kWh/m^2-year when used for space heating. In combination, 95% of the collected energy went to DHW heating. Results of this simulation may not be representative due to different equipment configurations and temperature set points.

Combined Heating and Cooling

Baer (2001) designed a system to heat and cool a building using unglazed collectors. The design used an unconventional heat transfer medium of ceiling-mounted PVC pipes filled with water. The system was tested as a small physical mockup rather than a simulation of a realistic building, and the measurements of the heating response were only taken over the course of a few days. The results showed that indoor temperatures (6 feet above the floor) stayed between 60 °F and 87 °F as outdoor temperatures fluctuated between 24 °F and 65 °F.

Burch et al. (2004) simulated a system that utilized unglazed collectors to charge separate hot and cold water tanks, which each serviced either a hot water coil or cold water coil within a forced air system. Domestic hot water was also drawn from the hot water tank. They simulated the performance in TRNSYS using three different collector areas (of 6 m^2, 23 m^2, or 93 m^2) in the climates of Albuquerque, Madison, and Miami. Auxiliary space heating was performed by a separate system

coupled directly to the zone to bring the air temperature to 20º C, while a chiller was run in series with the cold water tank to bring the water temperature down to 12.8° C before reaching the cooling coils. A tankless water heater was placed in series with the hot water tank to achieve a DHW temperature of 55º C. The 185 m^2 building model contained R3.35 (SI) / R19 (IP) stud frame walls, an R5.28 (SI) / R30 (IP) ceiling, and a concrete slab floor with R1.75 (SI) / R10 (IP) perimeter insulation. The building's footprint was square, with windows placed uniformly across all facades. In Albuquerque, the total energy savings (on heating, cooling, and DHW heating) for a 23 m^2 collector area were 56%. The savings for Madison and Miami at the 23 m^2 collector area were 36% and 31%, respectively. They found that collector performance is highly sensitive to wind speed for heating but generally insensitive to wind conditions for cooling

Variation of Performance with Tilt

The collector array simulated in the system by Burch et al. (2004) was 30 degrees, assumed to be flush with the roof. Marion and Wilcox (n.d.) stated that maximum annual insolation can be captured by using a tilt angle approximately equal to the location latitude. However, as Baer (2001) pointed out, increasing the tilt angle will decrease the cooling capacity due to less "view" of the sky from the collector face. It is accepted that there are aesthetic objections to arrays that are not flush with the roof surface, so the experimental design used in this study did not deviate from this constraint proposed by Burch et al. (2004) in their simulation.

Variation of Performance with Wind Conditions

Burch and Casey (2009) noted that the Solar Rating Certification Council's (SRCC) ratings have been biased in favor of unglazed collectors because, at the time of the published article, the SRCC had been testing glazed collectors according to American Society of Refrigeration and Air Conditioning Engineers (ASHRAE) Standard 93, which specifies wind speeds of 5 to 10 mph, but unglazed collectors under ASHRAE Standard 96, which specifies wind speeds below 3 mph. Although they stated that wind effects were "mostly negligible" (p. 1) for glazed collectors, they showed that even the range of wind velocities allowed within ASHRAE 96 can approximately halve

the efficiency of unglazed collectors tested in no-wind conditions. The International Organization of Standardization (ISO) 9806 Standard, which the SRCC transitioned towards at the time of the article, provides collector efficiencies as a function of both $(T_i - T_{amb})/I_{sun}$ and wind speed; therefore, it is preferable to analyze unglazed collectors rated according to this criterion.

The efficiency of unglazed collectors may also vary with wind turbulence, which may differ between test sites and sites of actual installation. Intelligent Energy Europe (2012), under the auspices of the European Commission, stated that artificial wind generators tend to produce more turbulent wind than air flowing naturally over a collector array at the same speed, which creates greater heat loss. However, International Standards Organization (ISO) 9806 stipulates that the wind produced by generators must be tested and confirmed to fall in the range of 20% to 40% turbulence to simulate natural wind conditions.

Variation of Performance with Mounting Method

ISO 9806 states that the thermal performance of collectors is affected by the method of mounting and specifies standard test configurations. Generally, it is stated that "…an open mounting structure shall be used which allows air to circulate freely around the front and back of the collector" (p. 33). However, a subsection on unglazed collectors states "If mounting instructions are not specified, the collector shall be mounted on an insulated backing with a quotient of the materials thermal conductivity to its thickness of 1 W/(m^2·K) ± 0,3 W/(m^2·K)…" (p. 33) and suggests 3 cm of polystyrene foam as an example.

The International Energy Agency (1993) described an equation developed by Svendsen (1985) that accounts for convective and radiative losses from the back of an unglazed, rack-mounted collector:

$$q_u = \alpha G_T - h_{c,p-a}(T_{pm} - T_a) - \varepsilon_p \sigma * (T_{pm}^4 - T_e^4) - h_{c,b-a}(T_{bm} - T_a) - \varepsilon_{bg}\sigma(T_{bm}^4 - T_g^4)$$

The convective and radiative losses from the back are:

$h_{c,b-a}(T_{bm} - T_a)$ and $\varepsilon_{bg}\sigma(T_{bm}^4 - T_g^4)$,

respectively. If the back of the collector is mounted flush with a roof or otherwise insulated from the air, it seems logical that these terms would be affected and that the performance of the installed collector may differ from the tested performance.

Variation of Performance with Incidence Angle

The maximum efficiency of glazed solar collectors are known to vary with the angle of incidence between incoming irradiance and the collector aperture, and this is accounted for in collector ratings by incidence angle modifiers (IAMs). However, a review of studies by the International Energy Agency (1993) concluded that the efficiency of unglazed collectors is not sensitive to the incidence angle.

Variation of Performance with Flow Rate

The SRCC (Solar Rating and Certification Council [SRCC], 2015a) certifies all collectors under ASHRAE-recommended flow rates (unless a model is specifically designed to operate under a different flow rate). ASHRAE Standard 96-1980 recommends testing methods for unglazed collectors and specifies a flow rate of 0.07 kg/s.m^2, while ASHRAE Standard 93-1986 provides recommended test procedures for glazed collectors (and other types) and suggests a flow rate of 0.02 kg/s.m^2. It warns that performance ratings are only valid at the tested flow rates.

TRNSYS

Overview

TRNSYS is a software package that is able to simulate a wide variety of dynamic processes, but is especially well-suited to those described in terms of heat and energy (TESS, 2015). TRNSYS consists of a core engine, or kernel, that performs mathematical operations and a set of components representing physical phenomena that communicate with the kernel. Both the kernel and the components are written in Fortran. The types of components are diverse and range from items as simple as a fluid pipe to systems as complex as a commercial building. Each component is defined by its source code and three types of attributes: inputs, parameters, and outputs. An input is a variable of a component that may change at any point in time, such as the flow rate through a collector. Inputs

are most commonly defined by the output of another component in the simulation, but they may also be held constant or dynamically modified based on user-defined equations. Functionally, a parameter is simply an input that must be held constant over time; for example, a parameter of most solar thermal collector components is the array area. An output is generated by the component's source code and may be plotted, saved into a text file, or routed to other components as an input. The entire model serves as an input to the TRNSYS kernel as a "deck" file, which is developed and visualized through the graphical interface of Simulation Studio. Simulation Studio displays the connections between inputs and outputs as well as each component's settings in table format. It is the graphical interface shown in schematics throughout this document, such as in Figure 1.

Utility

Sousa (2012) compared the features of TRNSYS with other software packages that were considered "among the most complete" (p. 9) simulation tools: Energy Plus, ESP-r, IDA ICE, and IES. He concluded that TRNSYS was the most complete tool of the group. A key feature described is the ability to incorporate custom routines and mathematical models into the simulation.

Accuracy

Burch, Huggins, Wood, and Thornton (1993) compared physical measurements on drainback systems to TRNSYS simulation results and found that the root mean square deviation between measured and simulated auxiliary energy used was 3%, with a maximum of 8% deviation. Ayompe (2011) compared TRNSYS simulation results to measurements of an experimental flat plate collector system. The error of TRNSYS relative to the measurements was 16.9% for the amount of heat absorbed by the collectors but only 6.9% for the amount of heat delivered to the load.

Building Loads

Internal Heat Gains

It is important to accurately estimate the building's internal heat gains because larger internal gains can shift energy consumption away from heating and towards cooling. This is especially true for energy-efficient buildings; Firlag and Zawada (2013) estimated about 20% of the heat lost from a

standard building can be recovered by internal gains, but up to 65% can be recovered in a "passive house" (p. 372). Huang, Hanford, and Fuqiang (1999), under the auspices of Lawrence Berkeley National Laboratory, stated that cooling loads in old buildings are evenly split "between the roof, walls, infiltration, solar gains, and internal gains," but that in new buildings solar gains and internal gains account for two-thirds of the cooling load. In their analysis of internal gains in a passive house in Germany, Firlag and Zawada (2013) estimated total average internal sensible heat gains of 623 W for a 120.1 m^2 living space, or about 5.2 W/m^2. Elsland, Peksen, and Wietschel (2014) created a model of predicted internal heat gains for various countries across Europe, accounting for appliances, electronics, lighting, and people and their behavioral patterns. The estimated range was an average internal gain of 3.8 to 6.6 W/m^2, depending on the country.

DHW Consumption Models

Edwards, Beausoleil-Morrison, and Laperrière (2015) measured the hot water consumption of 73 homes in Canada over the course of 60 to 165 days per house. The mean daily consumption was 189 liters (49.93 gallons), but the standard deviation was considerable, at 83 liters (21.93 gallons). The conditions used by the SRCC and the U.S. Department of Energy for rating water heaters assumes a draw of 64.3 gallons per day divided into six different intervals, each at a draw rate of 3.0 gallons per minute (SRCC, 2015b).

Radiant Floor Systems

Affordability

A literature review performed by the University of California at Berkeley's Center for the Built Environment (Moore, Bauman, & Huizenga, 2006) found that radiant cooling systems can be competitive with forced-air systems in up-front costs, and can achieve energy savings from 17% to 42% over all-air, variable-air-volume (VAV) systems in cool, humid climates and hot, dry climates, respectively. The article mentions a case study of buildings in Germany with four different types of radiant cooling systems that suggested that slab systems have both the lowest first cost and lowest life cycle cost.

Thermal Comfort

It is necessary to review thermal comfort parameters to determine what floor temperatures will be acceptable to occupants during heating and cooling seasons. ASHRAE Standard 55 provides guidance on how the parameters of air temperature, mean radiant temperature, air speed, humidity, occupant activity, and clothing level combine to determine acceptable comfort ranges (Brandemuehl, 2005). The CBE Thermal Comfort Tool (Hoyt, Schiavon, Piccioli, Dustin, and Steinfeld, 2013) automates the prediction of thermal comfort levels using the methods and parameters of ASHRAE Standard 55.

To assess the effect of floor temperature on thermal comfort, assumptions must be made about other thermal comfort parameters. Because the building has no forced air system, the mean air speed is likely lower than what might be expected in a house that does use forced air (Betz, 2014). Occupants are assumed to be standing and relaxed with clothing levels appropriate to the seasons:

- Internal Air speed = 0.04 m/s
- Metabolic Rate = 1.2 met (represents standing, relaxed)
- Heating Season Clothing = 1.0 (represents typical winter clothing, indoor)
- Cooling Season Clothing = 0.5 (represents typical summer clothing, indoor)
- Humidity = 50%

Olesen (2002) stated that for a person sitting in a 6 m by 6 m room in a commercial building, the floor temperature will only make up 40% of the overall mean radiant temperature. If other surfaces are assumed to be equal to air temperature, thermal comfort level can be assessed for some potential floor surface temperature set points. For example, during heating season at an indoor air temperature of 20 °C and floor surface temperature of 25 °C, the mean radiant temperature becomes 22 °C and conditions are in compliance with ASHRAE Standard 55. During cooling season with an indoor air temperature of 27 °C and a floor surface temperature of 23 °C, the mean radiant temperature becomes 25.4 ° and the conditions are also in compliance. This review is used, in

conjunction with estimated heat transfer coefficients described in section Modeling Procedures, as a starting point for testing different floor surface temperature set points in TRNSYS.

Heat Transfer Coefficients

The *Radiant Cooling Design Manual* by Uponor (2013) provides an estimated heat transfer coefficient of 11 $W/m^2.K$ for radiant floor heating and 7 $W/m^2.K$ for radiant floor cooling. Therefore, for a 24° C floor surface adjacent to 20 °C air, the rate of heat transfer would be 44 W/m^2. This is similar to a figure provided by Olesen (2002): For a floor surface temperature of 23.9 °C and air temperature of 20 °C, the estimated heat flux is 40 W/m^2.

Thermal Storage Capacity

Some of the thermal energy from the collectors can be stored directly in the floor system. The storage capacity is a function of its specific heat, thickness, area, and allowable temperature range. The allowable temperature range is considered to be the difference between the temperature set point when using solar thermal energy and the temperature at which auxiliary energy must be used. The parameters are as follows:

- Specific Heat: 0.96 kJ/kg-K
- Thickness: 0.12 m (4.72 inches)
- Area: 167.23 m^2
- Heating Season Range: 23 °C to 25 °C
- Cooling Season Range: 21 °C to 23 °C

These parameters define the thermal storage capacity, $Q = m*C*\Delta T$, where Q is thermal storage capacity, m is mass, C is specific heat, and T is the allowable slab temperature range. The equation provides the thermal capacity of the floor without being recharged by the collector array. This equates to about 102,300 kJ of storage within the floor. In contrast, a 0.3 m^3 (79.2 gallon) tank of water heated 30 °C above its set point only provides 37,700 kJ of heat storage.

Concrete Thermal Lag

VanGeem, Fiorato, and Musser (1982) tested the time lag between a temperature stimulus on one side of a concrete wall and its resultant response on the opposite side for three different concrete densities, each with an approximate thickness of 8.25'' to 8.5''. The high, medium, and low concrete densities produced thermal lags of 4 hours, 5.5 hours, and 8 hours, respectively. The different densities also affected the R-Values of the concrete, with the low-density having higher R-Value.

Chapter Three: System Design

Overview

A model of an energy-efficient house was designed and implemented in TRNSYS. The model used the most stringent set of criteria for ENERGY STAR certification among the locations simulated (Raleigh, NC; Jacksonville, FL, and Albuquerque, NM). Key features were a 0.12 m (4.72 in.) slab-on-grade foundation with insulation underneath and around its perimeter, a low R-Value floor finish, a square single-story floor plan, a 30º pitched roof, and evenly distributed windows with overhangs along the south-facing windows.

The house model was heated and cooled by three different types of heating systems. The control case was a radiant floor system heated and cooled only by an air-to-water heat pump with domestic hot water heated by a tankless water heater. The second case contained unglazed collectors servicing hot and cold water storage tanks. Each tank was plumbed to an air-to-water heat pump that provided auxiliary heating (or cooling) to the fluid stream before entering the radiant floor system. A tankless water heater also provided auxiliary heating to water drawn from the hot storage tank to meet DHW demand. The third case was similar, only with glazed collectors.

The concrete slab, in all cases, had PEX tubing embedded at 0.06 m (2.36 in.) depth per the recommendation of Siegenthaler (2013). The solar collectors were mounted on the south face of the roof and connected to hot and cold storage tanks. The flow from the collectors ran through a controlled diverter valve to charge the appropriate tank based on the mode of operation. The PEX tubing also carried flow through a diverter valve outside of the radiant slab to direct flow through a heat exchanger within either the hot or cold tank. However, heating and cooling were modeled in separate simulation in TRNSYS due to problems with integrating all elements into a single model.

Solar Collector System Design

The system contained two controllers as illustrated in Figure 1: one to control heating and cooling of the floor system, and a second to regulate flow between the tanks and solar collectors. The floor temperature controller sent output signals (i.e., “on” or “off”) to both the hydraulic pump and the auxiliary heat pump. When the water in the storage tanks was hot or cold enough to meet space conditioning demands, the controller simply signaled the hydraulic pump to circulate fluid from the appropriate tank through the floor. When the circulating fluid was not sufficiently hot or cold to meet demands, the controller also signaled the auxiliary heat pump to turn on. When auxiliary energy was required, the controller used a slightly lower set point in heating mode and a higher set point in cooling mode in order to utilize as much “free” energy from the tanks as possible. These set points are outlined in the description of System Design under “Controls and Set Points.” The control of the tankless water heater was internal to the component and turned on when the DHW stream was less than 50 ºC.

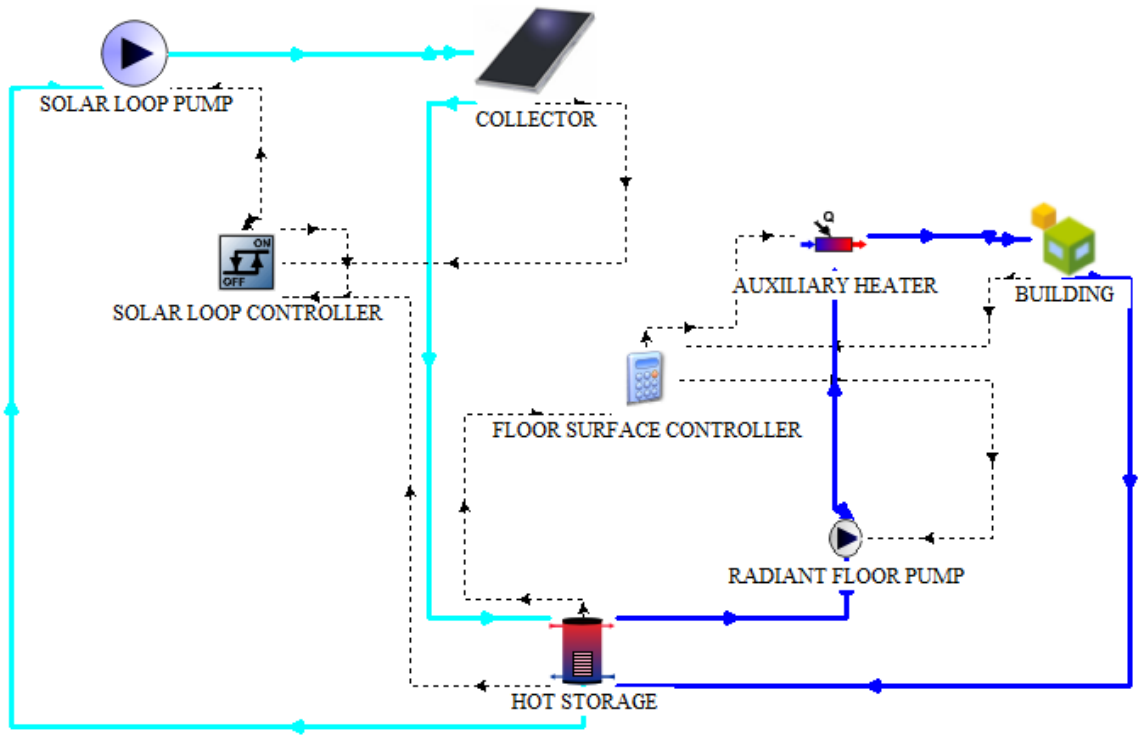

Figure 1. Simplified schematic of controllers in TRNSYS. Dotted lines represent controller readings and signals. Bold lines represent hydraulic flow. Cold storage not shown.

Collector Definition

The SRCC (2015c) describes collectors according to equations generated from tests performed under ASHRAE or ISO standards. The glazed collector equation depends on solar radiation and ambient temperature, while the unglazed collector equation utilizes these inputs with the addition of wind speed. The variables used in the SRCC performance curves are defined in Table 1, and are used throughout this document.

Table 1. *ISO Equation Variables*

Symbol	Meaning	Unit
u	Wind Speed	m/s
P	T_i - T_a	°C
T_i	Collector Inlet Temperature	°C
T_a	Ambient Temperature	°C
G	Radiation	W/m^2

A Rheem RS40-BP glazed flat plate collector is defined by the ISO equation for a flow rate of 0.02 kg/s.m^2:

$$\eta = 0.718 - 2.29060\left(\frac{P}{G}\right) - 0.04398(\frac{P^2}{G})$$

A Fafco Sungrabber unglazed flat plate collector is defined according to the ISO equation under a tested flow rate of 0.07 kg/s.m^2:

$$\eta = 0.941(1 - 0.0412u) - (11.6348 + 5.0697u)(\frac{P}{G})$$

The TRNSYS component types used to model the provided equations are Type 539 for the glazed collector and Type 553 for the unglazed collector.

Thermal capacitance.

The SRCC (2015c) also provides measurements that help determine the thermal capacitance of a collector. The thermal capacitance affects how quickly it responds to changing ambient conditions. TRNSYS assumes that the thermal capacitance parameter includes the capacitance of the contained fluid (in addition to the collector materials themselves). Although the glazed collector is made from heavier materials, SRCC data show it has a lower fluid capacity of 1.26 L/m^2, versus 2.87 L/m^2 for the unglazed collector. The total capacitance of the glazed collector was estimated from an example provided by Goswami, Kreith, and Kreider (2000, p. 109) by considering the ratio of collector areas; it is approximately 29.45 kJ/K for a 3.8 m^2 collector. The capacitance of the unglazed collector was estimated by assuming the primary material is propylene and adding the known capacitance of the contained fluid; it is 34.88 kJ/K for a 2.27 m^2 collector.

Incidence angle modifiers.

The amount of irradiance being absorbed by a collector is known to vary with the angle at which the sun enters the aperture. For glazed collectors, less irradiance is absorbed as the angle increases. For unglazed collectors, there is negligible difference. The SRCC (2015c) provides incidence angle modifiers (IAM) in terms of a table of values from 10° to 70°. TRNSYS, however requires IAMS to be defined in terms of an equation at an incidence angle of θ:

$$IAM = 1 - b_0\left(\frac{1}{\cos\theta} - 1\right) - b_1\left(\frac{1}{\cos\theta} - 1\right)^2$$

The IAM equation was fit to the SRCC IAM values using Excel's Solver function to determine the coefficients b_0 and b_1 (resulting in $b_0 = 0.038$ and $b_1 = 0.14$). The resulting values described in Table 2 replicate the Rheem RS40-BP values fairly closely.

Table 2. *Incidence Angle Modifier Comparison between SRCC Values and Equation-Based Values*

Angle (θ) in Degrees	SRCC Provided Value	Equation Best-Fit Value
10	1	0.96
20	0.98	0.96
30	0.96	0.95
40	0.91	0.95
50	0.84	0.92
60	0.71	0.82
70	0.44	0.44

DHW Consumption

DHW consumption was assumed equal in all climates, but the loads varied slightly because of different mains water temperatures. The occupant's draw on the water was modeled using a Type 14b forcing function according to a specified schedule to accumulate a total of 64 gallons per day of hot water usage. The step function of Type 14b (shown in Figure 2) can become truncated or distorted by the length of the TRNSYS time step, so the draw rate was chosen to add up to 64 gallons when divided into one-hour blocks. This flow rate worked out to 0.53 GPM (121.3 kg/hr).

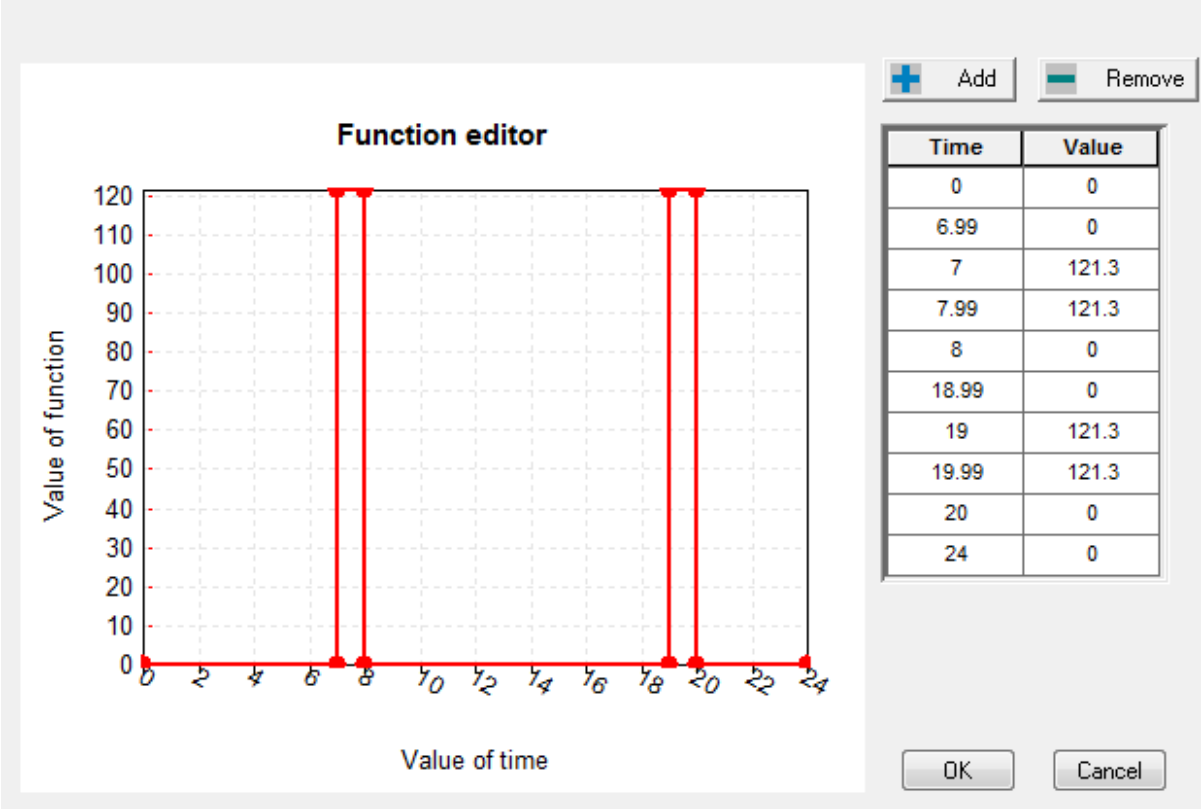

Figure 2. Hot water draw schedule using TRNSYS Type 14b.

Tank Definition

Two tanks of equal design (except for differences in number and locations of ports) were modeled for hot and cold storage. Each tank was a vertical stratified cylindrical storage tank with an internal heat exchanger coil. The heat exchanger was assumed to be copper. Tank dimensions were acquired from specification sheets for a line of solar water tanks (DudaDiesel), and heat loss coefficients were estimated from a survey of heat losses from 19 vertical solar DHW tanks by Furbo (2004). The TRNSYS component selected was Type 534-Coiled for reasons discussed in the Modeling Procedures section.

The parameters for the hot and cold storage tank were similar but differed mainly by the specified locations of inlets and outlets (for reasons also discussed in the Modeling Procedures section). Each tank had at least one set of ports in addition to the heat exchanger for the circulation of the tank fluid through the radiant floor system. Additionally, the hot storage tank had a second set of

ports that was used for providing domestic hot water and replacing it with fresh water from the mains. The tank properties are defined in Table 3.

Table 3. *Tank Properties*

Parameter	Value
Heat Loss Coefficient ($W/m^2.K$):	0.525
Tank Storage Fluid:	Water-Glycol Mixture
Fluid Thermal Conductivity (W/m.K):	0.6
Fluid Dynamic Viscosity ($N.s/m^2$):	0.001002
Fluid Thermal Expansion Coefficient (1/K):	0.000214
Number of Nodes:	5
Supply to Radiant Floor:	Hot Tank: Node 1 (Top)
	Cold Tank: Node 5 (Bottom)
Return from Radiant Floor:	Hot Tank: Node 5 (Bottom)
	Cold Tank: Node 1 (Top)
Heat Exchanger Conductivity (W/m.K):	401
Heat Exchanger Fluid:	60% Water, 40% Propylene Glycol

The collector fluid, which is a mixture of water and glycol, runs through the tank heat exchanger. This fluid has different heat transfer properties than the water stored in the body of the tank and had to be specified in the model. The thermal properties of the water-glycol mixture were modeled at 20 °C in cooling mode and 40 °C in heating mode, based on product information for a water-propylene glycol mixture using DowFrost (DOW Chemical Company, 2001). The properties are listed in Table 4.

Table 4. *Properties of 60% Water and 40% Glycol Mixture*

Parameter	Heating (40 °C)	Cooling (20 °C)
Specific Heat (kJ/kg.K):	3.70	3.77
Density (kg/m^3):	1036.9	1026.5
Thermal Conductivity (W/m.K):	0.401	0.415
Dynamic Viscosity ($N.s/m^2$):	0.0056	0.0023

Building Design

The building was a one-story residential house with a conditioned volume of 407.9 m^3. The foundation was slab-on-grade with a polished concrete interior floor. General properties that were chosen without regard to climate are described in Table 5. Other building properties were chosen to qualify under the most stringent set of criteria for ENERGY STAR certification among the investigated climates, using guidance from the International Energy Conservation Code (IECC) (International Code Council, n.d.). These are described in Table 6.

Table 5. *General Building Parameters*

Parameter	Value
Width (m):	9.14
Length (m):	18.29
Height (m):	2.44
No. of Bedrooms:	3
Mechanical Ventilation (ACH):	0.4
Southface Shading:	2 ft overhang
Average Internal Gains (W/m^2)	6
Lighting Power Density (W/m^2)	2.5

Table 6. *ENERGY STAR Requirements*

Climate	Location Represented	Ceiling R-Value	Wood Frame R-Value	Slab R-Value	Fenestration U-Factor	Fenestration SHGC
Zone 4	Raleigh Albuquerque	38	13	10 (2 ft deep)	0.35	N/A
Zone 2	Jacksonville	30	13	0	0.65	0.3

Overhang Design

A south-facing overhang was used consistent with basic energy efficient design in order to not exaggerate summer cooling loads. Based on the height of the window (1.37 m / 54 inches) and distance of the overhang above the top of the window (0.41 m / 16 inches), trigonometric calculations showed that a 0.62 m (2 foot) overhang will allow beam radiation to strike the entirety of the window face when the sun's azimuth angle is less than 45° and will shield the entire window face when the

angle is greater than 70°. Looking at the sun charts for the inspected climates, included in Appendix A, it can be seen that this works well in each location for eliminating beam radiation and excess cooling loads in summer while assisting passive solar heating in winter.

Air Exchange

For simplicity, all air exchange was modeled as mechanical ventilation to slightly exceed the requirements of ASHRAE Standard 62.2. The standard requires 0.03 cubic feet per minute (CFM) of ventilation per square foot of floor area plus 7.5 CFM for every occupant in the home. The modeled home requires 76.5 CFM, or 129.97 m^3/hr, which for a 407.76 m^3 living space works out to 0.32 ACH. Calculations were performed using the Residential Energy Dynamics Tool (Residential Energy Dynamics, LLC, 2013). Air exchange was modeled as 0.4 ACH to include potential air leakage.

Controls and Set Points

It is impractical to attempt to control air temperature directly because the thermal capacitance of the slab is orders of magnitude greater than the enclosed indoor air. However, the air temperature will approach the floor surface temperature at a rate proportional to the ΔT between floor and air temperatures, and if the floor surface temperature is kept constant, the air temperature will be controlled. This worked well under most conditions, but there were sometimes minor fluctuations and potential excursions from ideal thermal comfort. Slab surface temperature was held at the following set points during the heating season and cooling season, respectively:

- Heating using tank water: 25 °C
- Heating using auxiliary heat pump: 23 °C
- Cooling using tank water: 21 °C
- Cooling using auxiliary heat pump: 23 °C

Type 56 Parameters

The overall building was modeled with a Type 56 component. Type 56 can create multi-zone building energy models that are compliant with ASHRAE and LEED energy modeling standards. A

TMY2 weather file was processed by a Type 15 component to calculate meteorological values such as ambient temperature, wind speed, and radiation incident on surfaces of various orientations, which were inputs to the collector array and Type 56 building. The radiant floor system was defined as an "active wall layer" according to the program terminology, which received the inputs of fluid temperature and flow rate from the tanks.

The Type 56 component was created and modified through an ancillary software package called TRNBUILD. TRNBUILD provides an interface for defining the physical characteristics of the building as well as new inputs and outputs to interact with other components in the simulation. There are many variables that can be selected as outputs of a Type 56 component including those related to thermal comfort, such as dry bulb temperature; mean radiant temperature; and relative humidity; as well as those related to energy balances, such as inside surface temperature; outside surface temperature; and rate of radiant heat flux. Heating and cooling equipment was defined by external components rather than within the Type 56 component. However, heating and cooling loads can also be "artificially" met using the Load Manager, which adds or removes as much latent and sensible heat as necessary in order to meet desired set points of the indoor air. The results from the Load Manager were used to verify the correct functioning of the radiant floor system and investigate dehumidification requirements.

The building was modeled in TRNSYS as two separate air nodes: an "Attic" node, which includes all enclosed space above the ceiling, and a "Zone1" node, which includes the living space. An air node is a fundamental element of the building defined by a volume and thermal capacitance and characterized by a uniform temperature at any point in time. Each air node is uniquely paired to a set of surfaces and has unique specifications for ventilation, internal gains, and HVAC set points. Heat balance calculations are performed by TRNSYS according to the building characteristics defined for each specific air node.

Air Nodes

Two air nodes were used because the attic and living space are expected to have very different temperatures from each other. The accuracy of the simulation could be increased by creating multiple air nodes within the living space to model vertical stratification of air temperature, but this would increase the model complexity for less incremental benefit than adding the second air node. This is because temperature between floor-level and ceiling-level of a single story home should not vary as much as between living space and attic. For simplicity and computational expediency, the living space was modeled as a single room. The air nodes are described in Table 7. "Coupling air flow" indicates the quantity of air leaking between the attic and living space.

Table 7. *Air Node Properties*

Name	Volume (m^3)	Thermal Capacitance (kJ/K)	Wall Types	Conditioned?	Coupling Air Flow (kg/h)
Attic	220.7	264.85	Roof (External) Gable (External) Ceiling (Adjacent)	No	10
Zone1	407.76	978.62	Exterior Wall (External) Ground (Boundary) Ceiling (Adjacent)	Yes	10

Orientations

An "orientation" in TRNSYS is not strictly defined by spatial orientation: Any surface that has a unique amount of radiation falling on it is considered a new orientation. The quality of radiation incident on each orientation is calculated by the Type 15-2 weather component. Three new orientations were defined beyond those provided by default: two to represent the north and south faces of the 30° sloped roof and a third to represent the effect of the south façade's overhang. Orientations are summarized in Table 8.

Table 8. *Defined Building Orientations*

Orientation Name	Usage	Tilt	Azimuth	Shading
N_180_30	North Roof	30°	180°	No
S_0_30	South Roof	30°	0°	No
N_180_90	North Façade	90°	180°	No
SHADS_0_90	South Façade	90°	0°	Yes
E_270_90	East Façade	90°	270°	No
W_90_90	West Facade	90°	90°	No

The new roof orientations were added to the Type 15 weather component by adding the roof slopes and azimuths to its list of parameters, which creates new outputs to connect to the Type 56 component. The Type 15 weather component does not directly calculate the south shaded orientation; instead, its southward radiation was routed through a Type 34 "Overhang and Wingwall" component to the building as shown in Figure 3.

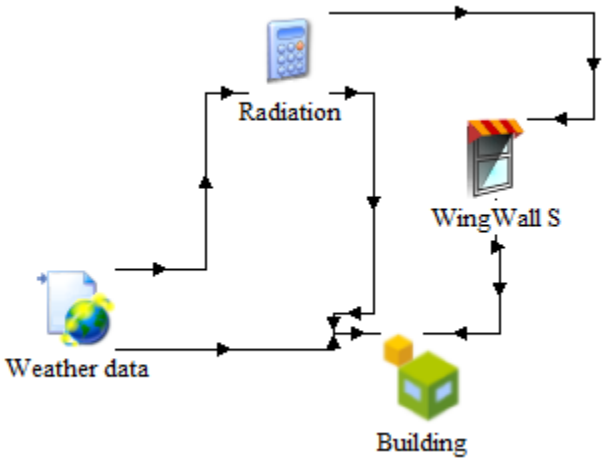

Figure 3. Overhang modeling.

Wall Parameters

The terminology of TRNSYS describes all elements of the building envelope such as ceilings, floors, walls, and roofing as "Walls." Walls are assembled from layers defined by properties of thickness, conductivity, thermal capacitance, density, solar absorptance, and thermal emissivity. Throughout the building enclosure, there are sometimes parameters of layers that are not applicable.

The solar absorptance is not applicable when a layer is not exposed to sunlight and thermal emissivity is not applicable when it is sandwiched in direct contact between other layers. In these cases, those parameters are marked "N/A."

Many wall types are pre-defined by existing layers in the TRNSYS libraries, but some materials or some of their parameters were not available and were instead retrieved from outside sources. Others were modified based on available literature; notably, the density of concrete was defined as 1,400 kg/m^3, but most sources place conventional concrete closer to 2,400 kg/m^3 (as outlined in *Density of Concrete* (Elert, 2001)).

Roof and ceiling.

The layers of walls connected to the attic air node are listed below; the roof is defined in Table 9, the gable in Table 10, and the ceiling in Table 11.

Table 9. *Roof Layer Parameters*

Material	Thickness (m)	Conductivity (kJ/hr.m.K)	Capacitance (kJ/kg.K)	Density (kg/m^3)	Absorptance	Emissivity
PLYWOOD	0.025	0.54	1.2	800	N/A	0.83
FELT MEMBRANE	.005	0.69	1.67	1121.3	N/A	N/A
ASHPALT SHINGLE	.01	0.223	0.92	2115	0.85	0.9

Table 10. *Gable Layer Parameters*

Material	Thickness (m)	Conductivity (kJ/hr.m.K)	Capacitance (kJ/kg.K)	Density (kg/m^3)	Absorptance	Emissivity
PLYWOOD	0.025	0.54	1.2	800	N/A	0.83
BRICK	0.09	3.2	1.0	1800	0.55	0.93

Table 11. *Ceiling Layer Parameters*

Material	Thickness (m)	Conductivity (kJ/hr.m.K)	Capacitance (kJ/kg.K)	Density (kg/m^3)	Absorptance	Emissivity
FIBERGLASS QUILT	0.27	0.144	0.84	12	N/A	0.75
GYPSUM	0.01	0.756	1	1200	N/A	0.85

Exterior walls and windows.

The exterior wall parameters are provided in Table 12. The exterior walls used discontinuous insulation in the form of a 2x4 stud wall cavity filled with mineral wool insulation. However, each TRNSYS layer is continuous, so the required thickness of each continuous layer of insulation was calculated. The resulting R-Value is 2.46 $K.m^2/W$, or 13.95 $hr.ft^2.R/Btu$.

Table 12. *Exterior Wall Layer Parameters*

Material	Thickness (m)	Conductivity (kJ/hr.m.K)	Capacitance (kJ/kg.K)	Density (kg/m^3)	Absorptance	Emissivity
GYPSUM	0.013	0.756	1	1200	0.3	0.85
ROCKWOOL	0.071	0.126	1.4	25	N/A	N/A
PLYWOOD	0.013	0.054	1.2	800	N/A	N/A
BRICK	0.090	3.2	1	1800	0.55	0.93

Windows were modeled as subcomponents of walls and were chosen from the TRNSYS library to meet the ENERGY STAR U-Value and SHGC constraints across all climates. TRNSYS defines them by the parameters of solar transmittance, solar reflectance, and visible transmittance. The window area within each building face is specified in Table 13 and the properties of each are specified in Table 14. Note that ENERGY STAR uses imperial units for U-Value while TRNSYS uses SI units, with a conversion factor of 5.678 $W/(m^2.K)$ to 1 $Btu/(hr.ft^2.°F)$.

Table 13. *Window Distribution on Building Faces*

North (m^2)	South (m^2)	East (m^2)	West (m^2)
4.26	4.26	1.42	1.42

Table 14. *Window Properties*

Description	U-Value ($W/m^2.K$)	SHGC	Solar Transmittance	Solar Reflectance	Visible Transmittance
LowSHGC,Ar, silber1.3 38/30	1.3	0.298	0.226	0.209	0.383

Floor system.

The floor was composed of the layers and parameters listed in Table 15. The PEX tubing was represented by the Active Layer, which is described in Table 16. Pipe dimensions and conductivity were obtained from manufacturer information for ½'-inch tubing, while spacing was set according to guidance in a design manual by Uponor (2013).

Table 15. *Floor Layer Parameters*

Material	Thickness (m)	Conductivity (kJ/hr.m.K)	Capacitance (kJ/kg.K)	Density (kg/m^3)	Absorptance	Emissivity
CONCRETE SLAB	0.06	4.068	1	2400	0.6	0.9
ACTIVE LAYER	N/A	1.37*	N/A	N/A	N/A	N/A
CONCRETE SLAB	0.06	4.068	1	2400	N/A	N/A
XPS	0.025	0.125	1.214	28.8	N/A	N/A

*Describes the conductivity of the pipe within the active layer.

Table 16. *Active Layer Specifications*

Material	Pipe Outside Diameter (m)	Pipe Wall Thickness (m)	Pipe Wall Conductivity (kJ/hr.m.K)	Pipe Spacing (m)	Number of Loops	Specific Heat of Fluid (kJ/kg)
PEX Tubing	0.015875	0.0018	1.37	0.2	8	4.18

Another important setting was the convective heat transfer coefficient for the top of the floor: this was set to "internal calculation," meaning TRNSYS calculated its value based on the floor and air temperatures rather than using a constant value. This was done solely for this surface because the slab is the most important location of heat transfer. The convective heat transfer coefficient for the underside of the floor was not needed because the floor is a slab-on-grade and does not interact directly with air.

Two new inputs were created for the Active Layer within the Type56 building to simulate the storage tanks connected to PEX tubing: "TankFlow" and "TankTemp," which received the flow rate from the tank and the temperature of the fluid stream immediately before entering the floor system.

Internal Gains

Internal gains were assumed to be consistent over each day of the week (except from clothes drying) and to come from the following sources: the human body, computers, artificial lighting, appliances, and miscellaneous gains from other sources. The usage schedule, sensible heat gain, latent heat gain, and equivalent moisture gain (in kg/hr) are provided in Table 17. Usage schedules may be more regular than typical activity, but being equivalent for both glazed and unglazed collectors, likely had negligible effect on this comparative study.

Table 17. *Internal Gain Schedule*

Type of Internal Gain	Times of Gain	Sensible Heat Gain		Latent Heat Gain		Equivalent Moisture Gain
		W	kJ/hr	W	kJ/hr	kg/hr
Human Body (per person)	5:30 PM to 8:00 AM	60	216	40	144	.06
Computers & Electronics	7:00 PM to 9:00 PM	280	1,008	0	0	0
Lighting	7:00 AM to 8:00 AM, 5:00 PM to 10:00 PM	418	1,505	0	0	0
Cooking	7:00 AM to 7:15 AM, 5:30 PM to 6:00 PM	1,125	4,050	375	1,350	0.6
Clothes Drying	1:00 PM to 3:00 PM (Sunday Only)	1,000	3,600	0	0	0
Washing Machine	11:00 AM to 1:00 PM (Sunday Only)	200	800	0	0	0
Dishwasher	11:00 PM to 12:00 AM (Tuesday and Thursday)	1200	4,320	200	720	0.17
Miscellaneous	Constant	520	1,872	0	0	0

Chapter Four: Modeling Procedures

A parametric analysis was performed to investigate the effects of tank size and collector array size on energy savings. Energy savings were found to vary little with tank size and a constant value was selected to allow for more direct comparison between different collector arrays. The simulation was performed in each chosen climate zone for each type of system at a number of different array sizes sufficient to reveal trends in the data. Outputs collected from the model included energy consumption by the auxiliary heat pump (in both heating and cooling modes) and energy consumption by the tankless DHW heater. The difference in energy and energy cost savings between glazed and unglazed collectors was calculated for each location.

Energy savings are displayed as graphs showing space heating, space cooling, and domestic water heating savings in each month for each climate. The total energy cost savings from glazed and unglazed collectors are also displayed in graphical and tabular format. The performance of the building, tank, and collector were investigated to make sure they performed realistically. Modeling procedures that were used to inform system design are also described here.

Floor System

Ground Coupling

The foundation is slab-on-grade, but the recommended procedure for accurately modeling coupling to ground temperature in TRNSYS is relatively complex. It requires modeling the building in Google Sketchup (Solar Energy Laboratory, 2009b) and greatly increases simulation run time, often taking up to several hours per simulated year (D. Bradley, personal communication, October 15, 2015). As a simplification, the below-slab ground temperature was estimated based on the ground temperature (outside of the building foundation) and typical indoor air temperature. The influence on heat loss from the underside of the slab was investigated based on two different hypothetical formulas:

$$T_{below} = (T_{indoor} + T_{ground})/2 \quad (high\ influence\ of\ ground\ temperature)$$

$$T_{below} = (3 * T_{indoor} + T_{ground})/4 \quad (low\ influence\ of\ ground\ temperature)$$

The temperature used for T_{indoor} is 23 °C, and T_{ground} was estimated from mains water temperature, which seems to work well as a proxy for ground temperature according to a soil temperature map. The TRNSYS Type 15 weather component does not produce an actual ground temperature output. The validity of each model was assessed by comparing the results of TRNSYS simulations with experimental results in the literature.

Chuangchid and Krarti (2001) compared a numerical model for concrete slab heat loss to an existing set of experimental measurements for a 4-inch thick heated slab with 2-foot deep perimeter insulation (and no continuous insulation below slab). When the outdoor air temperature was 30 °F (16.7 °C) lower than indoor temperature and the system was in steady-state, approximately 30% of the heat input to the slab was lost out of the bottom and edges.

A TRNSYS simulation was performed in Raleigh and Albuquerque for the month of February, for which the average differences between indoor and outdoor temperatures are 17 °C and 18 °C, respectively. The slab was heated to a constant 23 °C using an inlet water temperature of 29 °C and the amount of heat input to the slab was compared to the amount of heat lost through its bottom. Edge losses were not modeled and therefore all heat loss was accounted for through the bottom of the slab. The heat losses using each hypothetical model for below-slab temperature are shown in Figure 4.

At a high ground influence the simulation in the study comparing glazed and unglazed collectors agreed well with the experiment, showing about 31% heat loss through the underside of the slab. However, the simulated slab had 0.05 m of continuous insulation and should lose less heat than the experimental slab with only perimeter insulation.

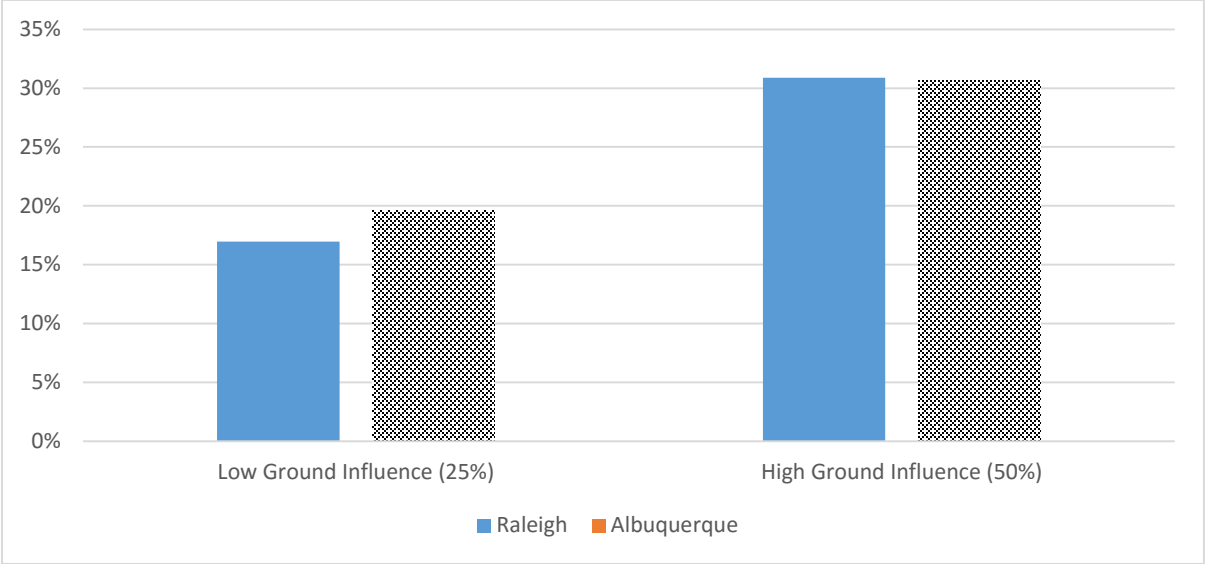

Figure 4. Percentage of heat loss through underside of slab using two different hypothetical formulas.

Chuangchid and Krarti (2001) also provided monthly estimates for the amount of heat lost through a slab with different levels of insulation. In February, a slab with "partial insulation" (understood to mean perimeter insulation) loses 60 W/m, but for continuous insulation at an R-Value of 2.0 m^2C/W the slab loses about 40 W/m. The estimated R-Value of the insulation in the simulation is 1.45 m^2C/W. Based on these figures, the rate of slab heat loss was attenuated to equal slightly more than 2/3 of the high ground-influence simulation. The formula representing low ground-influence produced heat loss rates that were (100% - 17% / 31%) = 45% lower in Raleigh and (100% – 20% / 31%) = 35% lower in Albuquerque than those produced by the formula representing high ground-influence. Therefore, a compromise between the formulas was chosen:

$$T_{below} = (2 * T_{indoor} + T_{ground})/3$$

Thermal Lag

The radiant system cannot respond immediately to loads because there is a lag between the time at which heat flows into the center of the slab and when it conducts to the surface. This time lag was investigated by removing all dynamic loads to the slab, varying the heat transfer fluid temperature at one point in time, and observing the slab surface temperature over time. All weather-

related inputs to the slab (or indirectly to the slab via the building walls) were set to zero, except for ambient temperature and the slab boundary condition, which were set to a constant 20 °C.

Under the simulated conditions, there was a large time lag for both heating and cooling response, taking about four hours for the slab surface temperature to approach about 50% of the difference between its initial temperature and its final temperature (using an inlet fluid temperature of 29 °C). However, the time lag is not an issue if the floor temperature is controlled to stay within an acceptable range. The thermal time lag is shown in Figure 5.

Inspection of a Raleigh TMY2 file showed that the coldest daily temperature, and therefore the highest demand, often occurs in early morning close to sunrise. A nighttime temperature setback was considered but decided against because the slab's thermal inertia may make it impractical to have the setback period immediately adjacent to the time of peak demand.

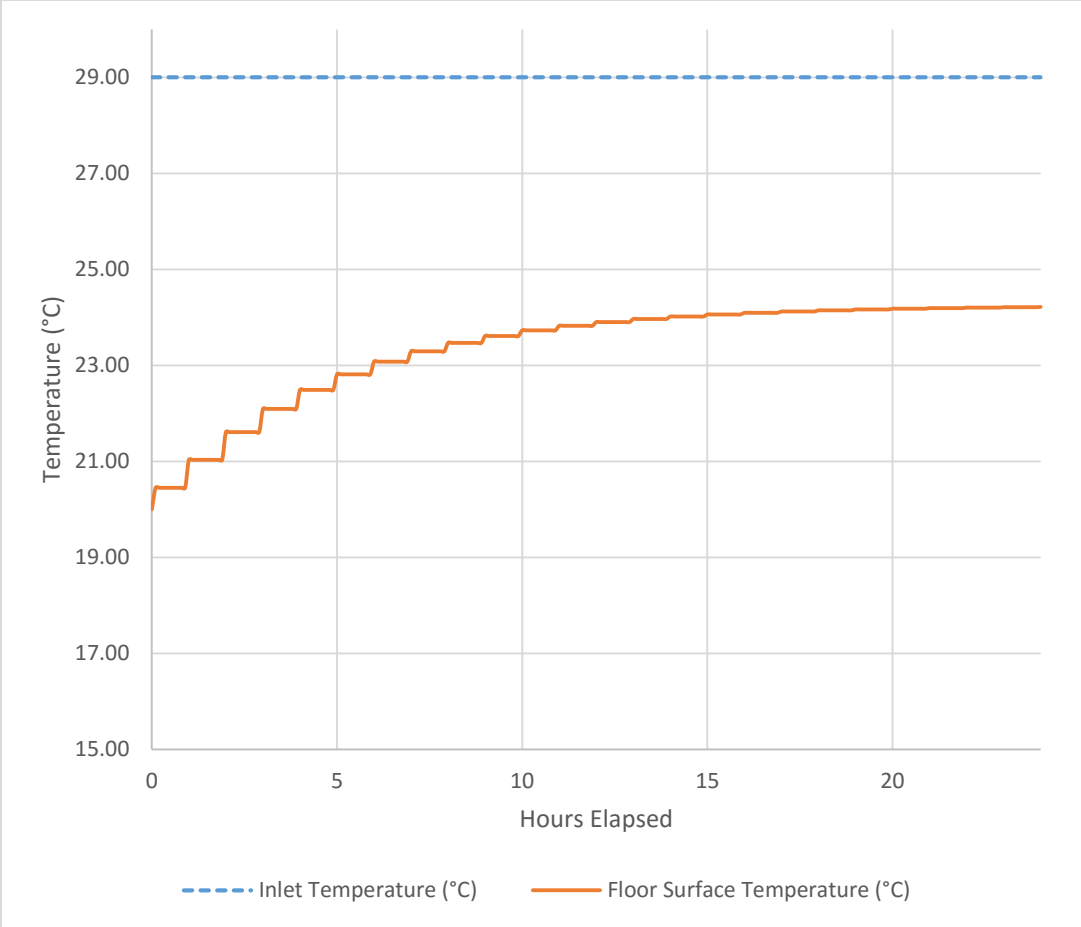

Figure 5. Floor surface temperature response during heating.

Determining Heat Transfer Fluid Set Points for Space Conditioning

The fluid set point temperatures for the radiant floor were chosen to maintain the floor surface-to-air temperature differential at the minimum practical value required to meet space heating and cooling loads. The Type 56 component requires the flow rate through to be high for turbulent flow. At these flow rates, the rate of heat transfer through the floor is not extremely sensitive to flow rate; varying the flow rate between 2,000 kg/hr and 20,000 kg/hr resulted in visually identical indoor temperature profiles. A flow of 2,000 kg/hr was selected.

It was decided to use the same fluid temperature set points in each climate. Inspection of the hourly building loads showed that the highest instantaneous heating load occurred in Raleigh (at a total of 4.32 kW) and the highest instantaneous sensible cooling load occurred in Albuquerque (at

3.47 kW). The floor temperature was controlled to prevent the indoor air from dropping below 21 °C during heating and from rising above 26 °C during cooling. Based on estimated heat transfer coefficients from Uponor (2013) of 11 W/m^2.K for radiant floor heating and 7 W/m^2.K for radiant floor cooling, the required floor temperature was calculated in order to be effective in each mode of space conditioning (Figure 6).

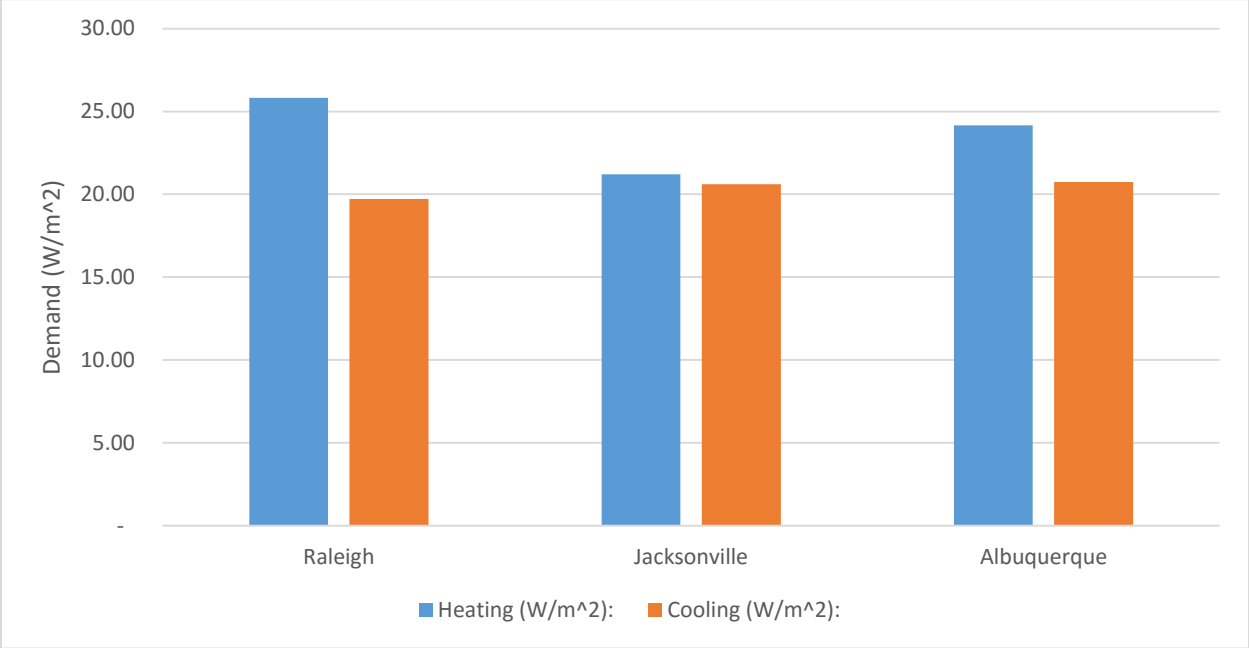

Figure 6. Maximum instantaneous heating and cooling load experienced in different climates.

The required temperature differentials between floor surface and air turned out to be quite small in order to achieve the required heat fluxes. The floor surface must be 2.35 °C above air temperature during maximum heating load (or above 23.35 °C) and 2.96 °C below air temperature during maximum cooling load (or below 23.04 °C). The fluid temperatures needed to maintain these floor surface temperatures were investigated by making adjustments to them in subsequent simulations in TRNSYS, and observing their effects on indoor temperatures. Heating and cooling were investigated in separate simulations (Figures 7 and 8).

A fluid temperature of 29 °C worked well for heating in Raleigh. The floor temperature stayed above 25 °C (the majority of time) and the indoor air temperature stayed above 21 °C. The

upper air temperature was artificially limited to 26 °C using the TRNBLD Load Manager in order to investigate heating separately from cooling.

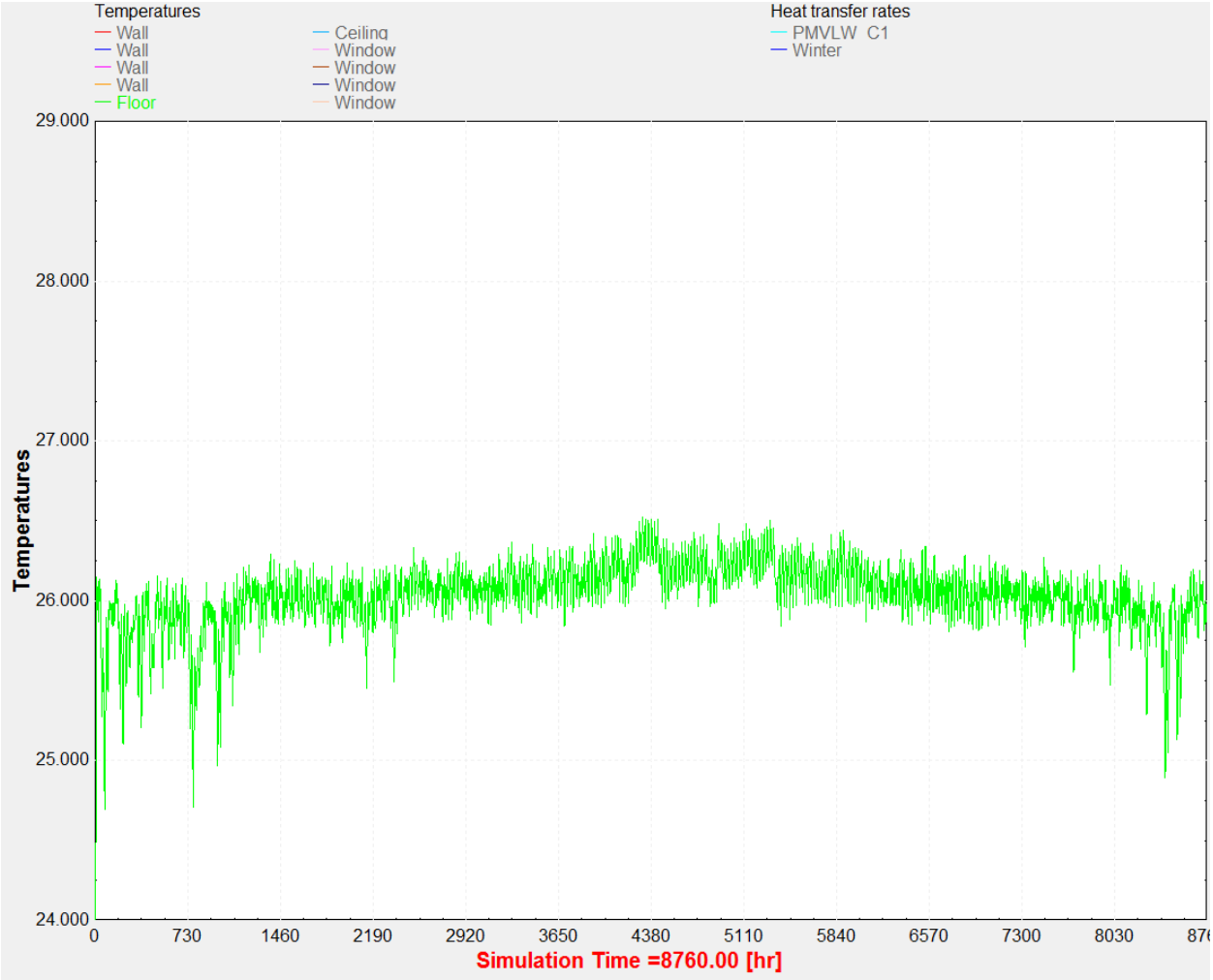

Figure 7. TRNSYS plotting tool showing floor surface temperature during heating season. Floor is only active during heating season. Fluctuations during cooling season are caused by passive modes of heat transfer (i.e., conduction to ground and convection to air).

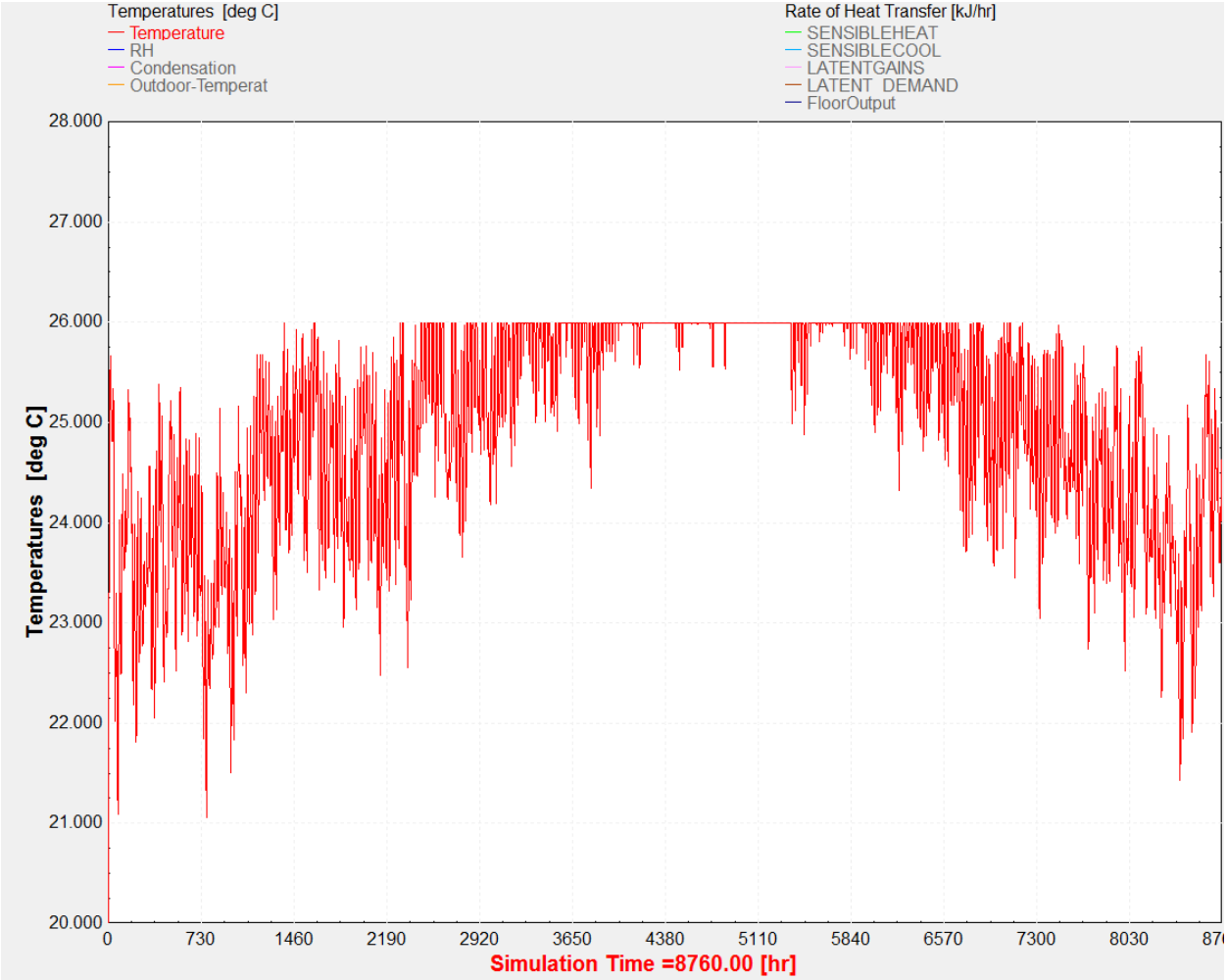

Figure 8. TRNSYS plotting tool showing indoor air temperature during heating season. The air is cooled by the Load Manager if it rises above 26 °C during summer months.

A water temperature of 20 °C worked well for cooling in Albuquerque. Figure 9 shows that the floor surface stayed below 23 °C, and Figure 10 shows that the indoor air temperature stayed below 26 °C. The operative temperature generally stayed below 25 °C, which the thermal comfort analysis showed is actually slightly on the cool side when wearing typical summer clothing. In the cooling analysis, heating was performed by the Building Load Manager when air temperature dropped below 22 °C.

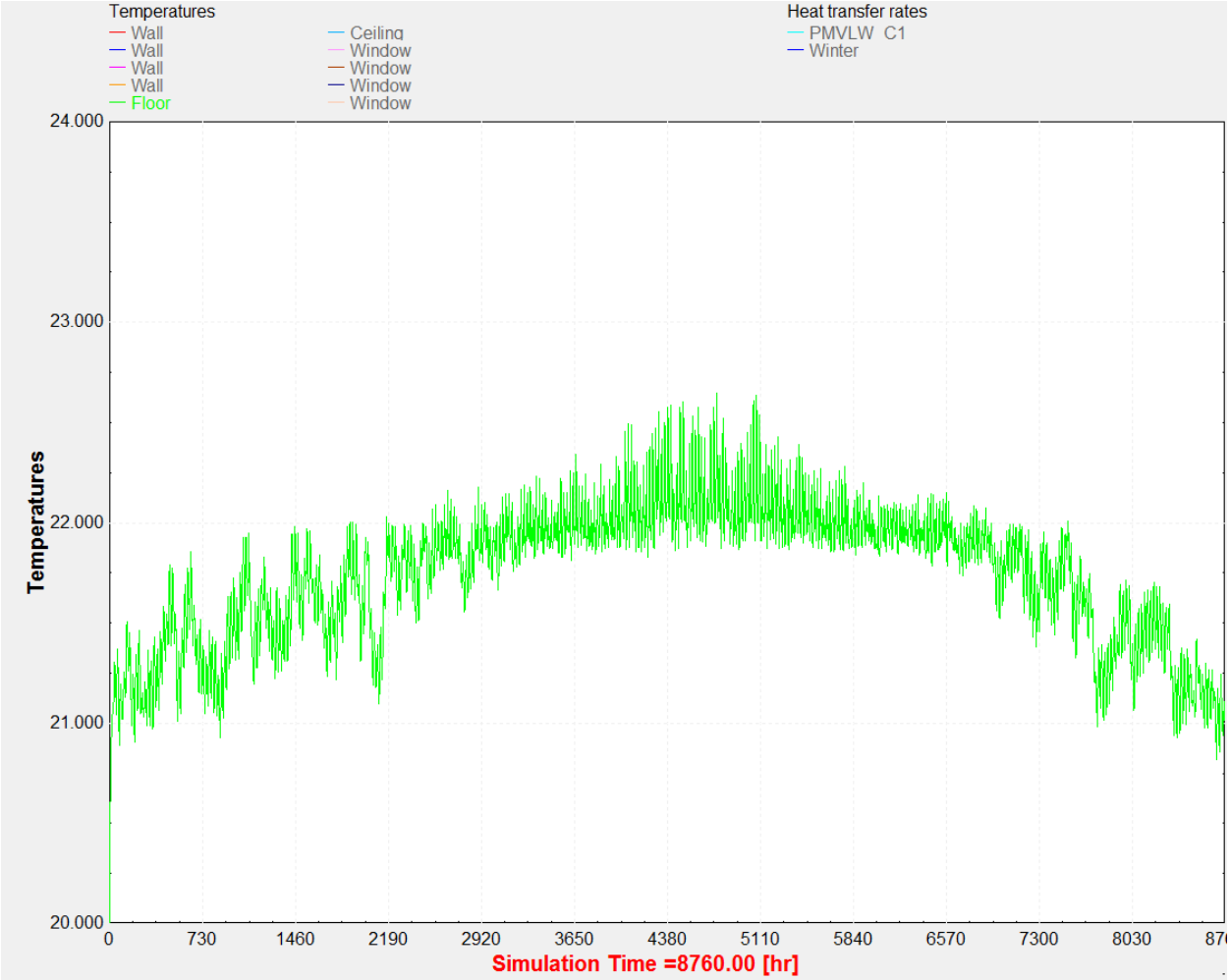

Figure 9. TRNSYS plotting tool showing floor surface temperature during cooling season. Floor is only active during cooling season. Fluctuations during heating season are caused by passive modes of heat transfer (i.e., conduction to ground and convection to air).

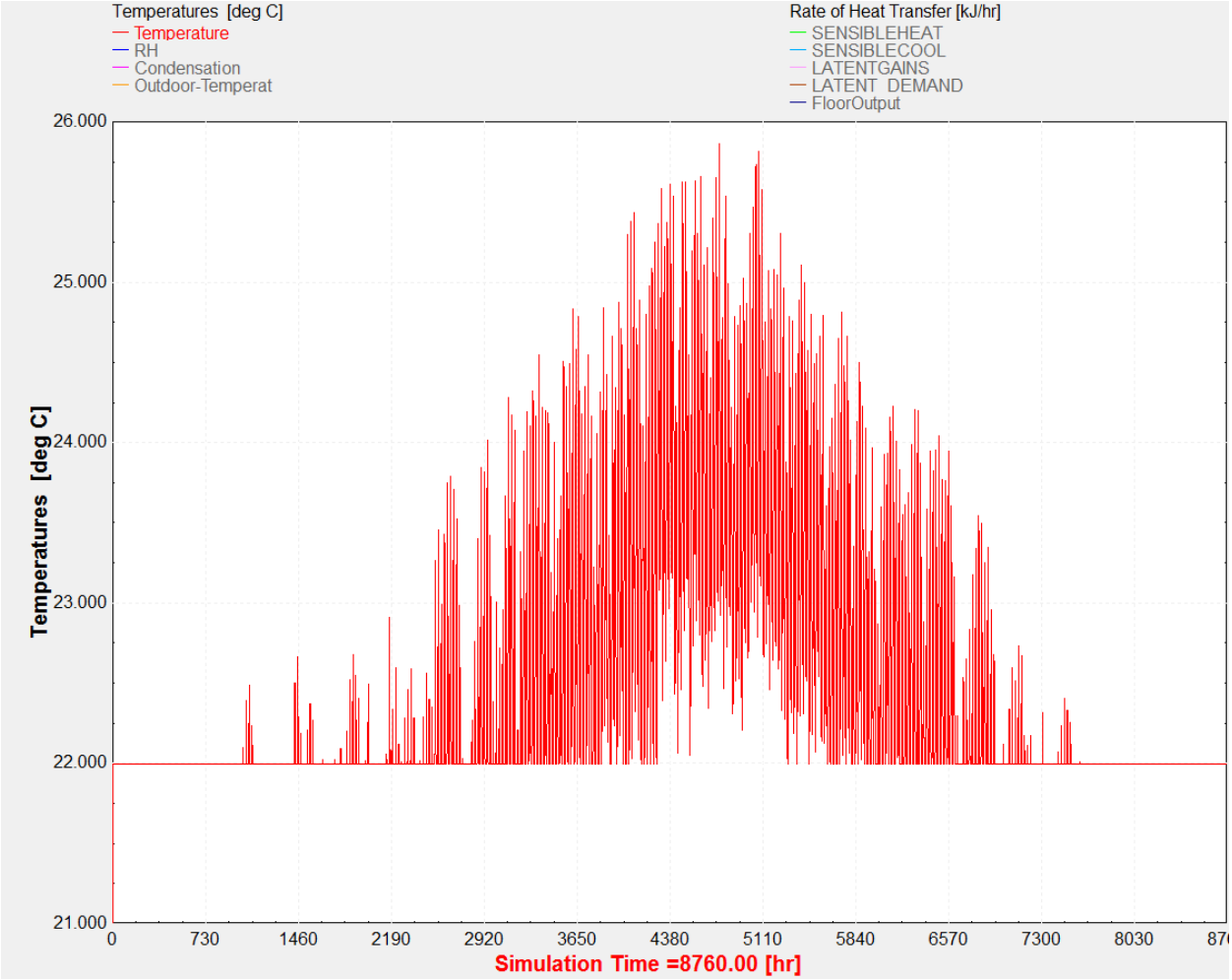

Figure 10. TRNSYS plotting tool showing indoor air temperature during cooling season. The air is heated by the Load Manager if it falls below 22 °C during winter months.

In summary, the fluid temperature set points for the inlet to the radiant floor are 29 °C for heating and 20 °C for cooling.

Tank Modeling

Considerations

The storage tank must have a large enough capacity to store the required heat for at least one day at a time, but should not be so large that its thermal inertia prohibits the collectors from heating or cooling it to usable temperatures. When undisturbed by forced circulation, the fluid will naturally stratify along a temperature gradient, modeled by N separate nodes in TRNSYS, with coldest at the bottom of the tank to warmest at the top. The heating tank is used most efficiently by delivering water

from the top node to the heating load (i.e., the radiant floor or auxiliary water heater) and from the bottom node to the heat source (i.e., the collector array). The cooling tank is used most efficiently by delivering water from the bottom node to the cooling load (i.e., the radiant floor) and from the top node to the cooling source (i.e., the collector array).

Tank Model Analysis

Different TRNSYS components were considered for the stratified storage tanks representing the hot and cold storage reservoirs. Type 4e did not show realistic stratification behavior. Type 60c showed better stratification, but a flaw in this component was encountered that the distributor verified as an error and recommended Type 534 instead. Type 534-Coiled (which contains an internal heat exchanger coil) was selected. It showed realistic temperature stratification (shown in Figure 11) and was further investigated by comparing 534-Coiled and 4e components side-by-side in equivalent solar thermal loops. Figure 12 shows that they behaved similarly, with a slightly lower temperature displayed by 534-Coiled, which makes sense because it uses an internal heat exchanger rather than direct mixing.

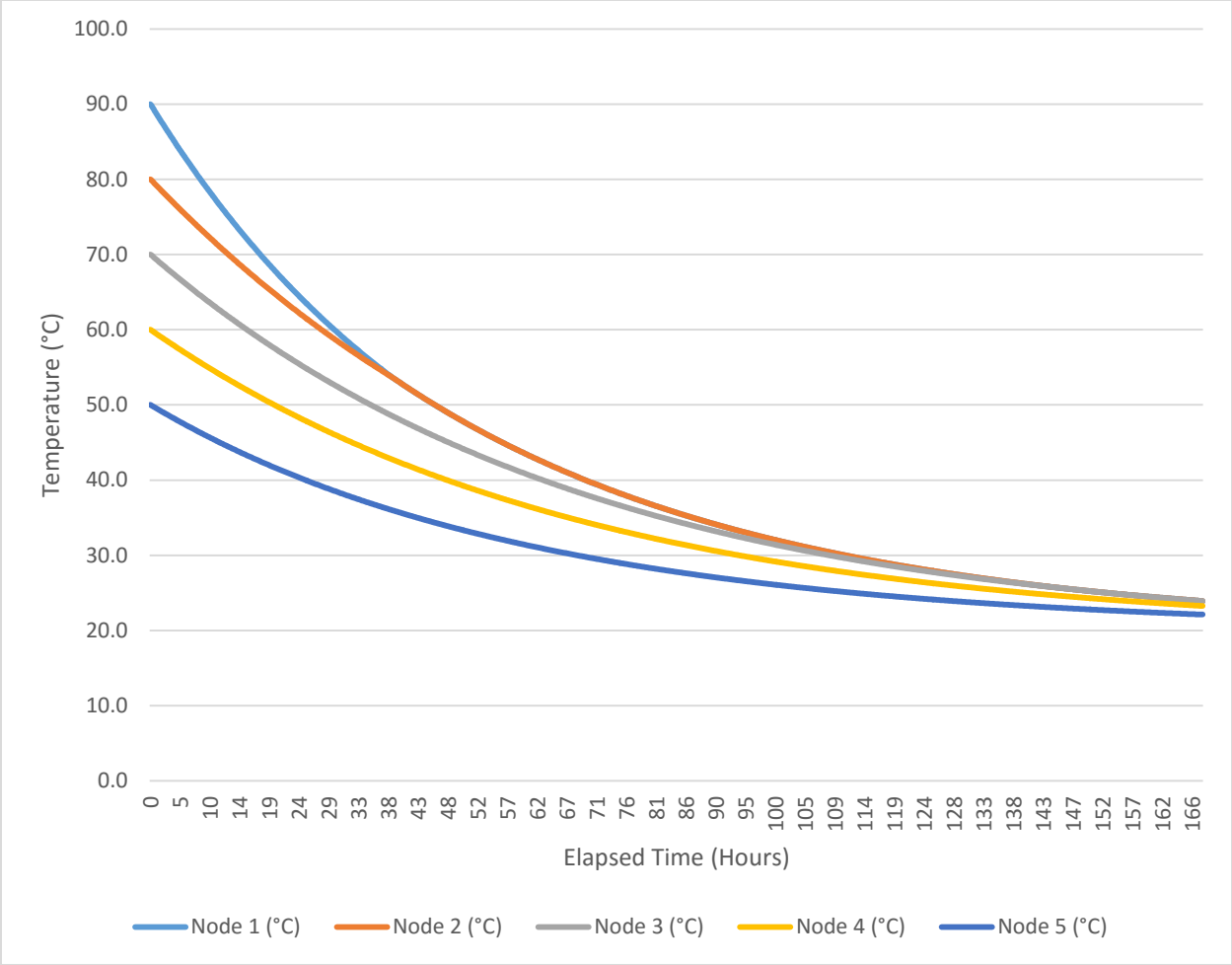

Figure 11. Stratification behavior of Type 534-Coiled as fluid cools over time.

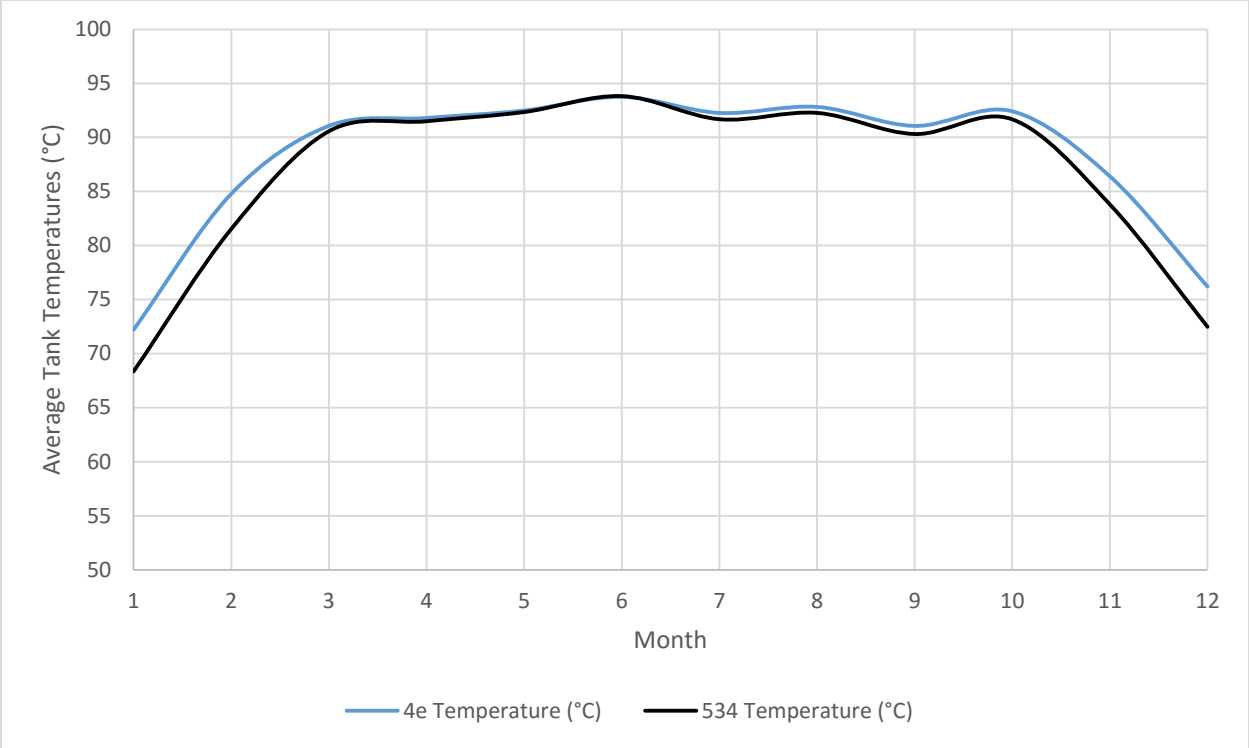

Figure 12. Average monthly temperatures produced by Type 534-Coiled and Type 4e tanks under similar conditions.

Tank Size Optimization

Burch et al. (2004) found that the optimal tank size for their unglazed collector array was about 80 L (or about 0.08 m^3) per square meter of collector, but of all sizes simulated, the amount of energy saved ranged between 0.85 and 1.15 times the amount of the base case. Several simulations with various tank sizes were performed in the Raleigh climate for a glazed collector array of 7.6 m^3 and an unglazed collector array of 15.2 m^3 (based on the understanding that glazed collectors tend to absorb more heat).

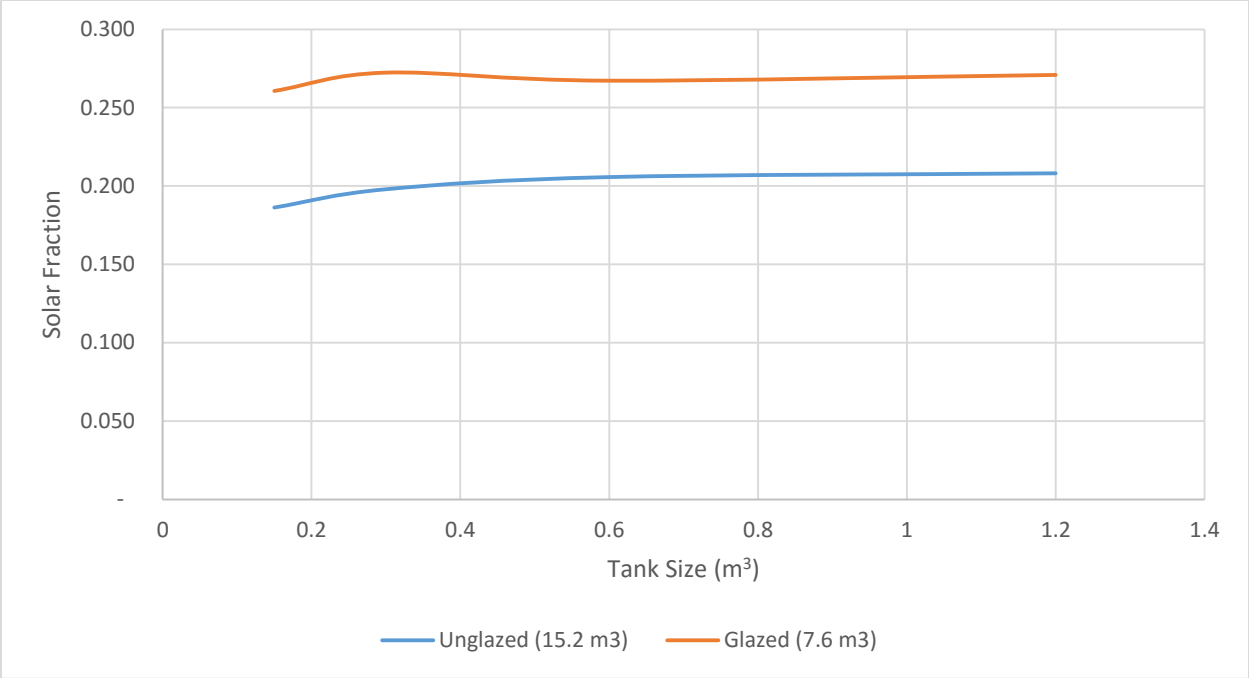

Figure 13. Total solar heating fractions (including space heating and DHW) versus tank size.

As seen in Figure 13, the performance was relatively insensitive to tank size. A tank size of 0.6 m^3 should be a robust value that does not greatly alter the solar fraction as array size is varied. There may be a slightly lower efficiency as the array is increased and the tank size is held constant; however, by maintaining a constant tank volume, the incremental cost per collector was much clearer.

Configuration Optimization

Two different configurations were tested to determine which yielded a better solar fraction. In the first configuration, the solar collector fluid ran through the heat exchanger within the hot water tank and potable water was stored in the tank for DHW and space heating. In the second configuration, the collector fluid ran directly into the tank and the DHW was pre-heated by running through the heat exchanger.

The total auxiliary energy consumption was tested by simulating each case with different sizes of unglazed collector arrays: one collector having an area of 3.8 m^2 and an unrealistic saturation case using 760 m^2 of collectors. Figure 14 shows that the configuration in which DHW is stored

directly in the tank yields a slightly better solar fraction under both minimum and maximum sizing conditions, and was chosen as for all system simulations.

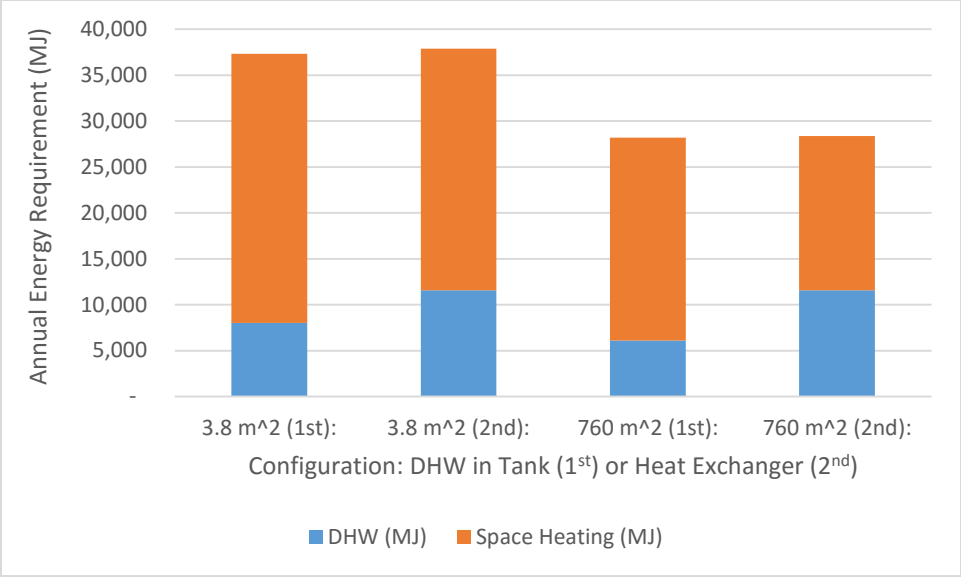

Figure 14. Total heating requirements with potable water stored in tank (1st configuration) or in heat exchanger (2nd configuration).

Collector Modeling

The solar thermal collectors were the most important components to accurately model in view of the research questions. Inaccuracies in the building or tanks generally affect both glazed and unglazed collectors equally, but inaccurate modeling of the collectors themselves would directly skew the comparison. Therefore, much attention was given to comparing the performance of the TRNSYS models against what would be expected based on the theoretical understanding of solar thermal collectors and measured performance curves. This section of the analysis first describes the basic equations governing collector performance and the TRNSYS components that are able to perform those calculations. Next I have outlined why certain TRNSYS components are better suited for answering the research questions than others in light of the calculations that had to be performed. I then discuss when theoretical models may become less predictive of actual performance, specifically for different models of convection. Finally, I describe the calculations that were performed to verify the TRNSYS models and compare the results between the two methods.

For reference, the collector models used in each type of simulation and their capabilities are listed in Table 18. The "Used" column describes whether the TRNSYS component can respond to changes in that variable. For example, the Type 539 component is based off of test results performed in a specified range of wind speeds, and therefore accounts for wind under typical conditions. However, it does not utilize wind speed directly as an input. Further justification for the choices is described in the following sections.

Table 18. *Collector Types Used and Variables Processed in Each Mode of Operation*

Function	TRNSYS Model	Solar Irradiance		Wind Speed		Sky Temperature	
		Used?	Needed?	Used?	Needed?	Used?	Needed?
Glazed Heating	Type 539	Yes	Yes	No	No	No	No
Glazed Cooling	Type 942**	Yes	No	Yes	Yes	Yes	Yes
Unglazed Heating	Type 553	Yes	Yes	Yes*	Yes	Yes	Yes
Unglazed Cooling	Type 553	Yes	No	Yes*	Yes	Yes	Yes

*Wind speed is indirectly processed by Type 553 as described later.
**Type 942 is indirectly used through a correlation function described later.

Collector Performance Theory

An accurate model of a solar thermal collector must correctly describe the rate of absorbed radiation as well as the rates of convective and radiative heat loss. This task can be divided into two parts: first determining the incident radiation spectrum, temperature, and wind speed meeting a collector aperture, and secondly, accurately modeling the collector's response to these environmental variables.

The collector's absorption of radiation is described by Duffie and Beckman (2006, p. 221), under the assumption that the diffuse sky radiation is isotropic:

$$S = I_b R_b (\tau\alpha)_b + I_d (\tau\alpha)_d \left(\frac{1+\cos ß}{2}\right) + \rho_g I_b \left(\frac{1-\cos ß}{2}\right)$$

In which:

S = Incident solar radiation, reduced by optical losses

I_b = Beam radiation

I_d = Diffuse radiation

$(\tau\alpha)_b$ = Transmittance-absorptance product for beam radiation

$(\tau\alpha)_d$ = Transmittance-absorptance product for diffuse radiation

ρ_g = Ground reflectance

R_b = Ratio of beam radiation on tilted surface to beam on horizontal

$\frac{1+\cos ß}{2}$ = View factor from the collector to the sky

$\frac{1-\cos ß}{2}$ = View factor from the collector to the ground

ß = Collector slope

The amount of irradiance reaching a surface at a specific tilt and azimuth is easily generated in TRNSYS using a Type15 weather component. The isotropic sky model of diffuse radiation is specified in a parameter named "Tilted Surface Radiation Mode" with a value of 1. The slope of the surface of interest (e.g., a building façade or collector absorber) is also a weather component parameter. Beam, diffuse, ground-reflected, and total radiation are outputs supplied at any tilt and azimuth entered into the weather component.

According to the *TRNSYS 17 Solar Library Mathematical Reference* (Thermal Energy System Specialists [TESS], 2009), isotropic diffuse sky radiation is also assumed by the models selected for the heating simulation; Type 539 representing a glazed collector and Type 553 representing an unglazed collector. The transmittance and absorptance of the collectors are included implicitly in their efficiency curves utilized by the components.

Radiative heat loss primarily depends on surface temperature and an output of the weather component called "effective sky temperature." This is calculated by TRNSYS and depends on humidity and cloud-cover. At a given ambient temperature, a collector tends to lose more heat when

the humidity is low and the sky is clear. The magnitude of radiative heat transfer is governed by the equation (Duffie & Beckman, 2006, p. 149):

$$h_r = \frac{\sigma(T_2^2 + T_1^2)(T_2 + T_1)}{\frac{1-\varepsilon}{\varepsilon_1} + \frac{1}{F_{12}} + \frac{(1-\varepsilon_2)A_1}{\varepsilon_2 A_2}}$$

In which:

σ = Stefan-Bolzmann constant (5.670373 x 10^{-8} $W/(m\text{^}2\ K)$)

T_1 = Surface 1 temperature in Kelvin

T_2 = Surface 2 temperature in Kelvin

ε_1 = Surface 1 emissivity

ε_2 = Surface 2 emissivity

A_1 = Surface 1 area in m^2

A_2 = Surface 2 area in m^2

F_{12} = View factor from Surface 1 to Surface 2

The selected collector components used to model cooling performance utilize sky temperature as an input and allow the emissivity of the absorber plate to be specified.

Convective heat loss depends on the temperature of ambient air and wind speed – both outputs of the weather component. However, wind speed varies based on the landscape and there are different mathematical models describing how much heat a surface loses in response to a given wind speed. According to Duffie and Beckman (2006, pg. 166) the convective heat loss coefficient for collectors mounted flush to the roof is:

$$h_w = \max\left[5, \frac{8.6V^{0.6}}{L^{0.4}}\right],$$

where V is the wind velocity, L is the cube root of the house volume in meters, and "max" indicates that a value of 5 W/(m^2.K) should be used if the calculated convection is less than this. Convective losses are calculated directly by some collector component types in TRNSYS but expressed as part of an overall heat loss coefficient in others.

TRNSYS Modeling

Unglazed collector.

Because both sky temperature (T_s) and wind speed (V) factor into the losses of an unglazed collector, the component model must utilize both of these inputs. There are multiple choices of unglazed collectors available between the standard TRNSYS component library and the proprietary components provided by Thermal Energy System Specialists (TESS). These include Type 553: "Unglazed Flat Plate Collector with Capacitance and Flow Modulation", Type 559: "Theoretical Unglazed Collector" (TESS, 2009) and Type 72: "Solar Collector, Performance Map" (Solar Energy Laboratory, 2009a).

Type 559 models the performance of a collector based on theoretical equations of heat gain and heat loss. In addition to the usual inputs of ambient temperature and incident solar radiation, it utilizes sky temperature and wind velocity in the calculation of its output. However, these are used in the calculation of the heat transfer coefficient, U_L, which is ultimately substituted into the Hottel-Whillier equation (TESS, 2009, p. 108):

$$Q_u = AI_tF_R(\tau\alpha)_n - AF_RU_L(T_i - T_a)$$

Where:

Q_u = Useful heat gain

I_t = Irradiation on tilted surface

F_R = Collector heat removal factor

A = Collector gross area

T_i = Inlet temperature

T_a = Ambient temperature

The Hottel-Whillier equation, referencing ambient temperature but not sky temperature, will yield a Q_u that approaches zero as irradiance becomes zero and the inlet temperature approaches ambient temperature. Therefore, it is not possible for the collector to cool a fluid below ambient temperature under night sky conditions according to this model, limiting its usefulness for modelling

night-sky radiative cooling. Moreover, varying the parameter of effective sky temperature while holding all others constant shows that the plate responds oppositely to what would be expected in a physical collector: as sky temperature increases in the model, plate temperature decreases. This error is documented in Appendix B and was discussed with the distributor for correction.

Type 553 models an unglazed collector according to a differential equation equating the rate of energy change in the collector to the difference between the rate of absorbed irradiance (minus losses) and the rate at which heat is carried away by the fluid (TESS, 2009, p. 89):

$$C\frac{dT}{dt} = A * F' * \left(S - U_L(T - T_a)\right) - \dot{m} * C_p(T - T_{in}),\ in\ which$$

$$S = IAM_b * I_{bt} + IAM_{ds} * I_{dsT} + IAM_{dg} * I_{dgT} - IAM_{ds} * \sigma\left(T_a^4 - T_{sky}^4\right) * \varepsilon/\alpha$$

In the equation for absorbed irradiance, S, the IAM terms represent incident angle modifiers for beam and diffuse radiation from the ground and sky. The complete mathematical model is long and complex, but a key feature of the model is the ability of the collector to drop below ambient temperature via longwave radiation to the sky. However, it does not directly utilize wind speed. Fortunately, the wind speed can be simulated by dynamically changing the efficiency curve of the collector, which is classified as an input of the component rather than a parameter. Type 553 therefore satisfies the critical requirements for modeling night sky radiative cooling and was selected for the simulation. The TRNSYS component model is shown in Figure 15.

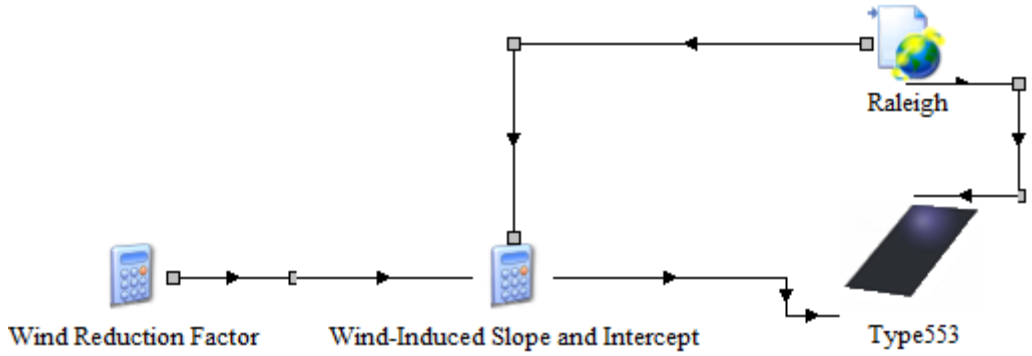

Figure 15. Modeling wind effects on Type 553 collector.

Glazed collector.

The TRNSYS component that utilizes the SRCC performance curve for a glazed collector does not account for wind speed. Although glazed collectors are not typically used for cooling, it was desired to investigate their performance in this mode in order to make a fair comparison to unglazed collectors. The Type 942 component is able to simulate the effect of these important variables on the collector, but it does not directly utilize the SRCC performance curve. This is circumvented by calibrating the Type 942 component to the Type 539 component, which directly utilizes the tested Rheem RS40-BP performance curve.

The Type 942 insulation thickness, plate absorptance and emissivity, and cover emissivity were varied until the outlet temperatures resembled the Type 539 outlet temperatures as closely as possible in the climate of Raleigh. For the purpose of calibration, the sky temperature was equated to the dry bulb temperature and the wind temperature was set to a constant 2 m/s. The outlet temperatures were the result of running a constant stream of 50 °C water at a rate of 0.02 kg/s.m^2 through the collector. Although the Rheem RS40-BP is classified as a nonselective collector, it was necessary to give the absorber plate slightly selective properties (with an absorptance of 0.94 and emissivity of 0.75) in order to closely emulate its performance. A comparison between the two models in winter and summer months are shown in Figure 16 and Figure 17, respectively.

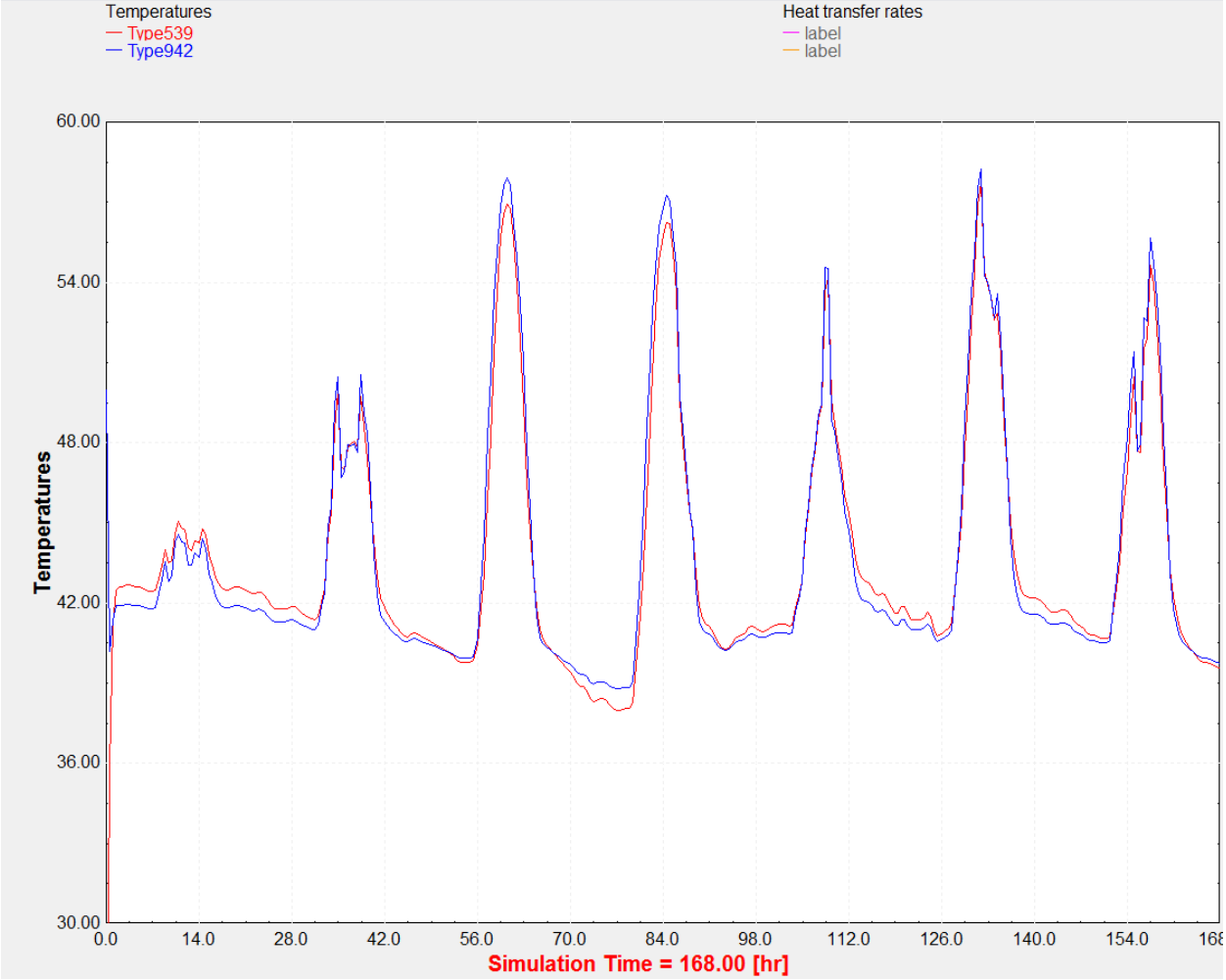

Figure 16. TRNSYS plotting tool showing comparison between Type 942 and Type 539 outlet temperatures in winter.

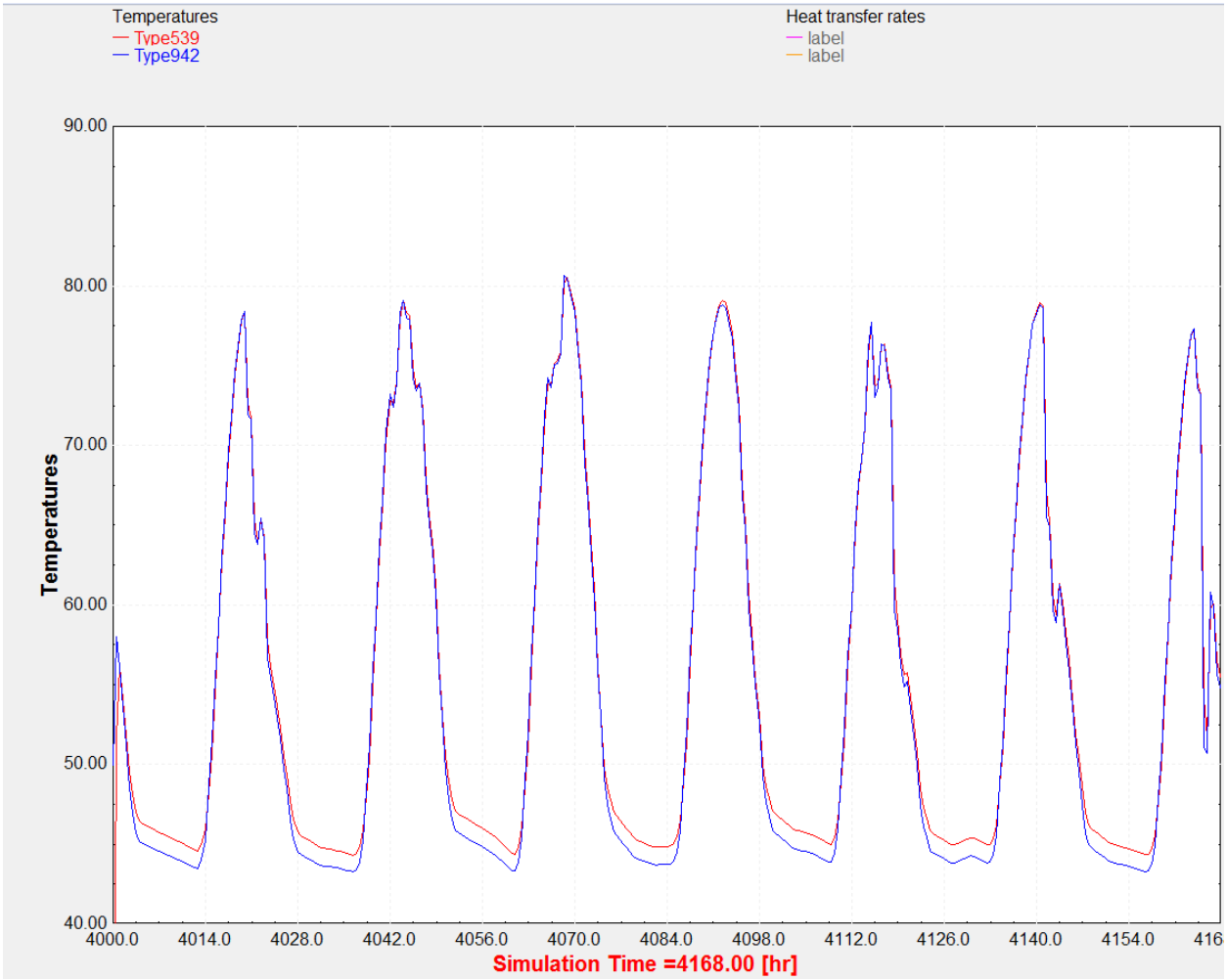

Figure 17. TRNSYS plotting tool showing comparison between Type 942 and Type 539 outlet temperatures in summer.

The Type 539 collector was used for heating simulations because it is the most direct replication of the SRCC performance curve; however, cooling simulations are based off of this calibration.

Wind Sensitivity

Wind effects are a great source of uncertainty in making an accurate comparison between glazed and unglazed collector performance. The first source of uncertainty is the difficulty of predicting the magnitude of wind at a site from TMY weather data. The second issue is that there are different models of how a collector will respond to wind. Although a convection coefficient may

describe the behavior of a collector at a test site very well, it may not work as well at the site of installation because of different mounting methods, wind directions, or turbulence levels. Duffie and Beckman (2006) argue that the size of a house on which a collector is mounted also affects the rate of convective heat loss.

Because the absorber plate of an unglazed collector is directly exposed to ambient air, convection is especially important in unglazed collectors. Convection can be modeled implicitly in the Type 553 component using the wind term, *u*, within the SRCC performance curve:

$$\eta = (0.941)(1 - 0.0412u) - (11.6348 + 5.0697u) * \frac{(T_i - T_a)}{G}.$$

Figure 18 shows the magnitude of the wind's effect on efficiency and Figure 19 shows the effect of natural wind conditions on unglazed collector outlet temperature in comparison to a collector exposed to no wind. The collector model in Figure 19 was simulated under no-flow conditions in order to see the maximum effect of wind. Wind is strongly counterproductive in heating conditions and also has a very slight adverse effect under cooling conditions (as indicated by the lower peaks and slightly higher troughs of the unglazed collector in the "Wind" condition).

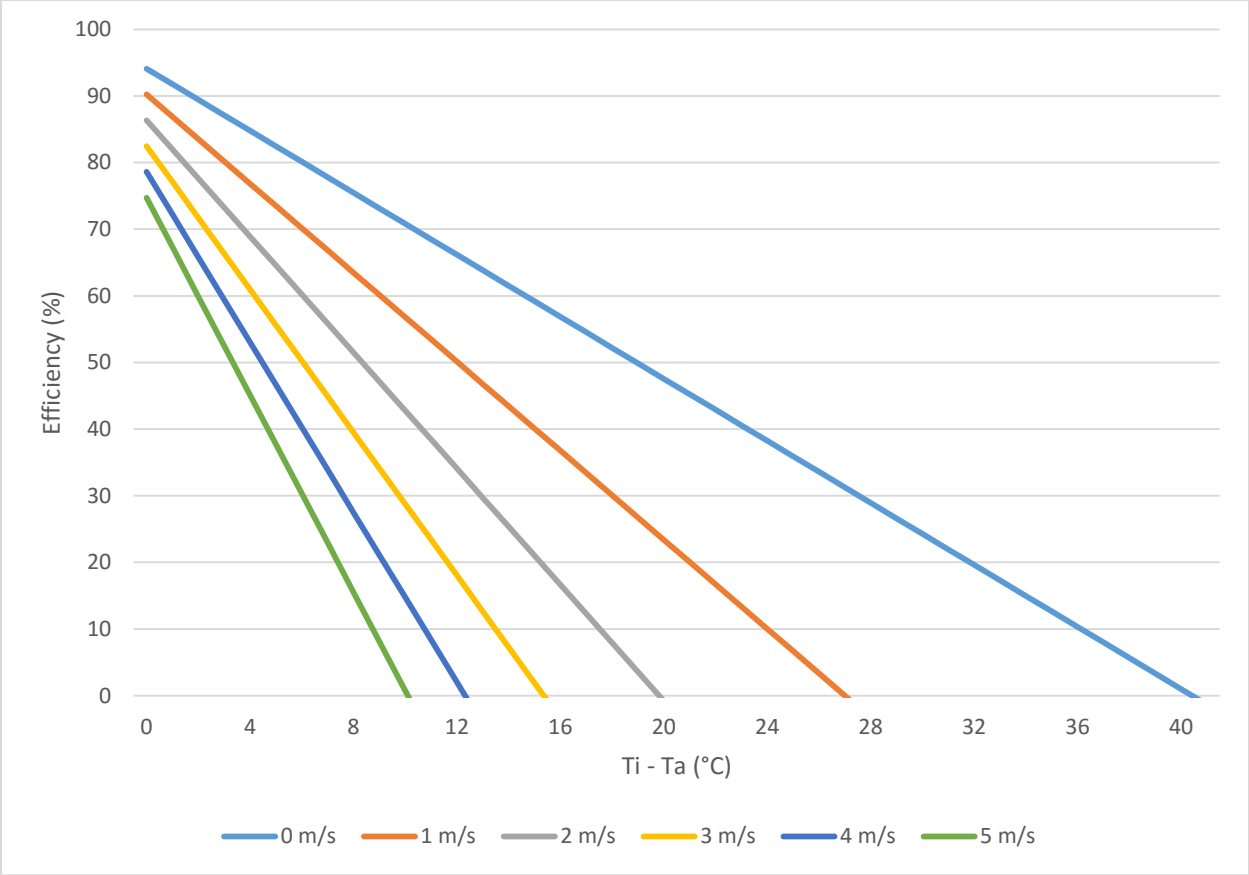

Figure 18. Unglazed collector efficiency versus T_i - T_a at irradiance of G = 500 W/m^2 for various wind speeds.

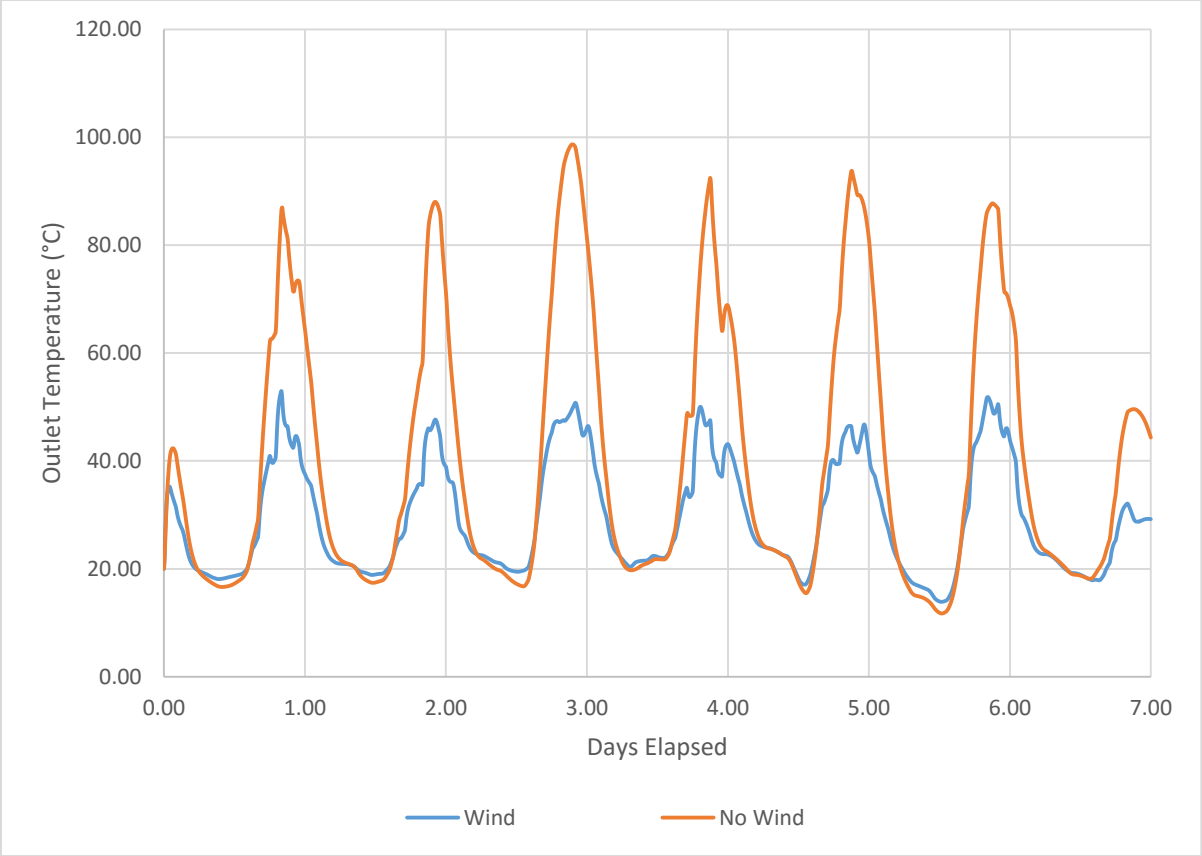

Figure 19. Unglazed collector outlet temperatures during summer in Raleigh in response to TMY2 wind speeds and windless conditions.

In contrast to the unglazed collector, the glazed collector proved to be insensitive to wind. The ISO equation for glazed collectors contains no wind term and ISO 9806 (International Organization for Standardization [ISO], 2013) only requires that they be tested at speeds between 2 m/s and 4 m/s. The wind sensitivity for glazed collectors was investigated by using a TESS Type942 component by alternating wind speed input between 0 m/s and 5 m/s at various inlet temperatures to derive the overall sensitivity of the collector to wind, as seen in Figure 20. The performance results shown in Figure 20 are for the Heliodyne Gobi Model 410 002, which has similar performance to the Rheem model. The Rheem was chosen later in the analysis for its non-selective absorber surface and thus superior cooling performance, making it a better choice for comparison to the unglazed collector.

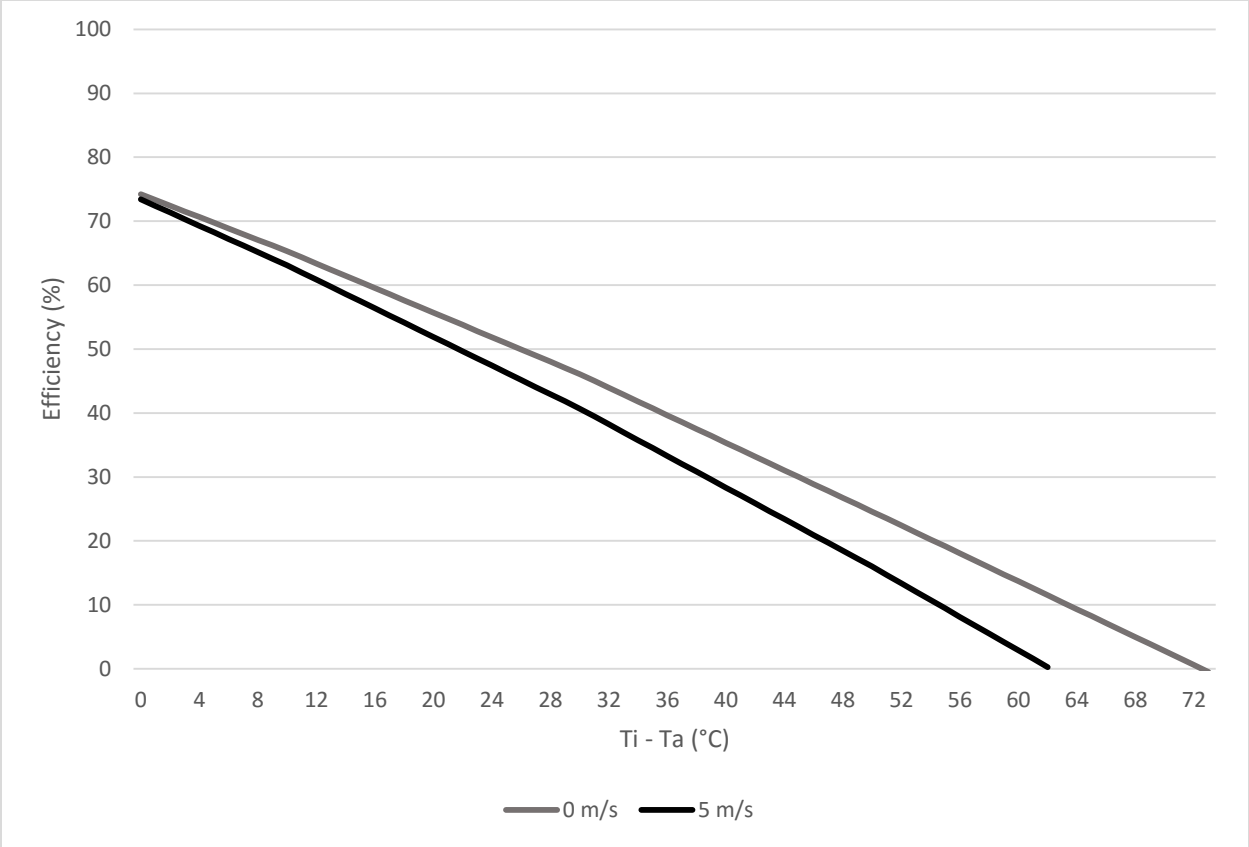

Figure 20. Glazed collector efficiency versus $T_i - T_a$ at irradiance of G = 500 W/m^2 for wind speeds of 0 m/s and 5 m/s.

Convective Heat Transfer Coefficients

There are several mathematical models that correlate wind speed with the convective heat losses from solar thermal collectors, often producing very different results. This created some uncertainty in verifying the accuracy of the unglazed collector model. The International Energy Agency (1993) provided an overview of convection coefficients used in unglazed collectors, referencing a study by Perers (1987) that compared four different models of convection against experimental measurements he performed on unglazed collectors. One convection model that seemed to fit the data well had the equation:

$$h_{c,p-a} = 5.7 + 3.8u$$

However, Duffie and Beckman (2006) reported that this coefficient likely includes free convection and radiation effects, and therefore suggested using a corrected form of the equation developed by Watmuff:

$$h_c = 2.8 + 3.0u$$

Duffie and Beckman (2006) suggested that the best model of convection losses for collectors mounted flush to a roof came from the experimental results of Mitchell, who tested heat transfer effects on differently shaped objects in a wind tunnel. The suggested equation is:

$$h_w = \max[5, \frac{8.6V^{0.6}}{L^{0.4}}]$$

The TRNSYS model of the unglazed collector predicts its performance based primarily on its ISO efficiency equation derived from experimental results, rather than on theoretical loss coefficients. This produces greater confidence in the model, but can also be a source of error if the collector mounting does not resemble mounting on a residential roof.

In order to decide on the best convection coefficient, theoretical heat gains under various convection coefficients were compared to the ISO curve-fit for the Fafco Sungrabber. The curve-fit adopted by Burch et al. (2004) in their analysis of unglazed collectors was also modeled for comparison. The results shown in in Figure 21 are based on calculations that considered absorbed irradiance ($Q_{absorbed}$), long-wave radiation losses to the sky (Q_{rad}), and convection losses (Q_{conv}):

$$Q_{absorbed} = S - Q_{rad} - Q_{conv}$$

$$S = \alpha G$$

$$Q_{rad} = h_{rad}(T_{plate} - T_{sky})$$

$$Q_{conv} = h_{conv}(T_{plate} - T_{air})$$

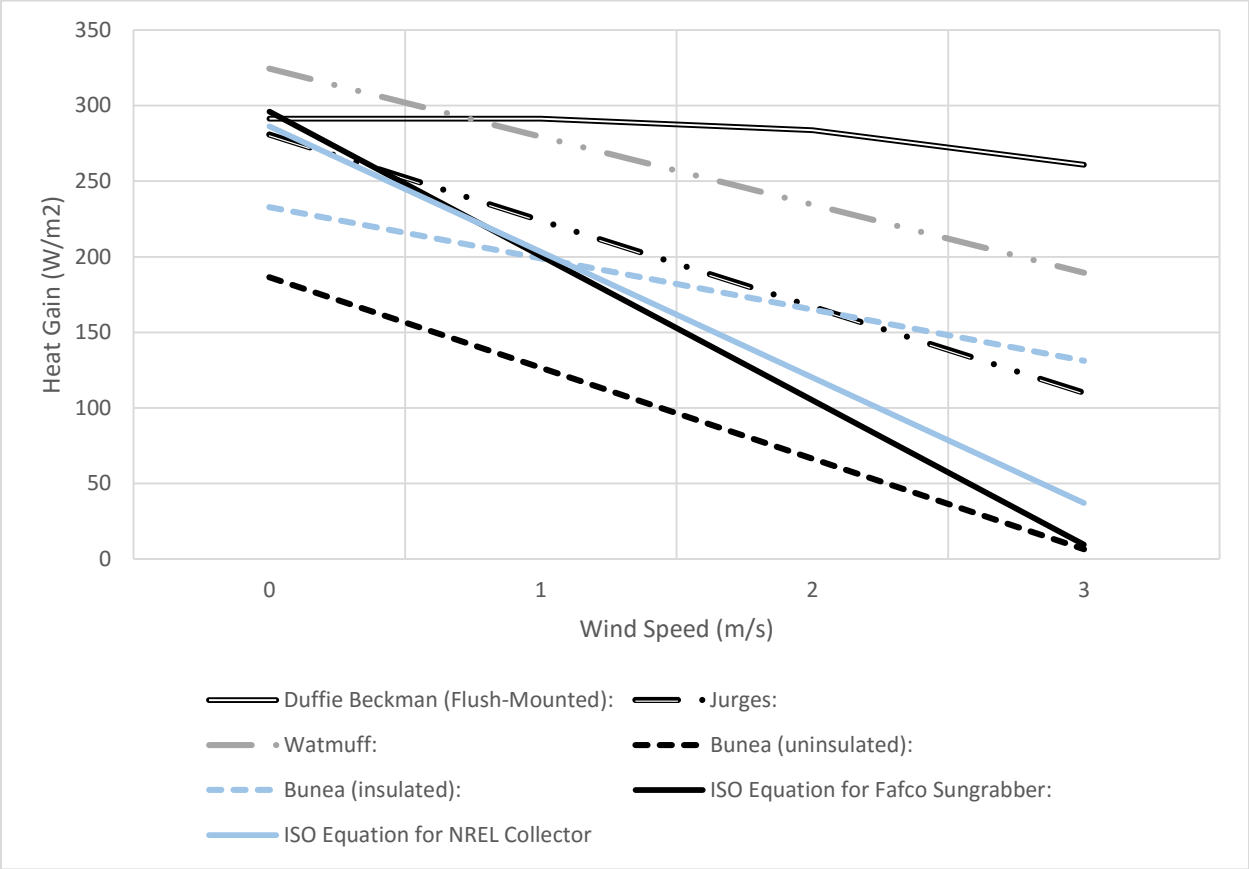

Figure 21. ISO-equation predicted performance and theoretical performance of unglazed collectors at an irradiance of G = 500 W/m2 and Ti – Ta = 15 °C for various convection coefficients.

Although long-wave radiation and conduction to other objects are ignored, Figure 21 demonstrates that many models diverge from the ISO performance curve as wind speed changes, showing the criticality of convection. The free convection predicted by the Jurges coefficient (International Energy Agency, 1993) and by Duffie and Beckman (2006) agree with the ISO performance curve under windless conditions but diverge significantly from the ISO curve at higher wind speeds. None of the theoretical models seem to adequately track the performance curve described by the ISO equation for the Fafco Sungrabber.

These results forced a decision between using a performance curve generated from test results and modeling performance based on the theoretical mechanisms of heat exchange. Based on its description, the Duffie Beckman convection coefficient for a roof-mounted collector would be the

most fitting theoretical model for this application. However, it is also most sharply at odds with the heat loss that can be inferred from the SRCC performance curve. A possible compromise between these results would be to use the SRCC performance curve in conjunction with a larger wind reduction factor to correct for lower convective losses. However, choosing uncertain estimates for the unglazed collector parameters would make it more difficult to understand the causes of differences in performance between the collectors. A decision was made to use the SRCC performance curve to describe wind effects on the unglazed collector so that the model is anchored to physical measurements, and it can at least be understood that it may likely underestimate the efficiency.

Wind Reduction Factor

Burch et al. (2004) noted that the wind in residential areas is often much lower than measurements at airports, which often form the basis for TMY files. They applied a wind reduction factor of 0.3 to correct for this. The *User's Manual for TMY2s, Typical Meteorological Years* (Marion & Urban, 1995) provided the latitude and longitude of the sampling stations where the weather data was collected. The statement of Burch et al. (2004) was verified by viewing each set of coordinates on Google Maps: the Albuquerque station is at N36 3, W106 37, beside the Albuquerque International Sunport airport. The Raleigh station is at N35 52, W 78 47, beside the Raleigh-Durham International Airport. And the Jacksonville station is at N30 30, W 81 42, beside the Jacksonville International Airport.

Heisler (1990) measured the wind speed upwind of 15 residential buildings in four neighborhoods with differing tree densities to compare them to wind speeds measured at the closest airport. The measurements were obtained over the course of 14 days divided between summer and winter. Even in a neighborhood without trees, there was a 24% reduction in mean wind speed, while a neighborhood with a high density showed a reduction of 65% to 70% in winter and summer, respectively.

A middle-ground wind reduction factor of 0.5 was used in the simulations to describe the velocity in a residential neighborhood with average tree density. For the purpose of verifying cooling

performance of glazed and unglazed collectors, which are not described by any existing performance curves, the Jurges coefficient was used, understanding that there may be some error.

Collector Verification

Solar collectors are traditionally used for heating, and their performance is relatively well established through test results. The performance when used for cooling is less easily verified; therefore, theoretical cooling rates of glazed and unglazed collectors were calculated to assess the validity of the simulation's cooling response. The rate of heat loss from the absorber plate in a TRNSYS simulation was compared to theoretical calculations. Both the TRNSYS model and the theoretical calculations assumed the collector is in steady-state conditions.

The calculations for each of the two types were done at equal absorber plate temperatures at equal ambient conditions. In order to simplify the verification for the glazed collector, only the rate of heat transfer from the collector aperture was calculated while heat loss from the collector back and sides were minimized in the TRNSYS simulation by specifying insulation with an extremely low U-Value. The following parameters were assumed:

Ambient Conditions

Air Temperature: 20 °C (≈293 K)

Sky Temperature: 10 °C (≈283 K)

Wind Speed: 1 m/s

Irradiance: 0 W/m^2

Collector Conditions

Absorber Plate Temperature: 25 °C (≈298 K)

Absorber Plate Emissivity: 0.95

Plate to Glazing Spacing: 0.025 m (*glazed only*)

Glazing Emissivity: 0.88 (*glazed only*)

Glazing Transmissivity: 0.865 (*glazed only*)

Collector Tilt: 0°

Glazed collector.

The equations for convective and radiative heat loss from a collector assume that the temperature of the top surface is known; for a glazed collector, this is the cover temperature. I wanted to compare the cooling power of a glazed collector with an unglazed collector at an equal plate temperature, so the cover temperature had to be deduced based on the plate temperature and ambient conditions. This was an iterative process guided by the following steps:

1) An initial cover temperature was guessed.
2) Heat transfer coefficients were calculated based on this cover temperature.
3) An energy balance on the cover was performed using these heat transfer coefficients.
4) The cover temperature was adjusted and the process was repeated until the net energy flux across the cover was zero (indicating that the process is in steady-state).

The convective heat transfer coefficient between the absorber plate and cover was guided by an equation described by Duffie and Beckman (2006):

$$h_c = Nu * k/L$$

However, the Nusselt number is not directly known and the calculation ultimately ended up depending on the following variables:

$Nu =$ Nusselt Number (ratio of conduction resistance to convection resistance)

$Ra =$ Rayleigh Number (also indicates importance of conduction vs. convection)

$g =$ gravitational constant

$T =$ temperature of air within collector

$k =$ thermal conductivity of air

$\alpha =$ thermal diffusivity of air

$k =$ thermal conductivity of air

$k =$ thermal conductivity of air

ß′ = volumetric expansion coefficient of air $= 1/\mathrm{T}$

ß = angle of collector tilt

$$Nu = 1 + 1.44\left[1 - \frac{1708 * (\sin 1.8ß)^{1.6}}{Ra * \cos ß}\right] * \left[1 - \frac{1708}{Ra * \cos ß}\right]^{+} + \left[\left(\frac{Ra * \cos ß}{5830}\right)^{\frac{1}{3}} - 1\right]^{+}$$

$$Ra = \frac{g * ß' * \Delta T * L^3}{\nu * \alpha}$$

The properties of air had to first be estimated at 20 °C:

k = 0.0257 W/m.K (conductivity)

$\nu = 1.51 * 10^{-5}$ m^2/s (kinematic viscosity)

$\alpha = 2.12 * 10^{-5}$ m^2/s (thermal diffusivity)

The heat balance equation was then solved to arrive at the cover temperature:

$$h_{p-c,rad} * A(T_p - T_c) + h_{p-c,conv} * A(T_p - T_c) = h_{c-s,rad} * A(T_c - T_s) + h_{c-a,conv} * A(T_c - T_a)$$

The subscripts *p*, *c*, *s*, and *a* represent absorber plate, cover, sky, and ambient air, respectively. The subscripts *conv* and *rad* represent convective and radiative modes of heat transfer, respectively. For example, $h_{p-c,rad}$ represents the radiative heat transfer coefficient from absorber plate to cover.

Substituting the known values into the Nusselt and Rayleigh number equations provided the heat transfer coefficients, allowing the cover temperature to be solved for a value of T_c = 19.36 °C (performed iteratively with Excel). This implied a mean air space temperature of $(T_p + T_c) / 2$ = 22.18 °C, which was close enough to the original estimate such that its properties (such as conductivity) will change only minimally with subsequent iterations. The heat transfer out of the cover was finally calculated from the right side of the heat balance equation to get the cooling power of a glazed collector: 40.26 W/m^2. Thus, its cooling power was found to be only about 31.8% of the unglazed collector's capacity at the assumed conditions. This percentage could vary with different ambient or collector conditions.

Unglazed collector.

The rate of heat transfer from the unglazed collector is the sum of radiative and convective heat transfer. The radiative heat transfer coefficient was found by substituting the stated values into the previously defined equation:

$$h_r = 0.95 * 5.670373 \text{ x } 10^{-8} \frac{W}{m^2 K^4} * ((283\ K)^2) + (298\ K)^2)(283\ K + 298\ K)$$

$$= 5.286\ W/m^2 K.$$

The convective heat transfer coefficient was found by substituting wind speed (V) and characteristic length (L) into $h_w = 5.7 + 3.8u = 9.5 \frac{W}{m^2 K}$. Each of these heat transfer coefficients then determined actual heat flux:

$$Q_r = 5.286 \frac{W}{m^2 K} * (298\ K - 283\ K) = 79.28\ W/m^2$$

$$Q_w = 9.5 \frac{W}{m^2 K} * (298\ K - 293\ K) = 47.5\ W/m^2$$

Thus, the total rate of cooling for an unglazed collector under the stated conditions was $Q_r + Q_w$ = 126.78 W/m^2.

Cooling performance verification.

The parameters in the above analysis were replicated in TRNSYS component Type 942 (representing a glazed collector) and component Type 553 (representing an unglazed collector). Edge losses and back losses for the glazed collector were minimized by using thick (1 m) insulation with minimal conductivity. The Type 553 component, however, does not consider back and edge losses of the unglazed collector separately from overall collector losses. The plate temperatures of the theoretical cases could not be replicated exactly, but were achieved within 0.3 °C within the Type 942 components representing glazed collectors. The Type 553 components do not report plate temperatures but were inferred to be close based on the fluid outlet temperatures. The results of the verification process are shown in Table 19.

Table 19. *Verification of Cooling Performance for Glazed and Unglazed Collectors*

Method of Calculation	Cooling Power at 1 m/s wind (W/m^2)	Cooling Power at 3 m/s wind (W/m^2)
Glazed Collector		
Theoretical	40.26	39.26
Simulated	40.39	39.46
% Difference	-0.32%	-0.51%
Unglazed Collector		
Theoretical	126.78	164.78
Simulated	136.57	183.19
% Difference	-7.72%	-11.8%

Glazed collector cooling adjustment.

When the glazed collector inlet temperature was above ambient temperature, the model seemed to closely match theoretical calculations. However, once the collector reached ambient temperature, the Type 942 model did not allow the collector to cool further by radiating heat to the sky.

A correlation analysis was performed to model cooling performance at sub-ambient temperatures. A series of 27 side-by-side simulations were performed for the glazed collector and unglazed collector under a variety of combinations of air temperature, inlet temperature, sky temperature, and wind speed. Overall, in the above-ambient temperature range, the glazed collector cooling power ranged from 15.5% to 34.2% of the unglazed collector's cooling power. The ratio was most sensitive to wind speed.

A regression line was fit to the relationship between wind speed and the cooling power ratio to create an alternative means of calculating the glazed cooling power. Each point in Figure 22 is an average value for multiple simulations.

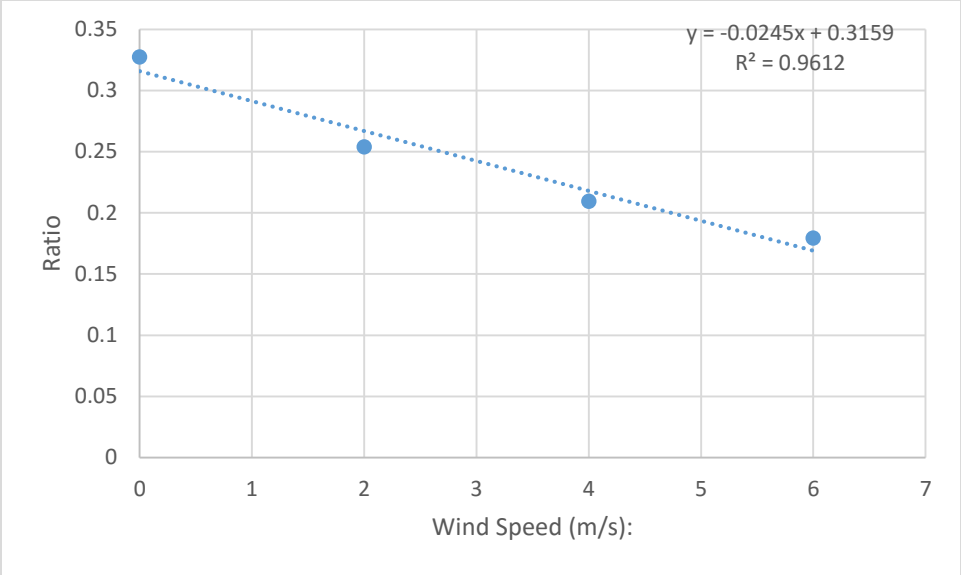

Figure 22. Ratio of glazed collector cooling power to unglazed collector cooling power as a function of wind speed.

The glazed collector was emulated by scaling the slope and intercept of the ISO efficiency equation for the unglazed collector according to the formula for the line of regression. The bold terms in the equations below show the adjustments to the ISO equation, in which *u* is wind speed and RF is the wind reduction factor equal to 0.5.

$$Slope = (\mathbf{0.3159 - 0.0245u}) * 3.6 * (11.6348 + 5.0697u * RF)$$

$$Intercept = (\mathbf{0.3159 - 0.0245u}) * (0.941 * (1 - 0.0412u * RF))$$

However, because it is possible for the slope and intercept to become negative at high wind speeds, causing TRNSYS to abort the simulation, the equations were run through a filter that returns a zero value if they are not positive.

Heating performance verification.

The parameters for the heating performance verification remained equal to those for the verification of cooling performance with the exceptions of ambient temperature, plate temperature, and solar irradiance. Plate temperature was increased to 30 °C and ambient temperature was dropped to 15 °C to be more representative of typical heating conditions. All solar irradiance was modeled as beam radiation at an intensity of 500 W/m^2.

The results of the verification process are shown in Table 20. The TRNSYS results for the glazed collectors were very close to theoretical values. The TRNSYS results for unglazed collectors, however, were markedly different than theoretical results. The problem was exacerbated at higher wind speeds. As previously discussed, this was likely because the measured performance curve did not fit the expectations of any discussed convection coefficients. This also describes why the difference would be greater in heating mode, when the plate temperature is further from air temperature.

Table 20. *Verification of Heating Performance for Glazed and Unglazed Collectors*

Method of Calculation	Heating Power at 1 m/s wind (W/m^2)	Heating Power at 3 m/s wind (W/m^2)
Glazed Collector		
Theoretical	348.22	339.7
Simulated	337.39	328.17
% Difference	3.1%	3.4%
Unglazed Collector		
Theoretical	223.98	109.98
Simulated	184.72	11.51
% Difference	17.5%	89.5%

Collector Absorptance Sensitivity

The absorber plate's emissivity and absorptance are implied when entering the slope and intercept of the Hottel-Whillier equation, $Q_u = AI_tF_R(\tau\alpha)_n - AF_RU_L(T_i - T_a)$, in which the intercept (i.e., the point of maximum efficiency) is defined by $F_R(\tau\alpha)_n$ and the slope is defined by F_RU_L. The loss factor U_L depends partly on the radiation loss coefficient, which is dependent on the emissivity (ε) of the absorber plate and/or cover. Therefore, both absorptance (α) and emissivity (ε) of the plate factor into the efficiency curve. However, the Type 553 model also requires explicit inputs for these parameters—not as part of the efficiency curve, but as completely separate parameters—so it had to be determined how this redundancy is processed by the model.

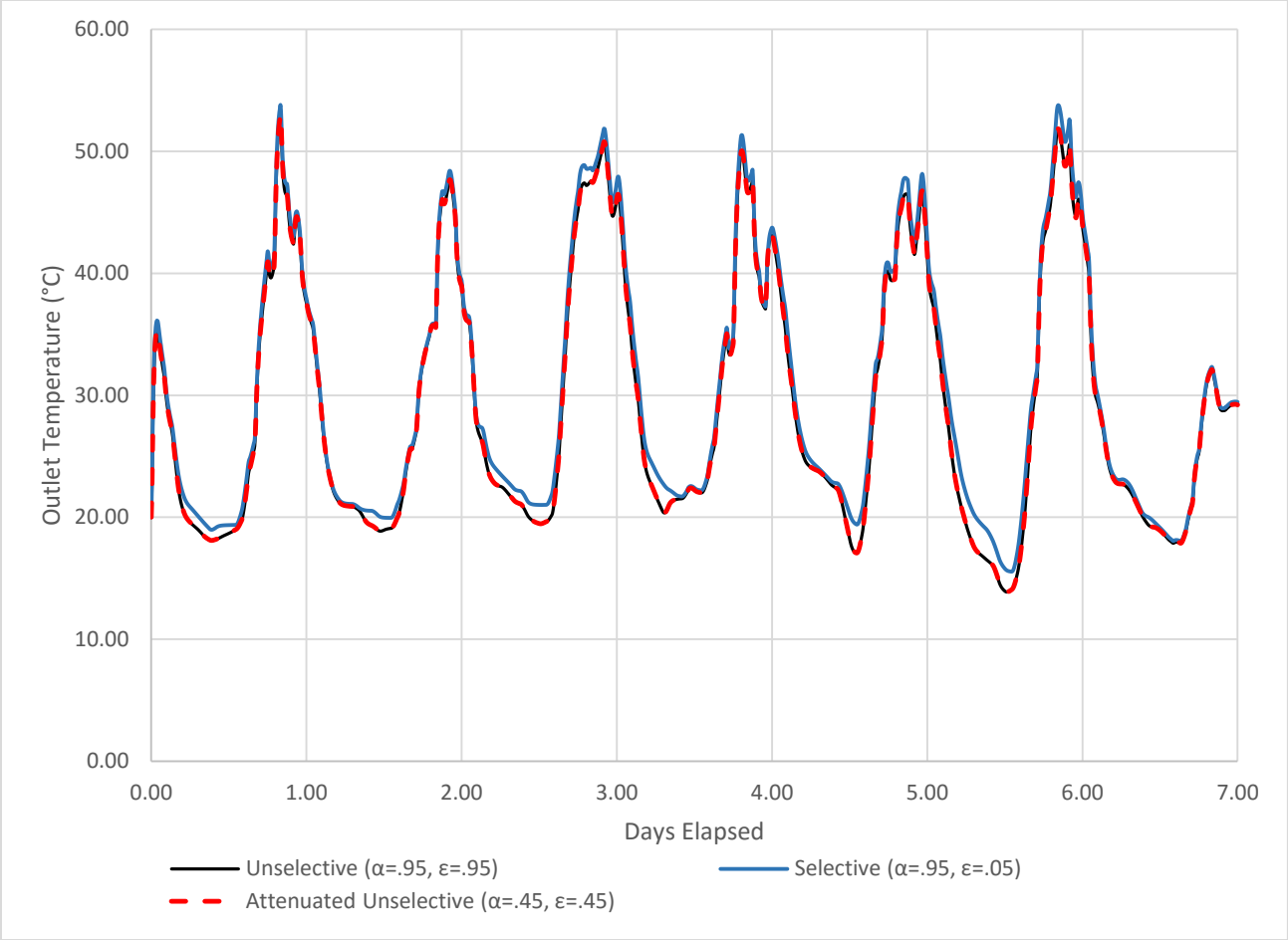

Figure 23. Type 553 unglazed collector sensitivity to absorptance and emissivity parameters.

Figure 23 shows that Type 553 was relatively insensitive to the parameters input for absorptance and emissivity; in fact, there was no change in collector temperature as long as a constant ratio of absorptance to emissivity was maintained. There was a minor increase in temperature overall when the emissivity was reduced to emulate a selective surface, but the performance was by far dominated by the slope and intercept of the efficiency curve. The actual emissivity and absorptance of the collector could not be obtained from the manufacturer and were therefore kept at values typical of an unselective surface with α=0.95 and ε=.095.

The Type 553 component has its limitations: For example, inspection of its equation shows that it is possible for the component to absorb irradiance even when absorptance is zero (if ε also equals zero), which would be physically impossible. However, the model may work well with typical

collector parameters. To test this hypothesis, Type 553 was compared against Type 559, which uses a theoretical model. At an arbitrarily chosen flow rate 250 kg/hr, the theoretical model was calibrated to match the performance of Type 553 by adjusting its heat loss coefficient. The outlet temperatures between the two models tracked each other very closely in the climate of Raleigh (seen in Figure 24), and it seems that the inability of Type 559 to model sub-ambient temperatures may not be very critical. However, in the climate of Albuquerque the difference was much more apparent. As shown in Figure 25, Type 553 got several degrees colder at night.

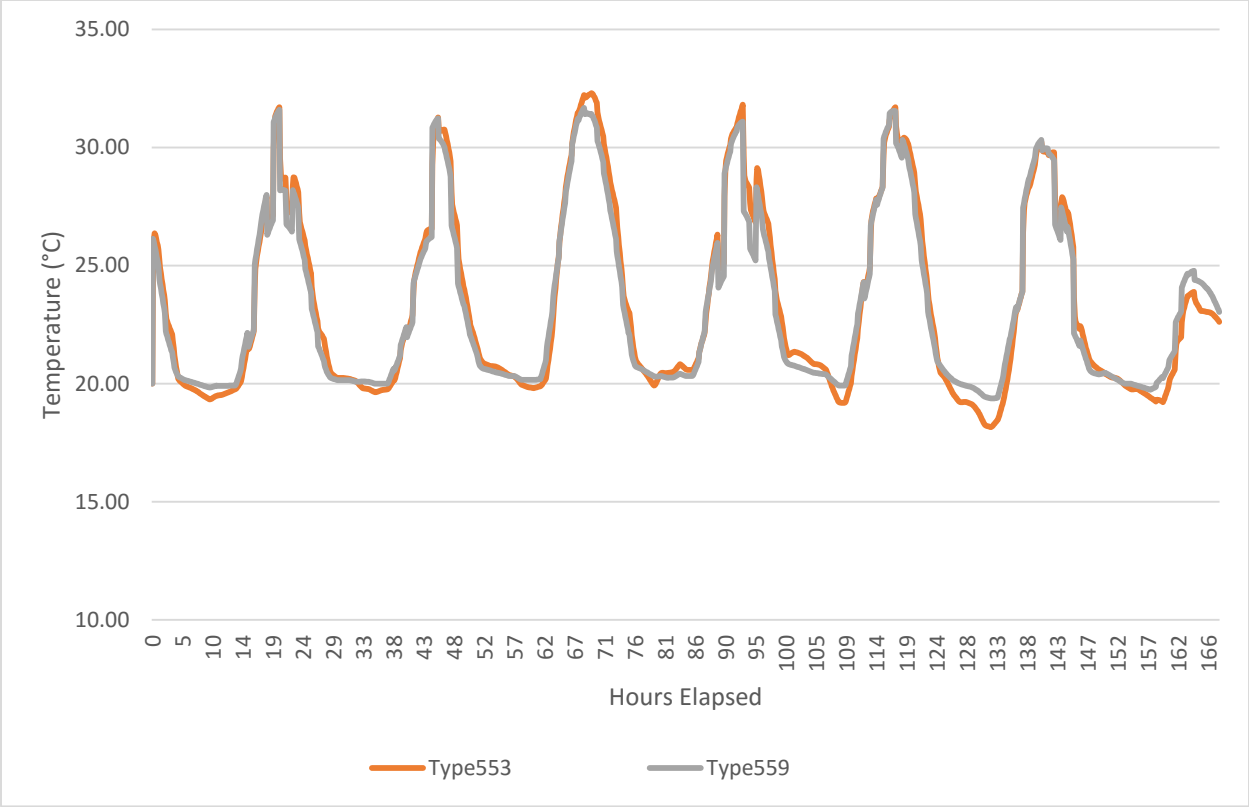

Figure 24. Type 559 and Type 553 performance during cooling season in Raleigh.

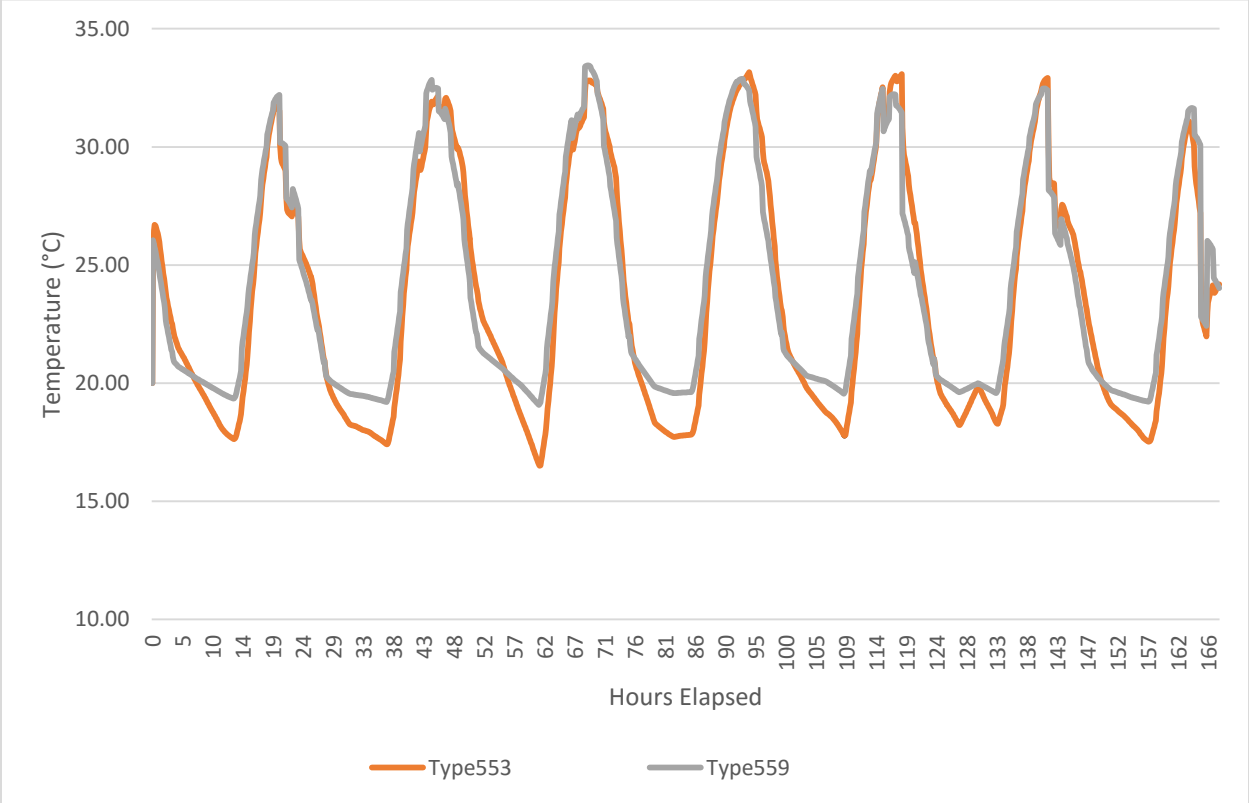

Figure 25. Type 559 and Type 553 performance during cooling season in Albuquerque.

Diffuse Radiation Sensitivity

According to ISO 9806 (ISO, 2013, p. 32), the performance of most collectors is better in response to beam radiation than diffuse radiation, and because there is "little experience with diffuse solar simulation," the test method is designed for a beam of radiation at nearly perpendicular incidence to the collector plane. Figure 26 shows that Raleigh and Jacksonville have very similar insolation profiles, but Albuquerque has a higher proportion of beam radiation.

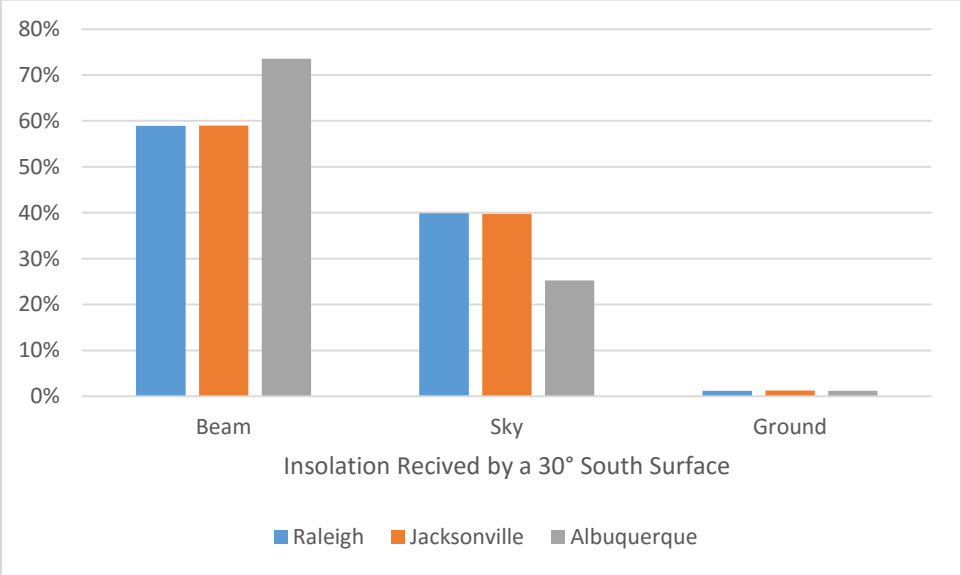

Figure 26. Percentage of insolation characterized as beam, diffuse sky, and ground-reflected radiation in each climate.

A sensitivity analysis was performed on the TRNSYS Type 559 glazed collector component and the Type 553 unglazed collector component. The fraction of beam radiation (in terms of total radiation) received by the collector aperture was varied between 100% and 70%. There was a reduction in collector heat gain of 4.5% and 5.3% for the glazed and unglazed collector, respectively. Although this may affect performance estimates for individual systems, the reduction in performance was similar enough between collector types that it did not significantly affect the comparison.

Freezing Potential

Both glazed collectors and unglazed collectors can be damaged by freezing conditions (Fafco Inc., 2009). The unglazed collector temperature was tested under stagnation conditions for the three

climates to determine the minimum temperature experienced annually and thus the amount of antifreeze required in the mixture. This temperature was obtained by connecting dry bulb temperature, effective sky temperature, and irradiance to the collector and simulating the outlet temperature over 12 months at a 0 kg/s flow rate. This was performed at windless conditions to obtain the worst-case scenario in terms of freezing.

There was not a great difference in minimum temperatures achieved between climates. Table 21 shows that Raleigh carries the greatest risk, followed in order by Albuquerque and Jacksonville. Based on manufacturing freezing-point data for propylene glycol (DowFrost), a 40% glycol to 60% water mixture, by weight, would be sufficient to prevent freezing down to -21.1 °C.

Table 21. *Minimum Ambient Temperature and Collector Temperature Experienced in Each Climate*

Type of Temperature	Raleigh	Jacksonville	Albuquerque
Ambient (°C)	-13.3	-7.2	-11.1
Unglazed Collector Outlet (°C)	-20.3	-15.1	-17.8

Sensitivity of Performance to Glycol

The Type 553, Type 539, and Type 942 components make adjustments to the collector efficiency based on the difference between the specific heat of the current fluid and the specific heat of the tested fluid. The certificate for each type of collector shows that it was tested with plain water. A sensitivity analysis was performed on both collectors at steady-state conditions of G_b = 700 W/m^2, $T_i - T_a$ = 10.7 °C between a glycol constitution of 0% and 40%. Table 22. shows that the resulting decrease in heat gain was negligible.

Table 22. *Sensitivity of Collector Performance to Fluid Type*

Collector Type	**Useful Energy using Plain Water (W/m^2)**	**Useful Energy Using 60% Water, 40% Glycol (W/m^2)**	**% Decrease**
Glazed	472.02	470.53	0.32%
Unglazed	410.95	408.99	0.48%

Boiling Potential

Frank, Mauthner, and Fischer (2015) described various problems that occur when water boils within a collector, including loss of the working fluid and damage to the collector and other components. A worst-case scenario was considered for each collector to assess the maximum fluid temperature at which it would continue to collect heat. Inspection of TMY3 files (used for their Excel-compatible format) for each region showed that these conditions could probably occur in Albuquerque, which achieves a high temperature of 36.95 °C (98.5 °F) in a typical meteorological year.

A quick inspection of the Rheem RS40-BP ISO equation made it obvious that boiling is a real risk for the glazed collector, but the risk of boiling in the unglazed collector needed closer inspection. A TRNSYS simulation of stagnation was performed with a flow of 0 kg/s through a Type 553 component in windless conditions. The maximum fluid temperature achieved in Albuquerque without wind was 107.2 °C. The maximum fluid temperatures occurring in Jacksonville and Raleigh in windless conditions were 102.7 °C and 99.4 °C, respectively. However, with the addition of wind (reduced by a factor of 0.5), the maximum annual temperatures became 81.0 °C, 87.4 °C, and 87.5 °C for Albuquerque, Jacksonville, and Raleigh, respectively. So, it seems that boiling is a very small risk for unglazed collectors.

Flow Rate Optimization

I originally intended to optimize the flow rate of the solar thermal system. However, there were various limitations to my ability to achieve this. The first issue is the different fluid capacities of the collectors; the unglazed collector holds much more fluid per unit area and therefore would require a naturally higher flow rate to achieve the same speed of fluid movement. A higher speed of fluid movement would imply a smaller temperature increase across the absorber plate and better efficiency, all other factors being equal. The collector certificates show that the unglazed collector holds 2.86 L/m^2 while the glazed collector only holds 1.26 L/m^2. Therefore the unglazed collector requires a higher flow rate.

The second issue with optimizing flow rate is an inability to determine the turbulence of the fluid. As discussed by Helvaci and Khan (2015), the heat transfer coefficient and efficiency of a collector depend on whether its flow is laminar or turbulent, with turbulent being more efficient. Turbulence is a direct function of the Reynold's Number, which depends on the diameter of the riser tubes. This information was not included in the SRCC certificate of the glazed or unglazed collector. Moreover, the TRNYS Type 553 component representing the unglazed collector does not utilize the parameters necessary to perform this calculation. Therefore, using values other than the rated flow rates may not accurately represent the collectors' efficiencies.

To test whether a crossover between laminar and turbulent flow might actually occur during optimization, a hypothetical example was investigated. A collector was assumed to have the following properties and conditions:

- Area: 3.8 m^2
- Number of Riser Tubes: 10
- Riser Tube Diameter (D): .01 m
- Fluid Dynamic Viscosity (μ): 0.000798 kg/m.s (water at 30 °C)
- Fluid Density (kg/m^3): 1,000 (liquid water)

It was determined that each tube in this example must have a fluid velocity of approximately 0.1 m/s to achieve the ASHRAE recommended flow rate of 0.02 $kg/s.m^2$. A Reynold's number of 1,253 was calculated from the formula below, indicating laminar flow. It is very conceivable that the fluid could transition into turbulence as flow rate is increased, or vice versa. Because it cannot be known where this transition actually occurs, the collectors were simulated only under the rated flow rates:

$$Re = \frac{\rho v D}{\mu} \quad [Laminar\ if < 2100, Turbulent\ if > 4000]$$

A sensitivity test was performed on two different sizes of unglazed collector arrays in Albuquerque to two different flow rates.

Figure 27 shows that the performance varied little. Another sensitivity test was performed on a 7.6 m^2 glazed collector in Albuquerque. Figure 28 shows that the performance varied significantly more, likely because the temperature increase across a glazed collector between inlet and outlet is much greater than for an unglazed collector, presenting a greater opportunity for heat loss. However, because of the issues discussed, there is a large amount of uncertainty in whether a similar degree of optimization can be equally applied to both collectors.

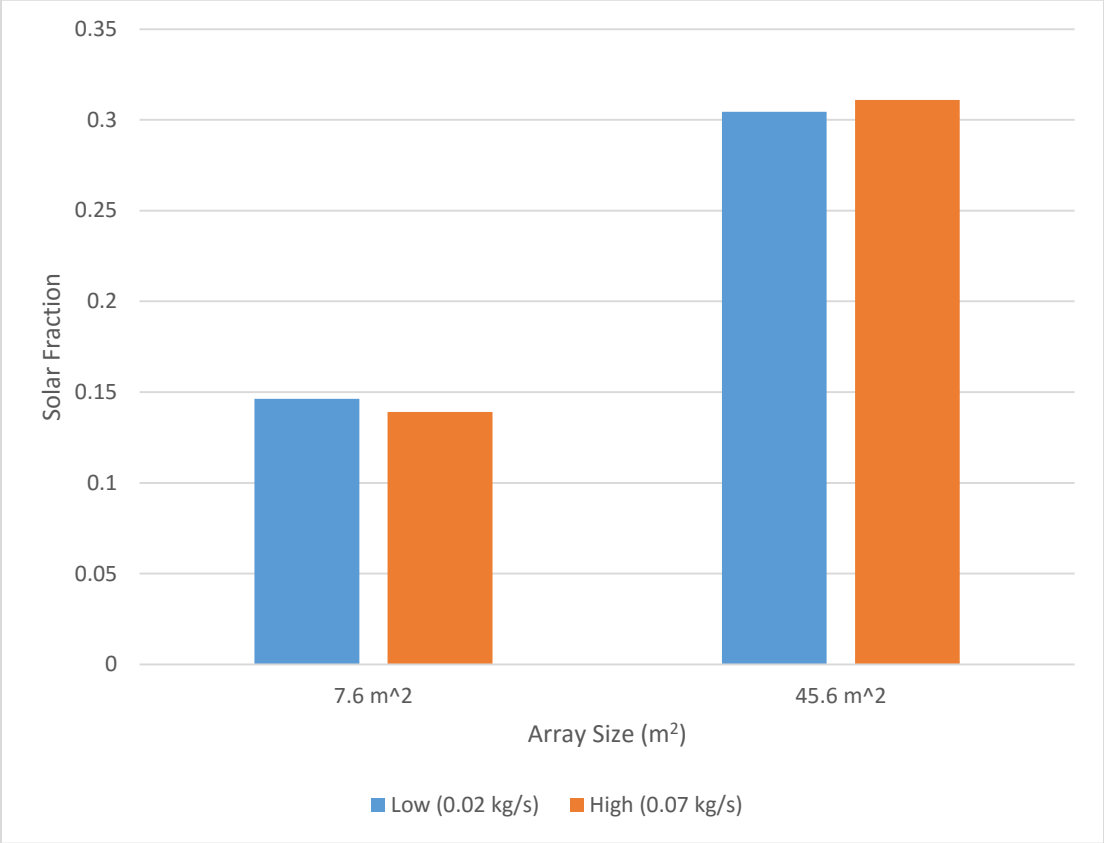

Figure 27. Solar fraction achieved by unglazed collectors at different flow rates.

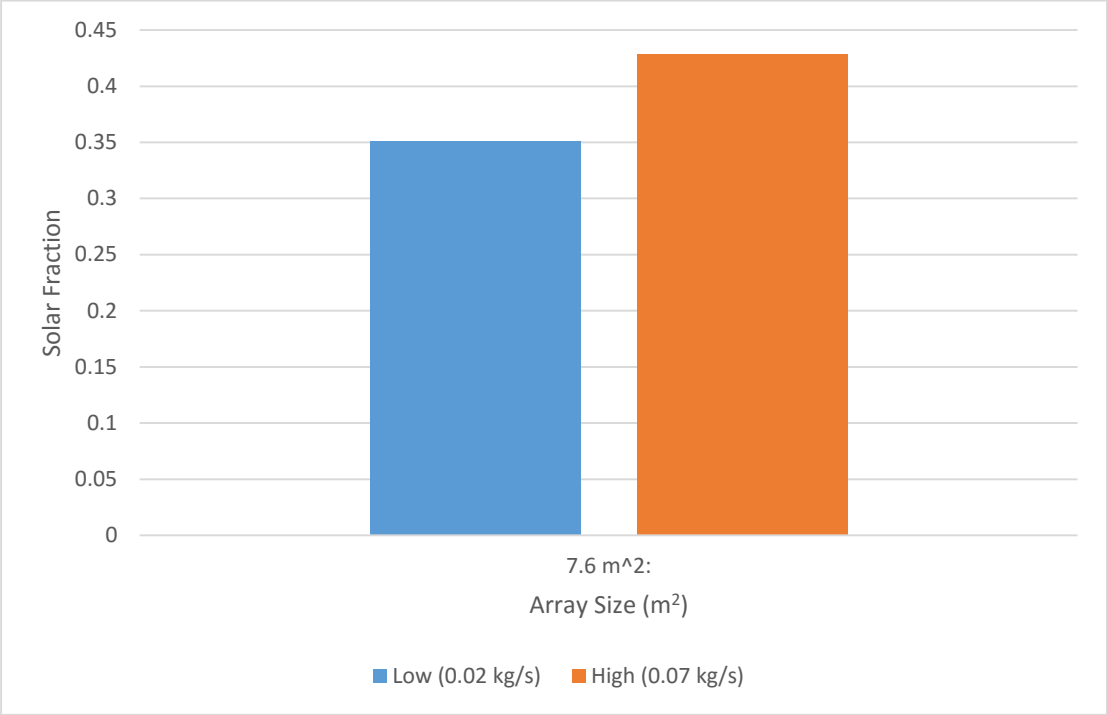

Figure 28. Solar fraction of glazed collectors at different flow rates.

Solar Loop Controls Optimization

The main controls consideration for the collector loop is the appropriate temperature differential for turning the pump on and off. The controller reads the difference between the temperature of the collector outlet and the tank heat exchanger outlet, and the temperature difference controls the pump state. The default setting for the Type 2b differential controller is a turn-on differential of 10 °C (required to turn the pump on) and a turn-off differential of 2 °C (required to turn the pump off). Analysis showed that any substantial turn-off differential above 0 °C is detrimental. Figure 29 shows the collector outlet temperature and the difference between collector and heat exchanger outlet under constant irradiance. The heat exchanger rapidly approaches the collector temperature. If there is even a 1 °C turn-off differential, the system begins to short cycle, signified by the rapidly fluctuating temperatures. If the turn-off differential is eliminated (i.e., set to 0 °C), the fluctuations disappear and the only variation is caused by hot water draw (Figure 30).

Figure 29. Controller performance using a turn-off differential of 1 °C between the collector outlet and tank heat exchanger outlet.

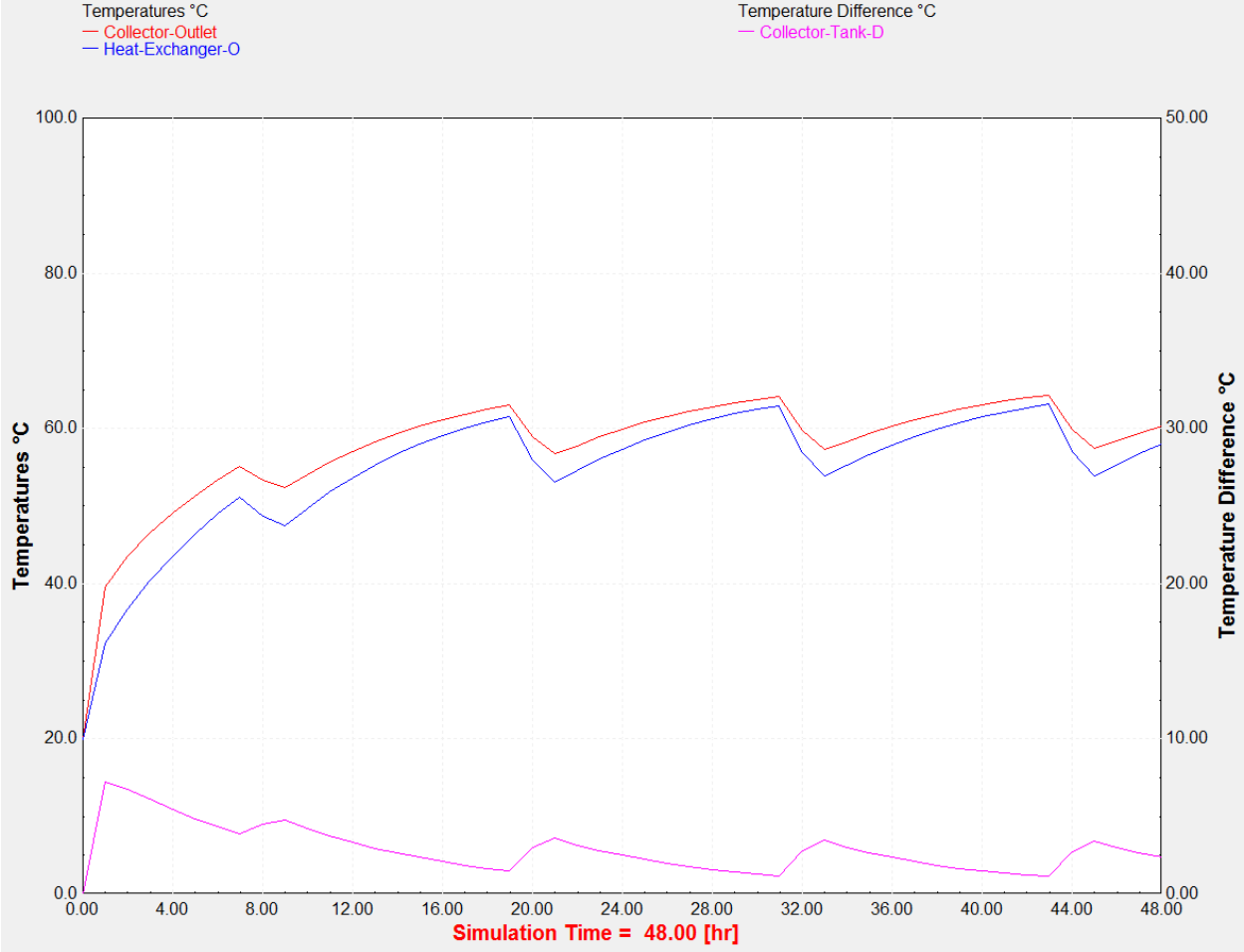

Figure 30. Controller performance using a turn-off differential of 0 °C between the collector outlet and tank heat exchanger outlet.

Chapter Five: Results and Conclusions

Climate Analysis

The collector heating performance depends on the ambient temperature, irradiance, wind speed, and to an extent, sky temperature. The most important variable to the performance of glazed collectors is probably irradiance, which Figure 31 shows that Albuquerque is clearly higher in. Unglazed collectors are more sensitive to daytime temperatures, especially in combination with higher wind speeds. Jacksonville may be slightly better for unglazed collector heating because of slightly higher ambient temperatures, as seen in Figure 32, and slightly lower wind speeds, as seen in Figure 33. The most notable difference in wind speed is that Jacksonville has a greater frequency of wind speeds below 2 m/s: a total of 15%, versus only 4% and 5% for Albuquerque and Raleigh, respectively.

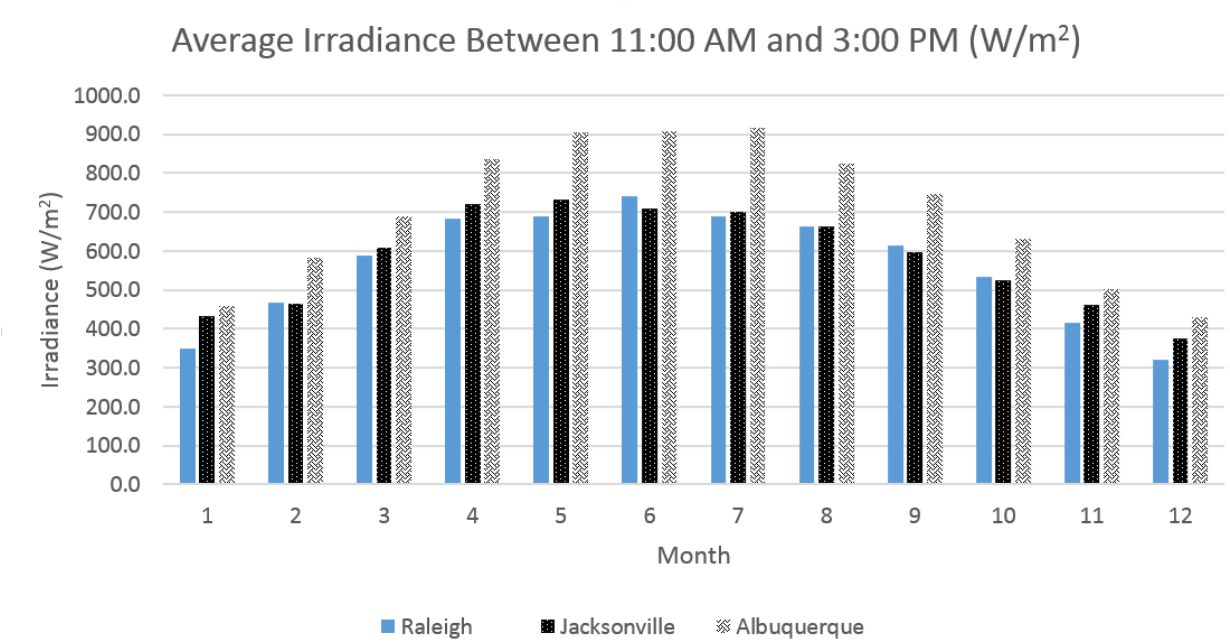

Figure 31. Average global horizontal irradiance from 11:00 AM to 3:00 PM for each month for different climates.

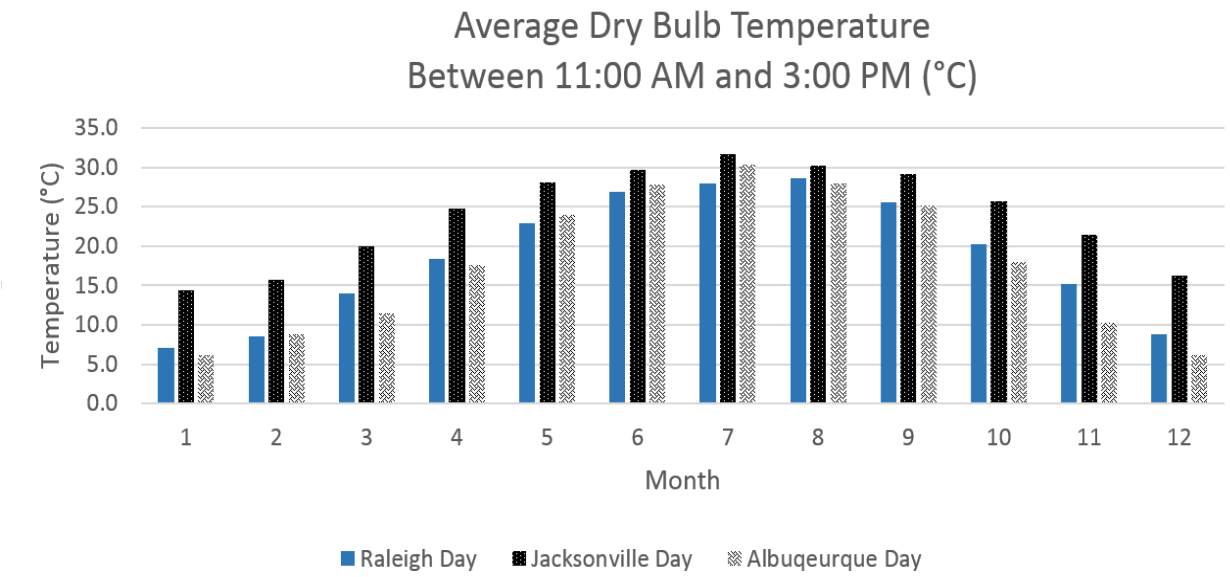

Figure 32. Average dry bulb temperature by month between 11:00 AM and 3:00 PM for different climates.

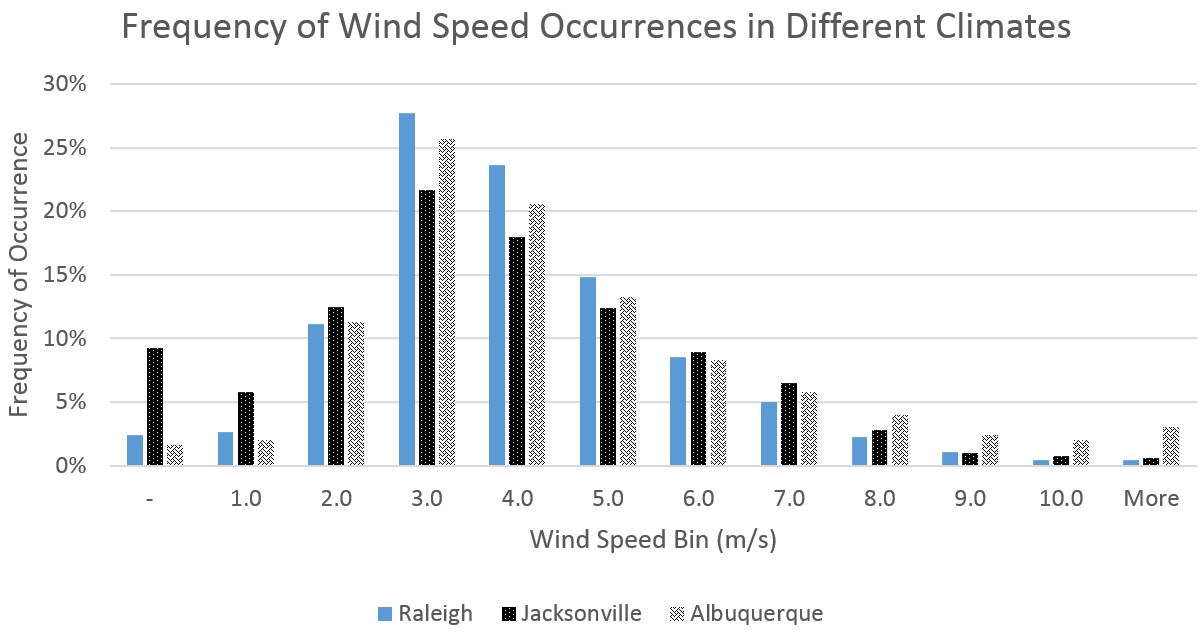

Figure 33. Percentage of time wind speed is within each speed interval in each climate. Each speed listed represents the lower bound of a 1 m/s range (e.g., "7 m/s" represents all speeds between 7 m/s and 8 m/s).

The cooling power of collectors is a function of ambient temperature, wind speed, and sky temperature. Figure 34 shows that the Albuquerque climate has the lowest night-sky temperatures, which gives it the greatest cooling potential. The variables of wind speed and ambient temperature have a compounding effect on each other because they codetermine the rate of convective heat transfer, which may be helpful or detrimental depending on whether ambient temperature is lower than collector temperature.

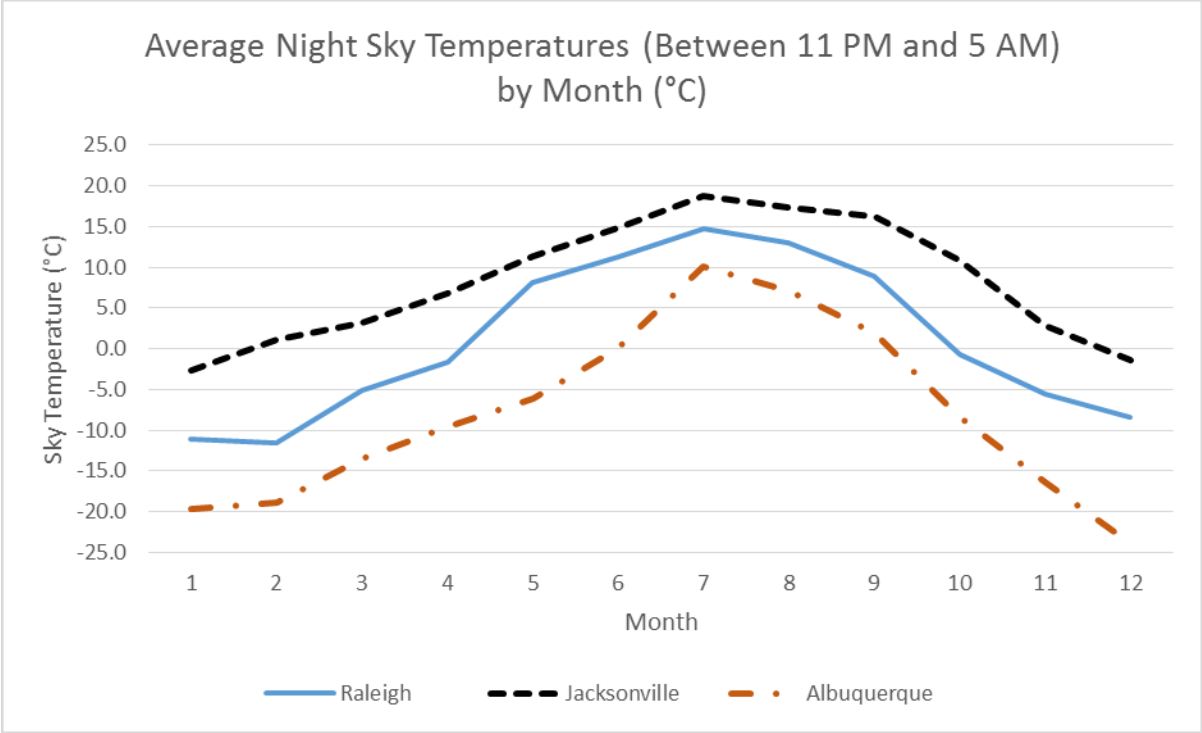

Figure 34. Average night-sky temperatures by month for each climate.

The building loads for Raleigh, Jacksonville, and Albuquerque are displayed in Figure 35, *Figure 36*, and Figure 37, respectively. Albuquerque has the highest heating requirement while Jacksonville has the highest cooling requirement.

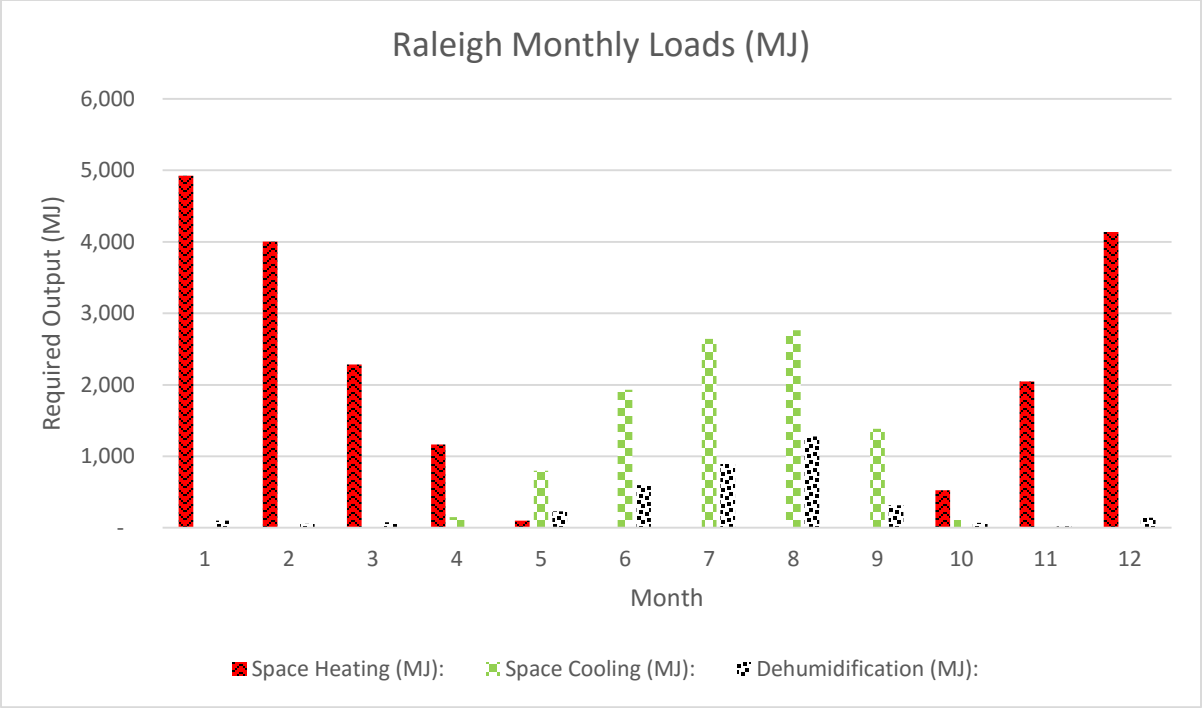

Figure 35. Total space heating, space cooling, and dehumidification load by month in Raleigh.

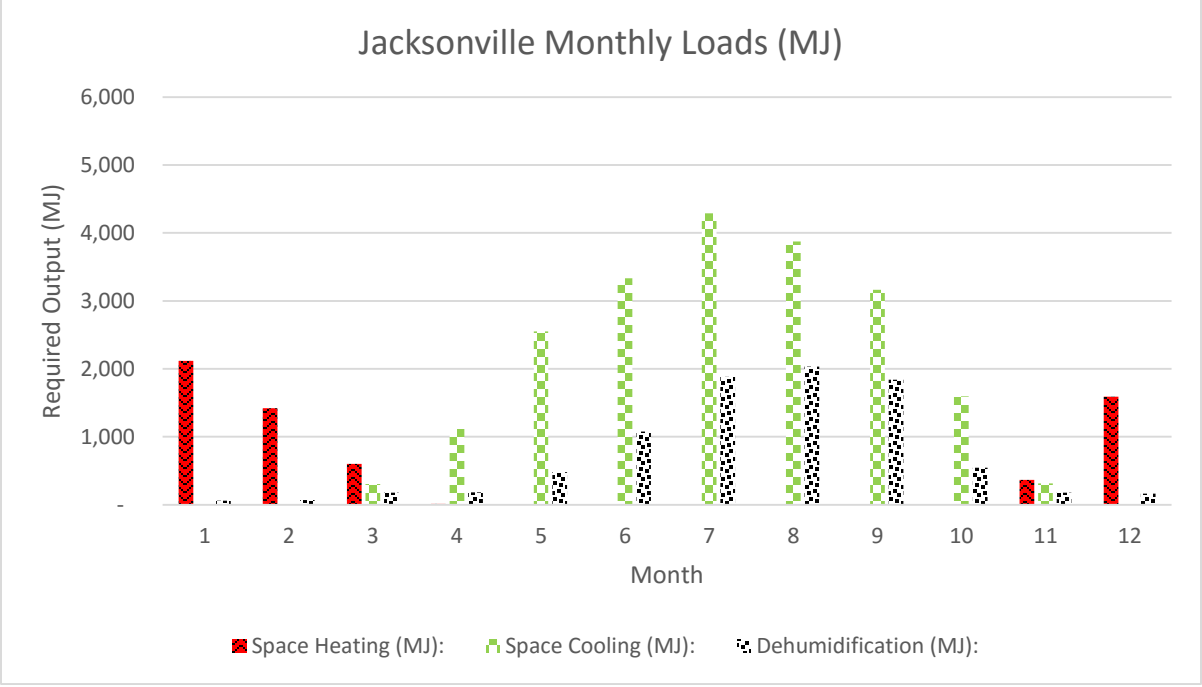

Figure 36. Total space heating, space cooling, and dehumidification load by month in Jacksonville.

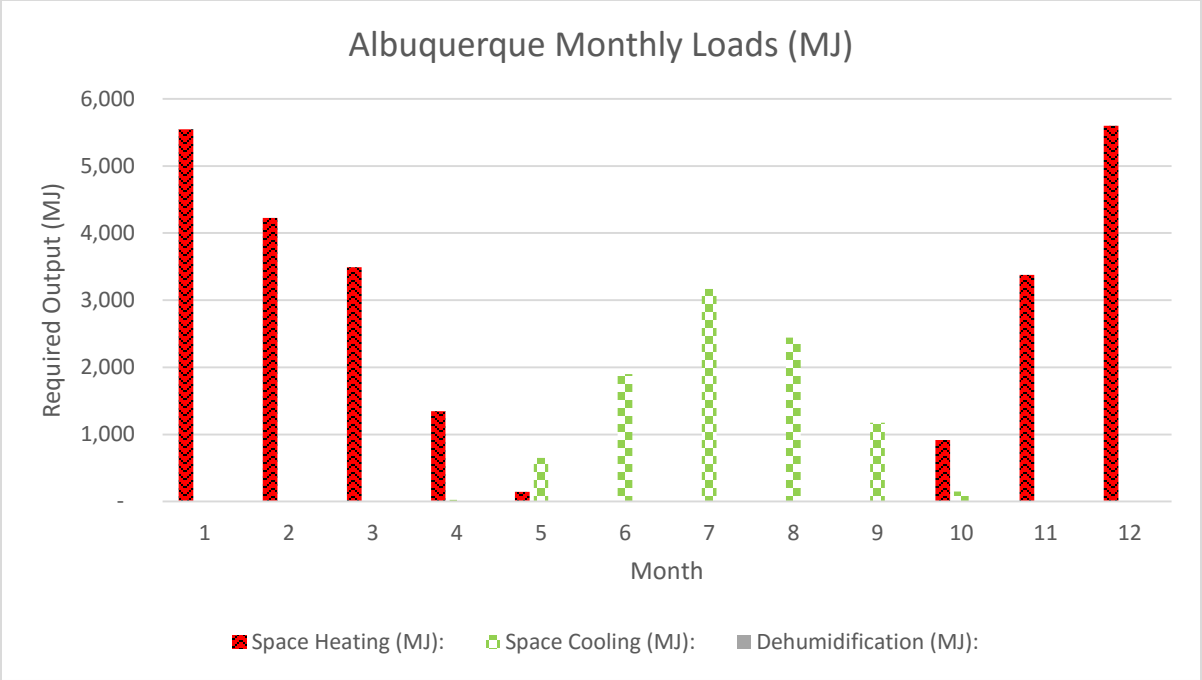

Figure 37. Total space heating, space cooling, and dehumidification load by month in Albuquerque.

System Performance

This section provides the annual solar fraction achieved in each climate by each type of collector. The monthly solar heating and cooling output is also displayed; an array size of 15.2 m^2 was chosen for both glazed and unglazed arrays to produce large enough effects in each mode of operation for monthly variations to be clearly visible. The annual trends are clear and generally as expected in heating mode, but there are some points that stray from the regression curve. One possible explanation is control error resulting from the functioning of the controls at the chosen time step; a value of one hour was used as a balance between precision and computational speed. A log function was fit to the data points purely on an empirical basis in order to predict the performance of different array sizes.

The results show that the glazed collectors are much better for space heating, while the unglazed collectors are much better for space cooling. The glazed collectors only attain a modestly higher amount of DHW savings compared to the amount they achieve in space heating. For example, over one year at equal array sizes in Raleigh, the unglazed collectors produce 65% to 73% as much

heat for DHW consumption, but only 23% to 26% as much heat for space heating. The glazed collectors provide a higher total solar fraction at all array sizes in all climates, although the disparity seems lowest in Jacksonville and highest in Albuquerque.

A limitation of the results is that the cooling performance does not account for condensation on the collectors, which may decrease the actual performance disproportionally in the more humid climates of Raleigh and Jacksonville. Further investigation must also be done into the cause of the glazed collector performance at the points when it does not increase with collector area. A final point that must be emphasized is that solar fractions only represent fractions of sensible heating and cooling loads; humidification and dehumidification are excluded.

Heating Savings

Because space heating and DHW supply are provided by the same tank, it seems natural to first look at them in combination, as displayed in Figure 38. However, this obscures the differences in space heating and water heating savings. Figure 39 shows that there is a very large difference between the space heating potential of glazed and unglazed collectors. However, the gap is much smaller when only DHW potential is considered, as seen in Figure 40. Figure 40 also shows that there is significant scattering of simulated loads from the regression curves when DHW heating is viewed in isolation. This may be partly because the available heat overlaps with the different types of demands at different times as it accumulates in the tank. However, it would be good to compare the results to findings that use separate DHW and space heating tanks in order to pinpoint how the savings influence each other.

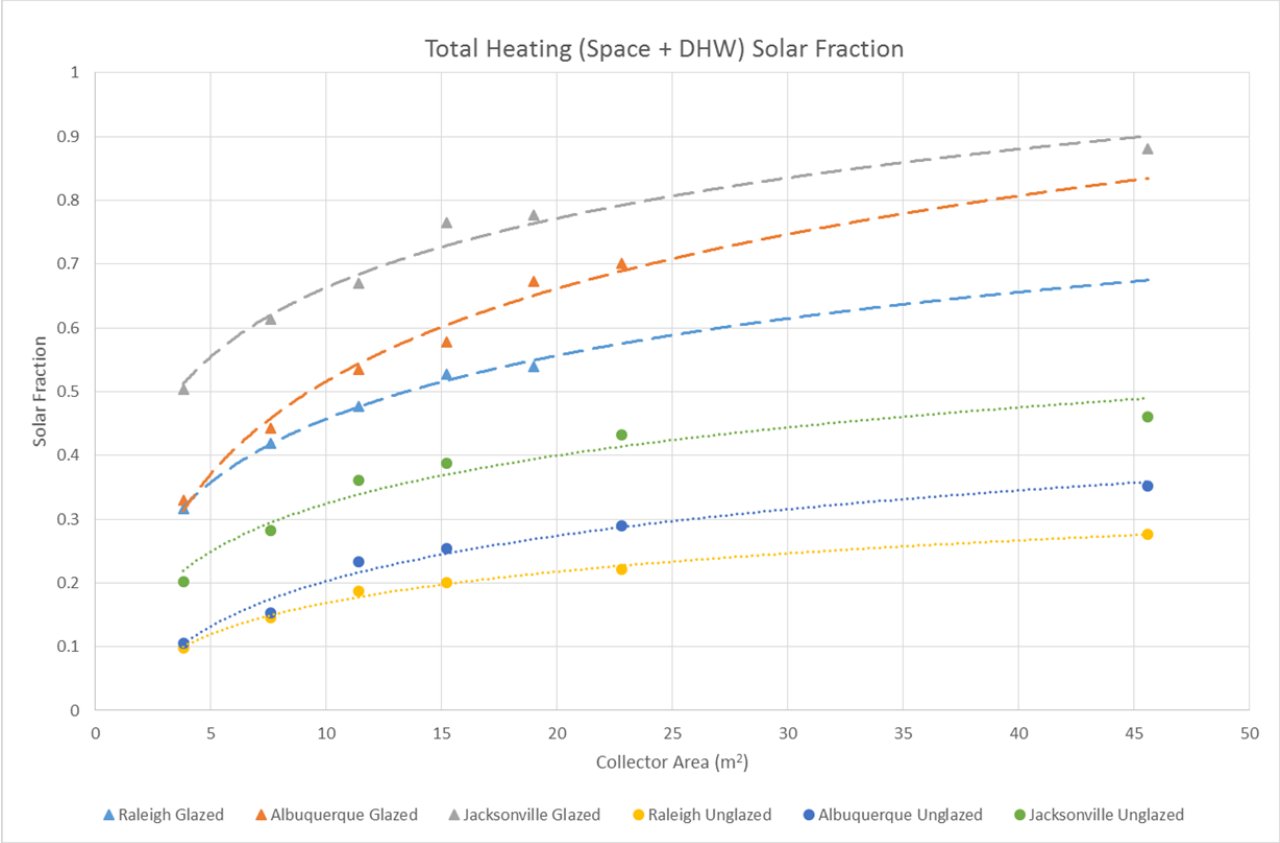

Figure 38. Total solar fraction (including space heating and DHW) for different array sizes of glazed and unglazed collectors.

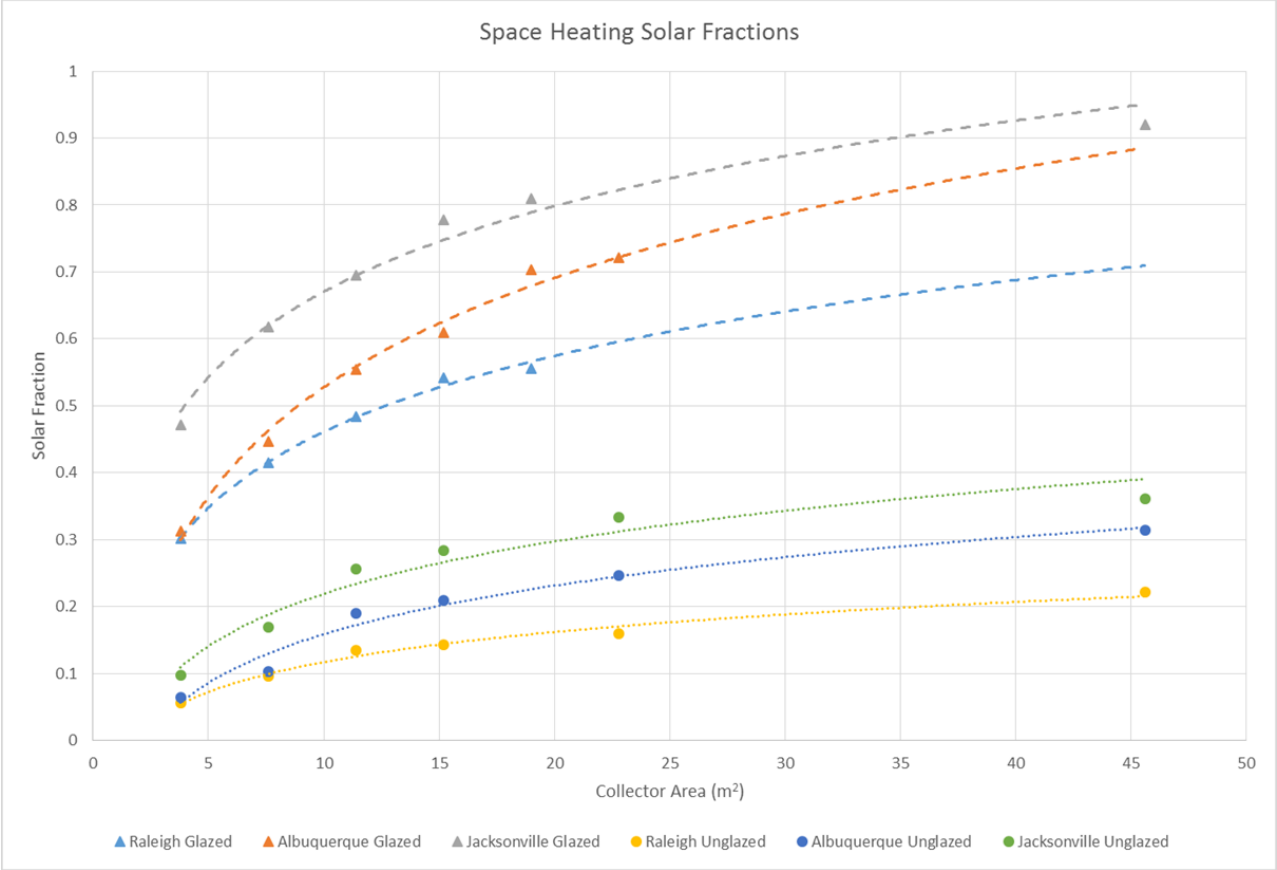

Figure 39. Space heating solar fractions for different array sizes of glazed and unglazed collectors.

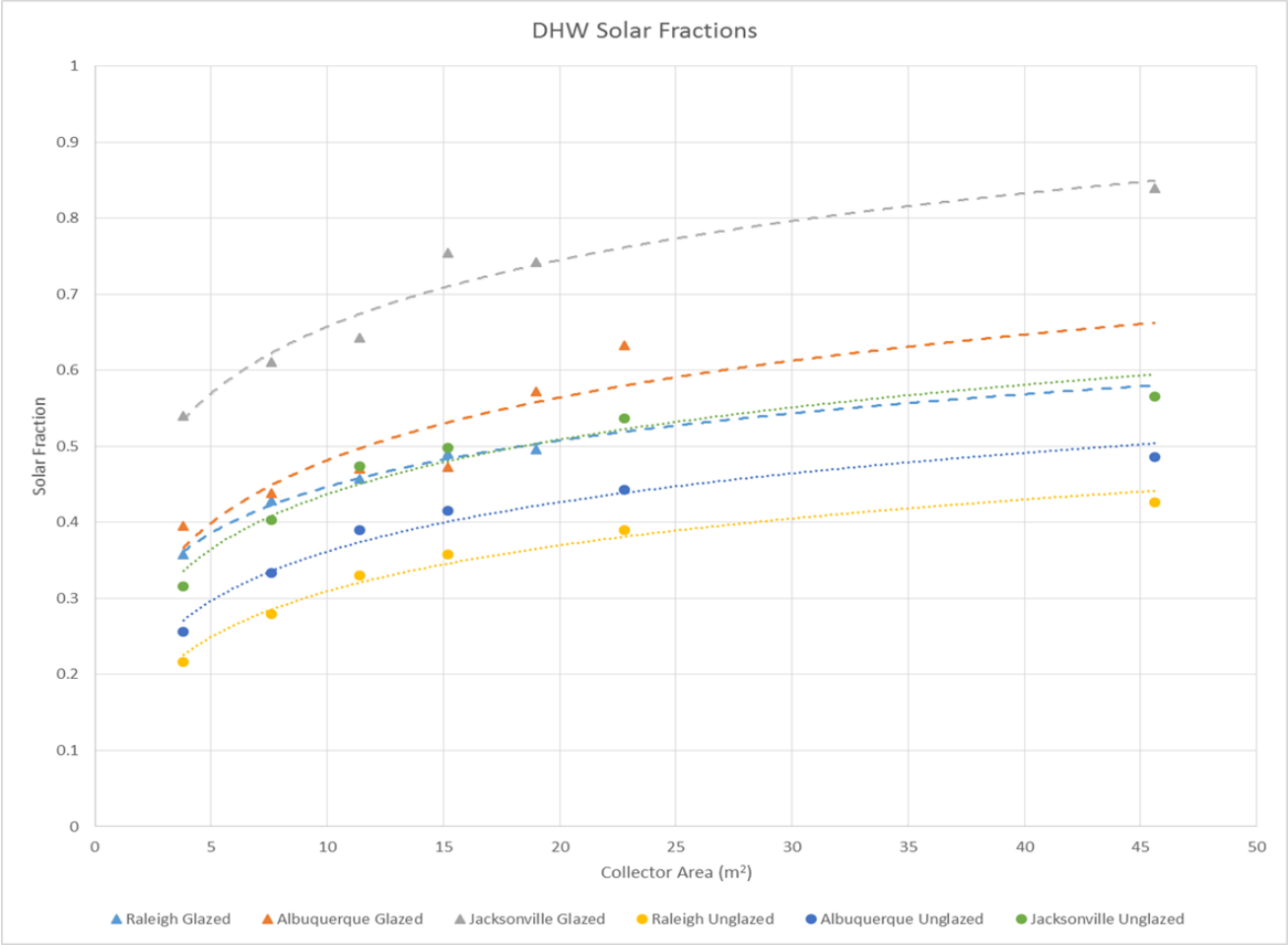

Figure 40. DHW solar fraction for different array sizes of glazed and unglazed collectors.

Figure 41, Figure 42, and Figure 43 show the heating energy savings in Raleigh, Jacksonville, and Albuquerque, respectively. Some competition can be seen between space heating savings and DHW savings. For example, the collectors harvest the most heat annually in Albuquerque, but achieve a substantially smaller amount of DHW savings than in Jacksonville, which has much smaller space heating loads. This seems to be because the system "prefers" to direct the stored water to space heating when it is available.

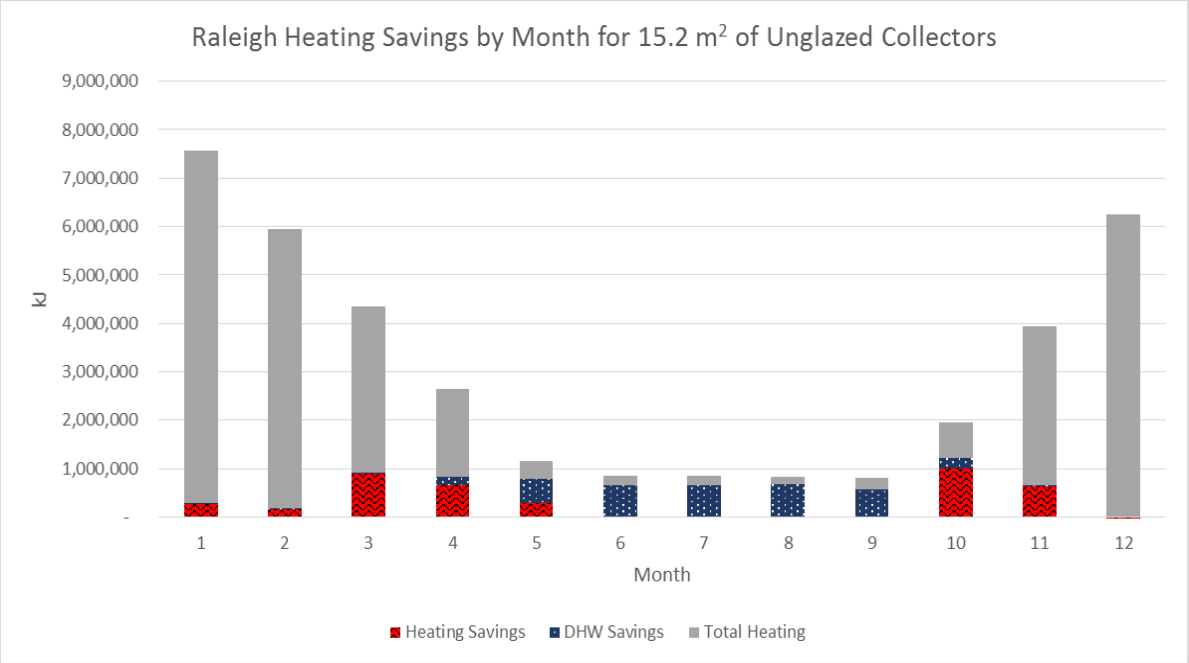

Figure 41. Heating savings for 15.2 m^2 of unglazed collectors in Raleigh, characterized by space heating savings and DHW heating savings.

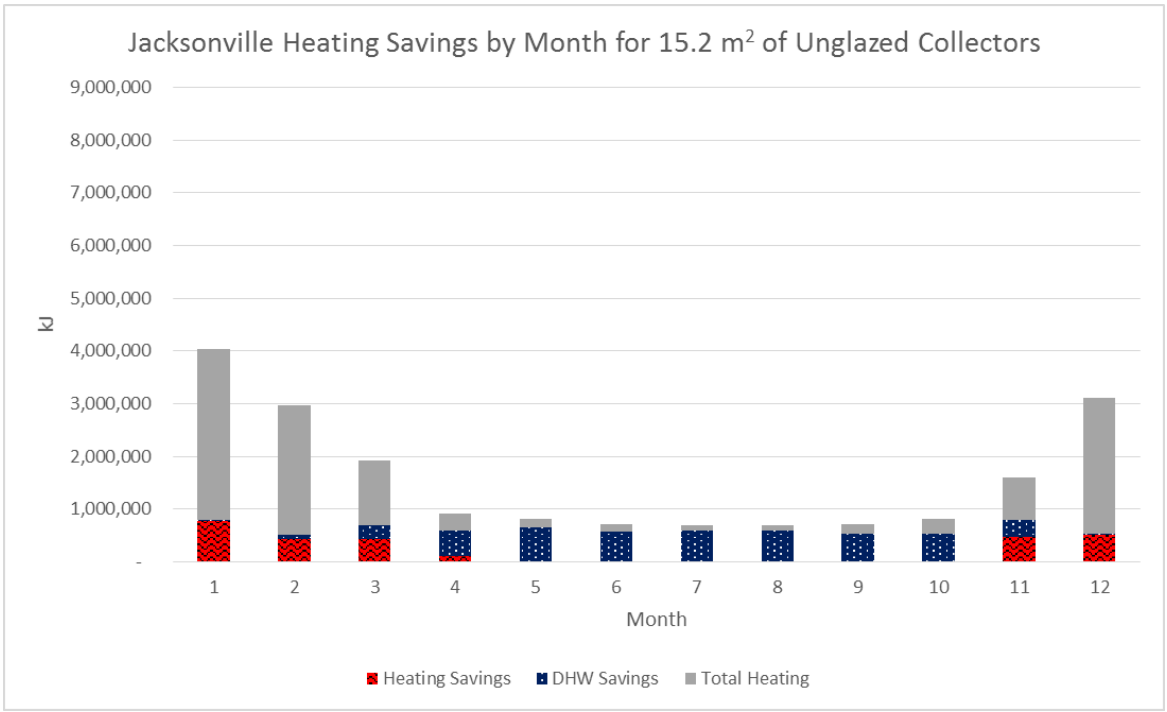

Figure 42. Heating savings for 15.2 m^2 unglazed collectors in Jacksonville, characterized by space heating savings and DHW heating savings.

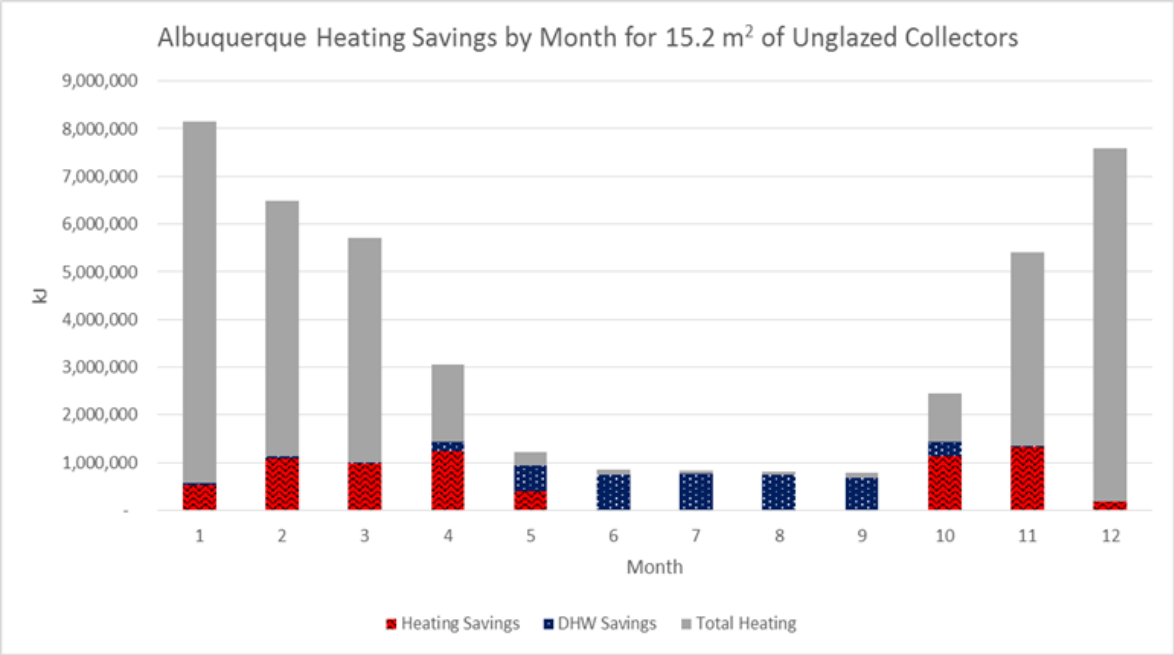

Figure 43. Heating savings from 15.2 m^2 unglazed collectors in Albuquerque, characterized by space heating and DHW heating savings.

Figure 44, Figure 45, and Figure 46 show the heating savings from glazed collectors in Raleigh, Jacksonville, and Albuquerque, respectively. The glazed collectors provide the most benefit in Albuquerque and the least benefit in Jacksonville.

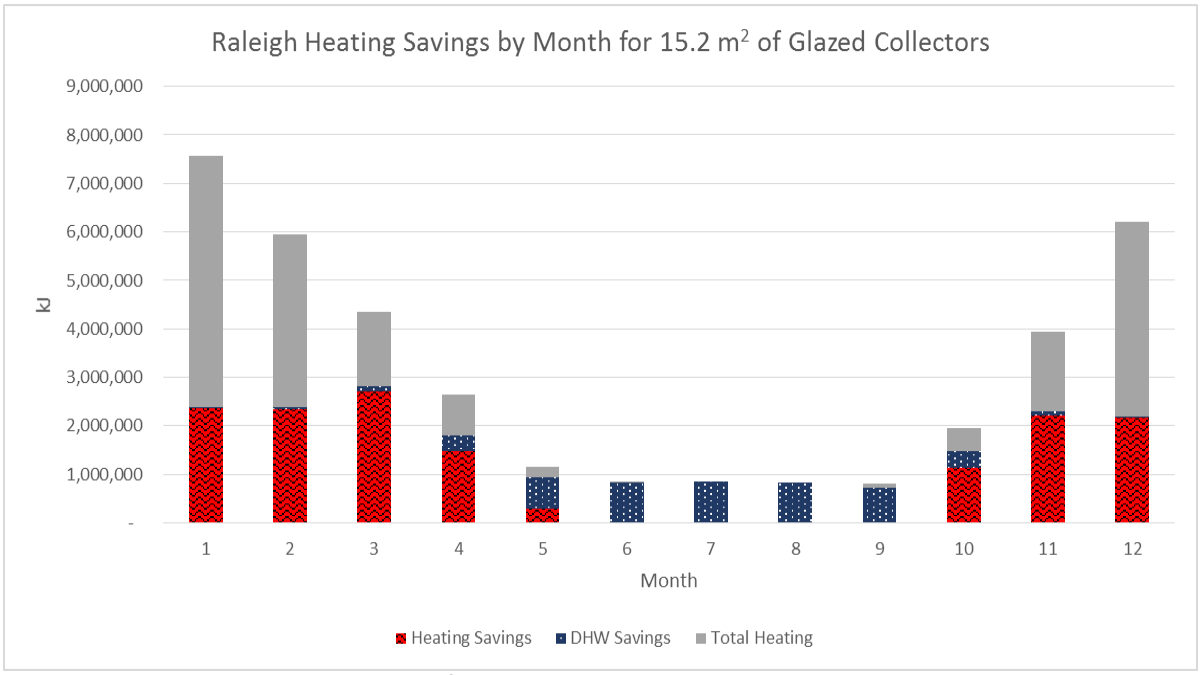

Figure 44. Heating savings for 15.2 m^2 of glazed collectors in Raleigh, characterized by space heating savings and DHW heating savings.

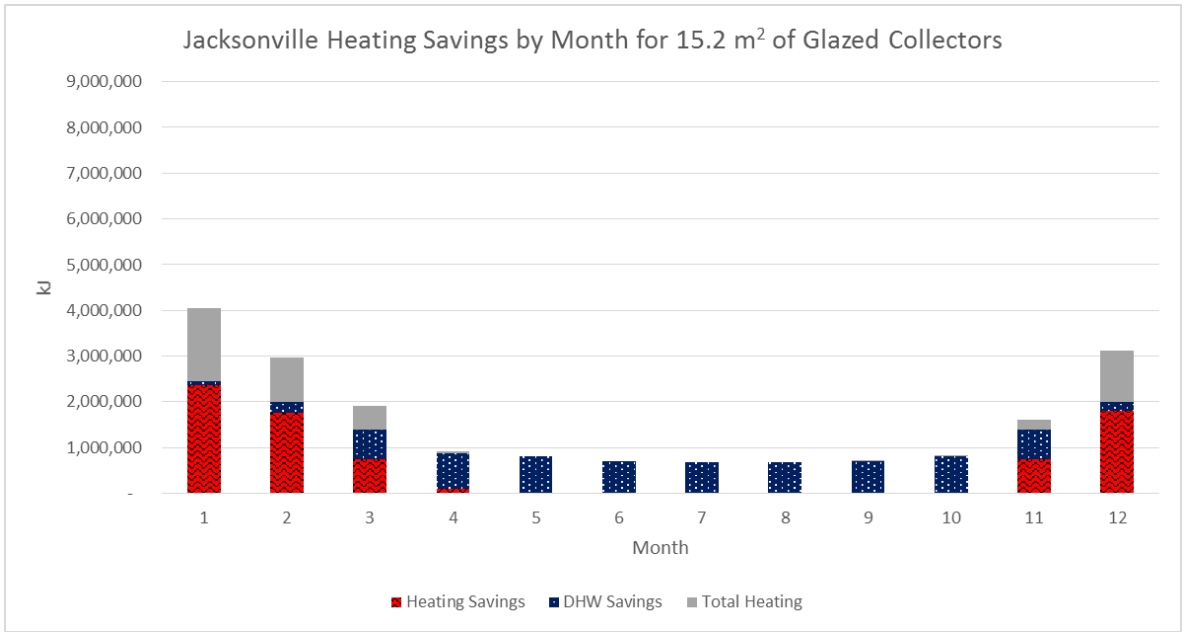

Figure 45. Heating savings for 15.2 m^2 of glazed collectors in Jacksonville, characterized by space heating savings and DHW heating savings.

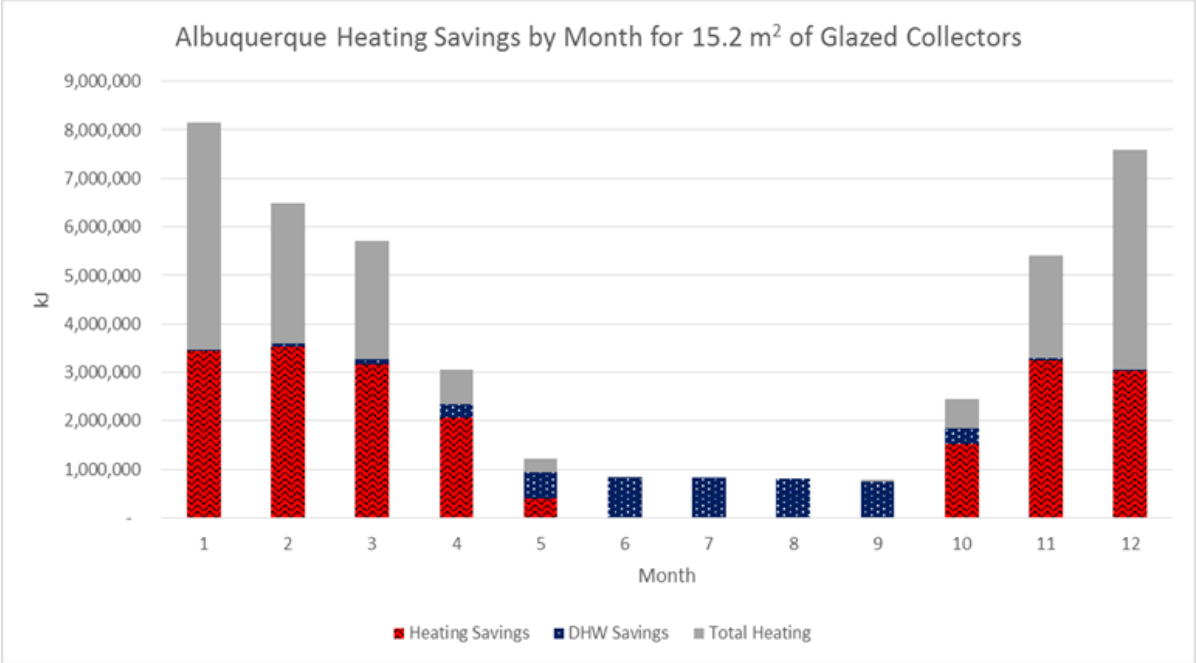

Figure 46. Heating savings from 15.2 m^2 of glazed collectors in Albuquerque, characterized by space heating and DHW heating savings.

Space Cooling Savings

The space cooling solar fractions from all collector array sizes are displayed in Figure 47. The benefit of Albuquerque's low night sky temperature is very apparent in the unglazed collector solar fractions. In fact, the glazed collectors in Albuquerque achieve a higher fraction of space cooling than the unglazed collectors in the humid climate of Jacksonville.

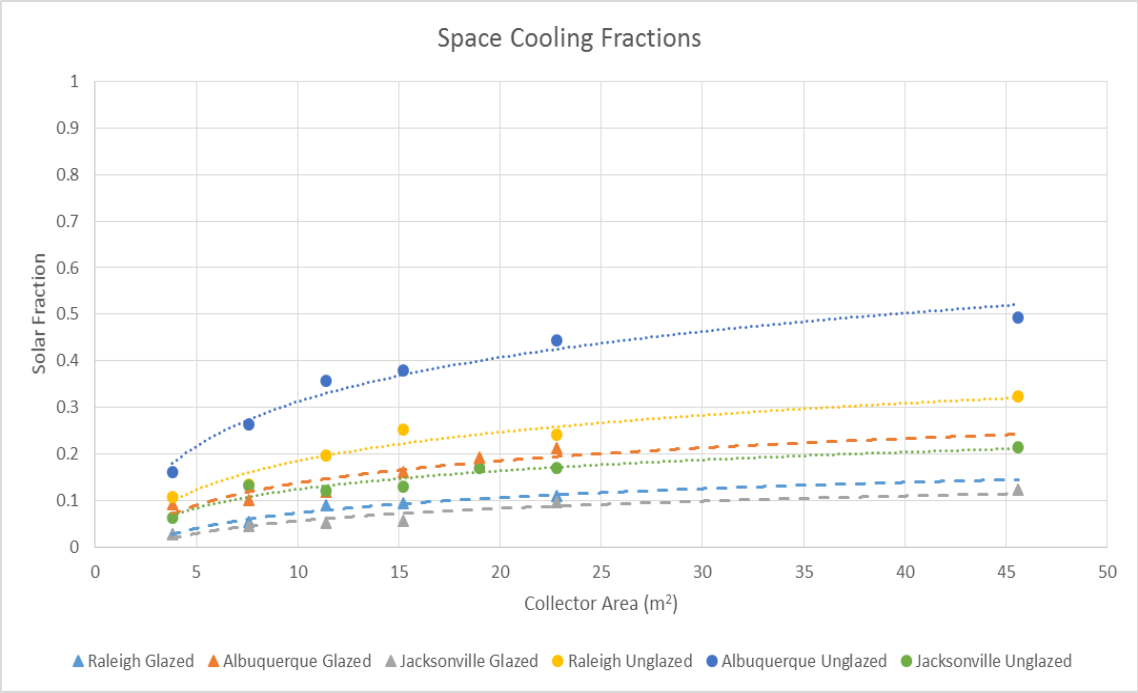

Figure 47: Space cooling solar fractions for different array sizes of glazed and unglazed collectors.

The monthly savings on space cooling for unglazed collectors are shown in Figure 48, Figure 49, and Figure 50 for Raleigh, Jacksonville, and Albuquerque, respectively. The monthly savings are generally better in the milder months.

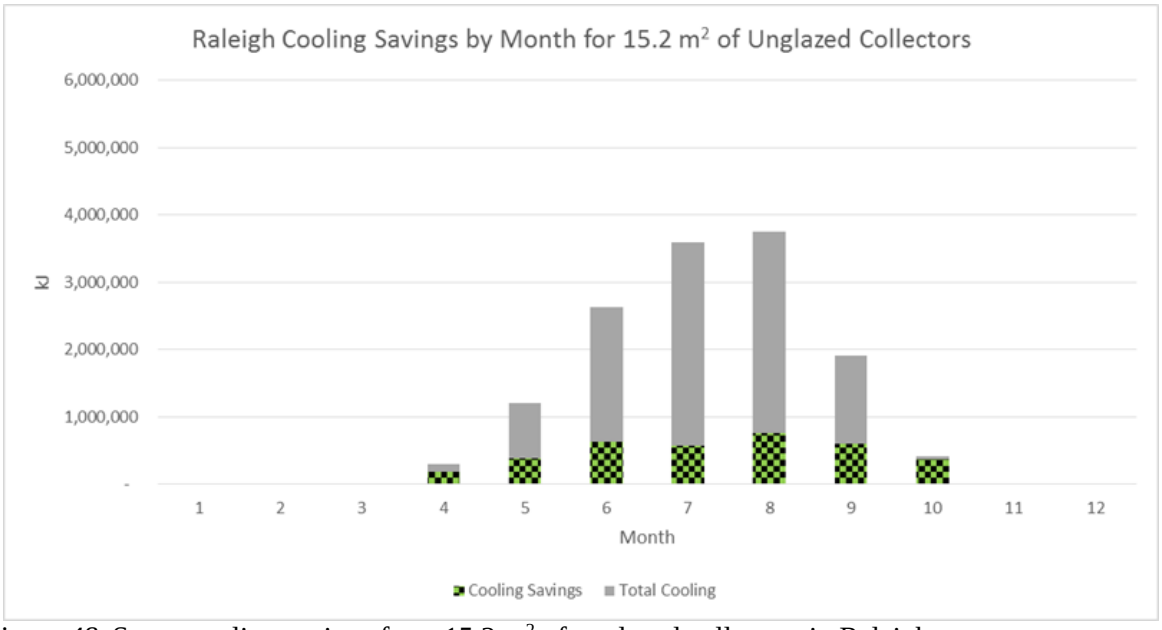

Figure 48. Space cooling savings from 15.2 m^2 of unglazed collectors in Raleigh.

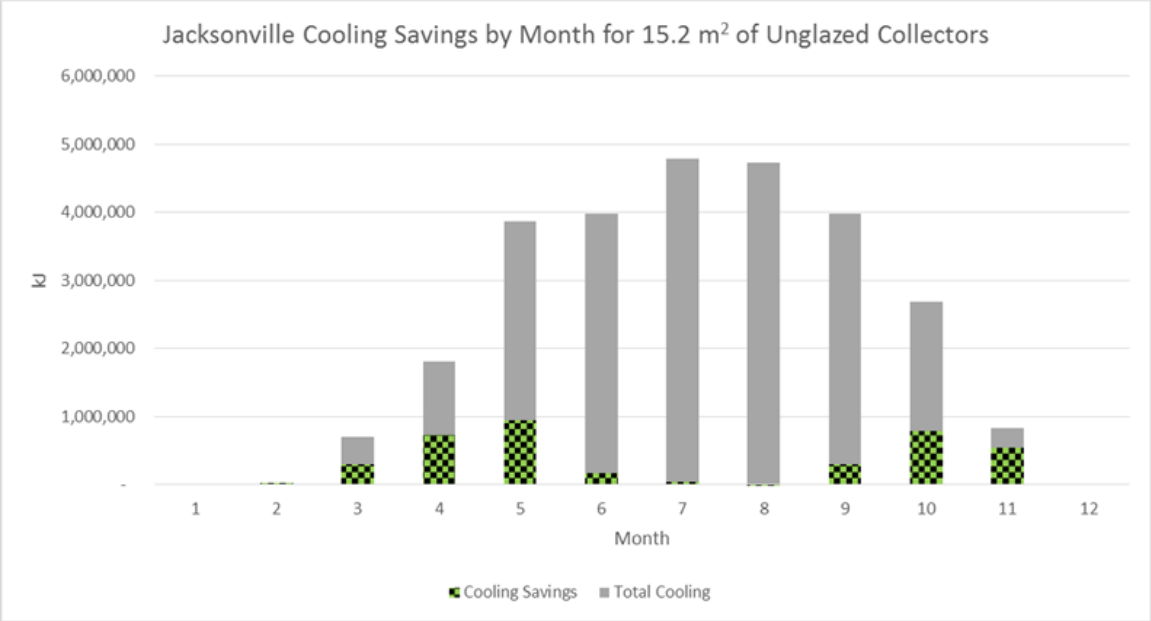

Figure 49. Space cooling savings from 15.2 m^2 unglazed collectors in Jacksonville.

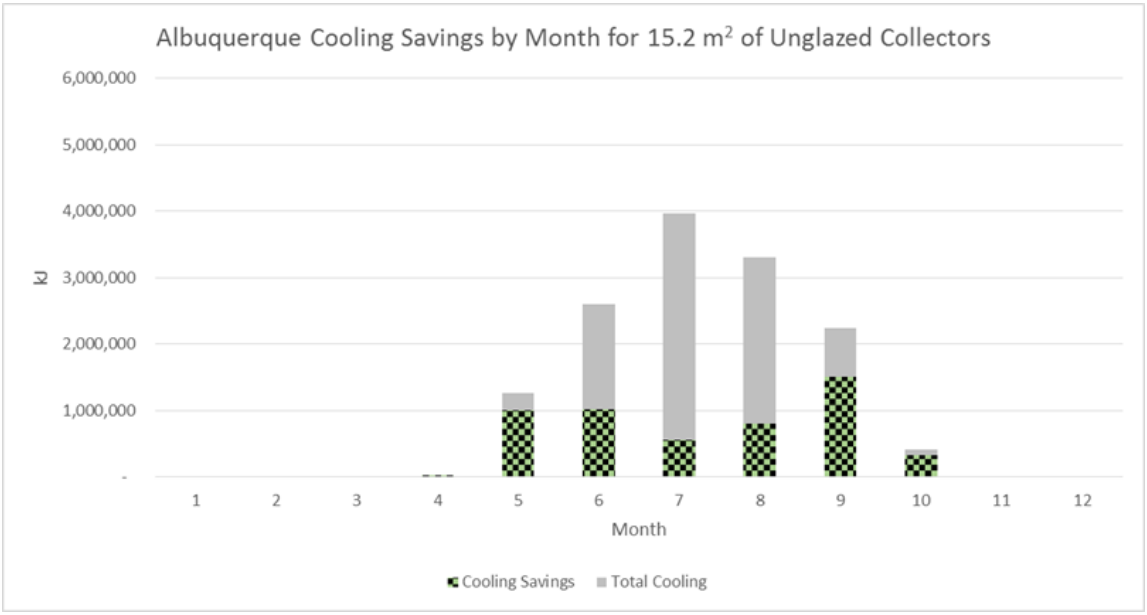

Figure 50. Space cooling savings from 15.2 m2 unglazed collectors in Albuquerque.

The monthly savings on space cooling for glazed collectors are shown in Figure 51, Figure 52, and Figure 53, respectively. They are consistently lower than the savings produced in the same climates by unglazed collectors, and are often near zero during the hottest months.

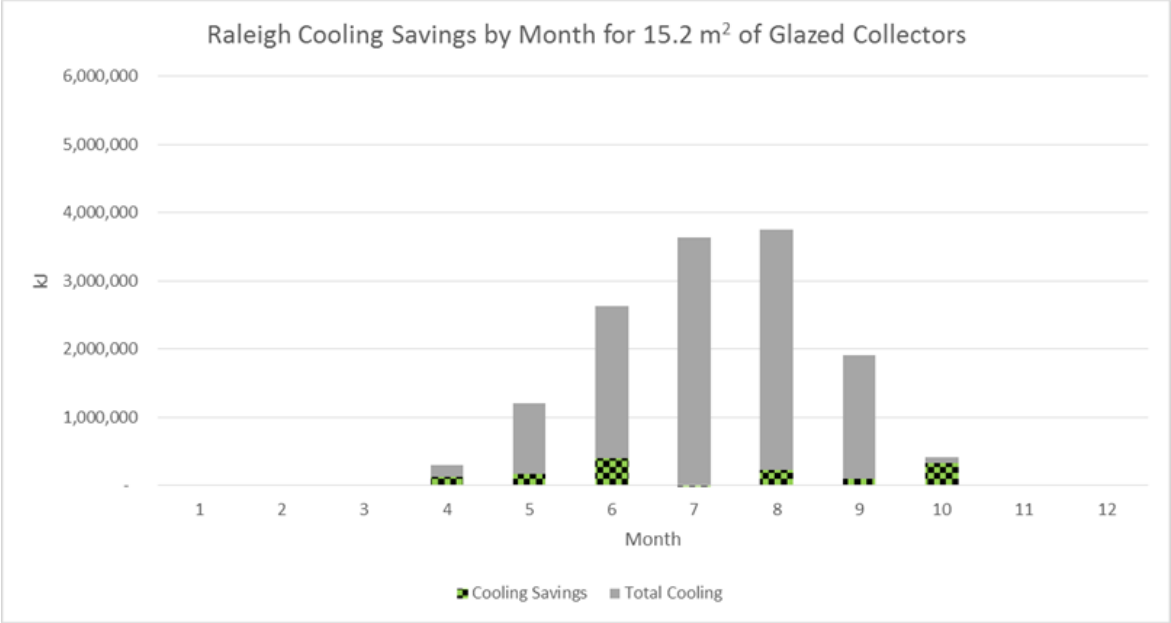

Figure 51. Space cooling savings from 15.2 m^2 of glazed collectors in Raleigh.

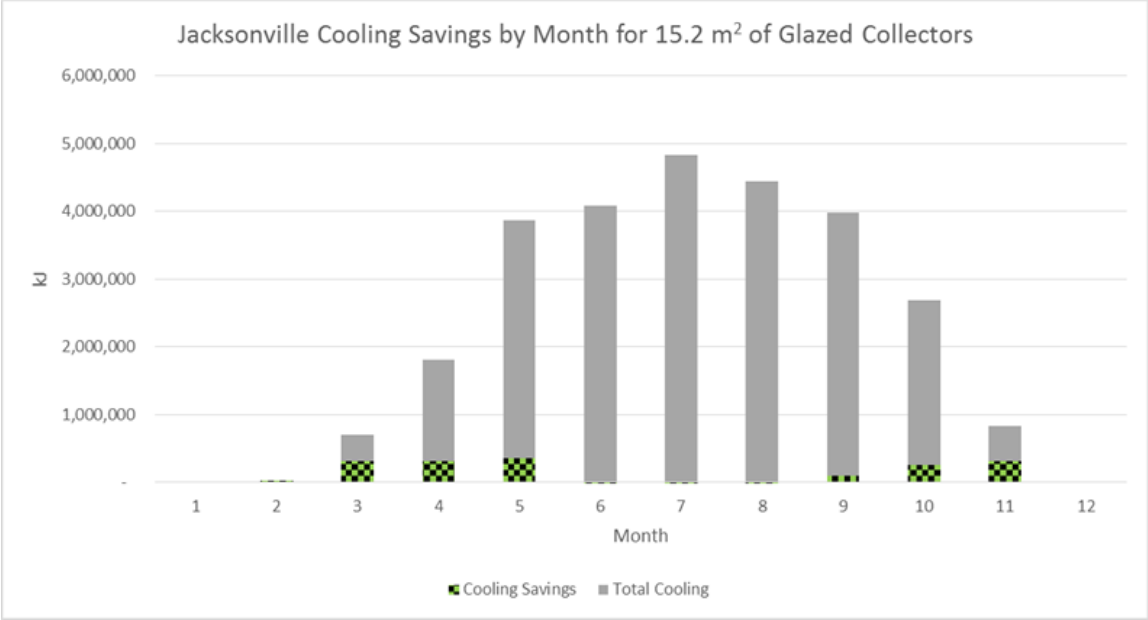

Figure 52. Space cooling savings from 15.2 m^2 of glazed collectors in Jacksonville.

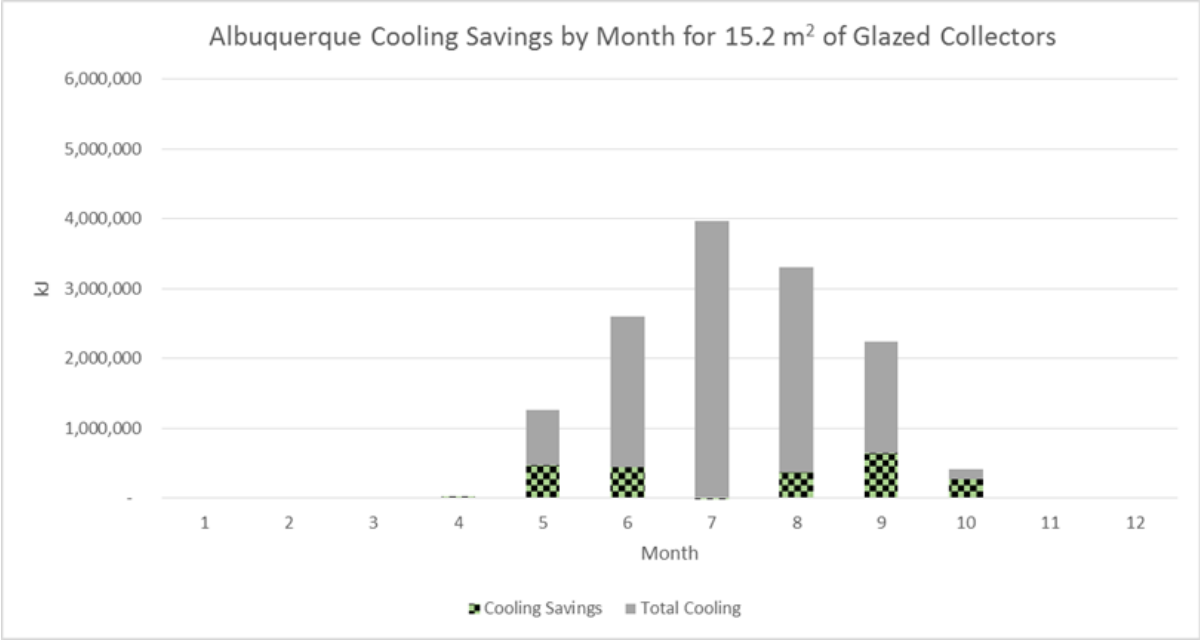

Figure 53. Space cooling savings from 15.2 m^2 of glazed collectors in Albuquerque.

Total Energy Savings

To understand how the heating and cooling solar fractions contribute to overall energy savings, the total solar fraction is plotted for each array size for each type of collector in Figure 54. Although the unglazed collectors save a significantly greater amount of cooling in Raleigh and Albuquerque, the building loads in these climates are dominated by heating and allow the glazed collectors to easily surpass the unglazed collector performance. The Jacksonville climate is cooling-dominated and shows the smallest absolute difference in solar fraction between glazed and unglazed collectors, but neither type of collector provides significant cooling at this location.

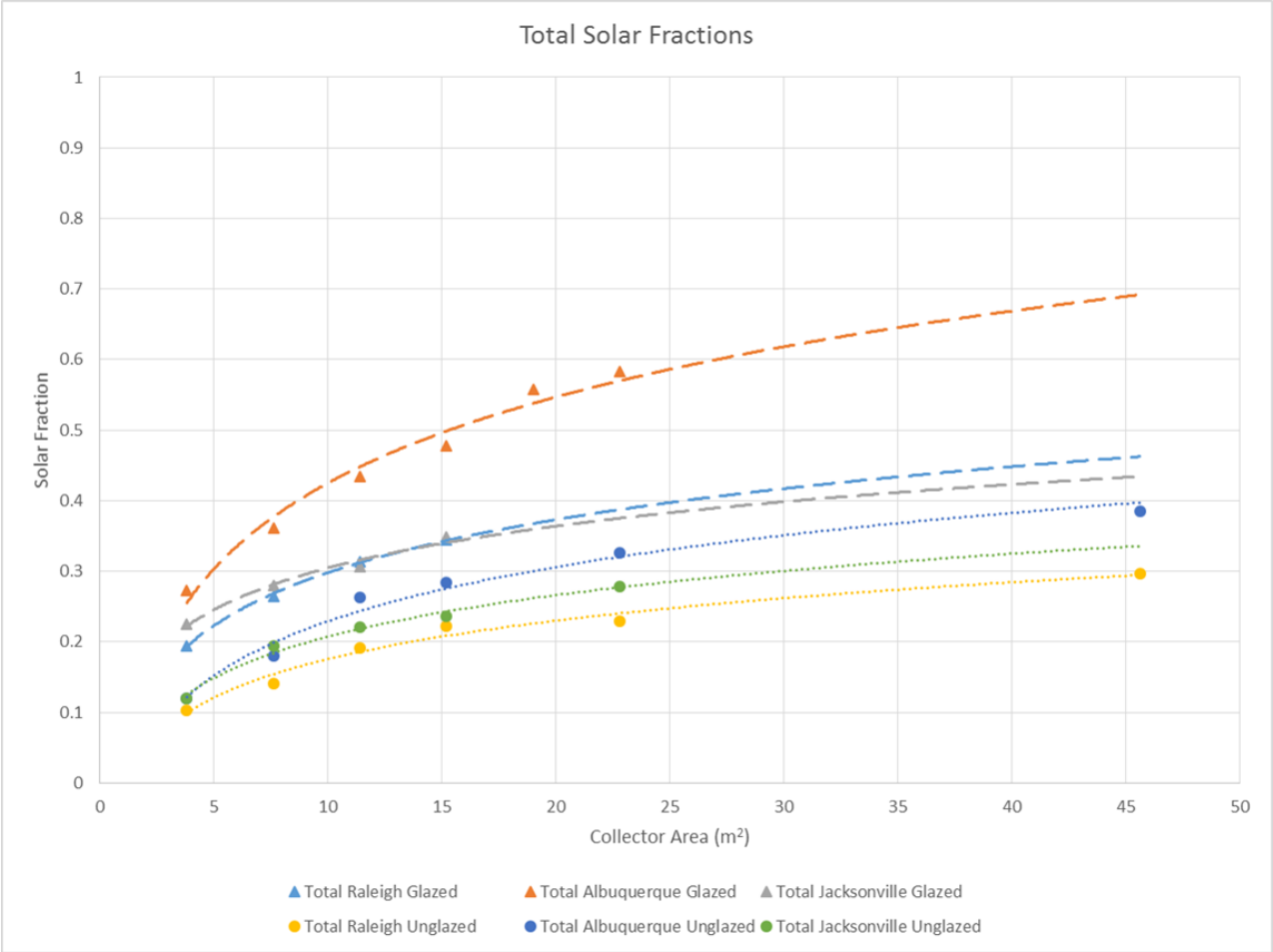

Figure 54. Total solar fractions at different array sizes for glazed and unglazed collectors.

Cost Savings Analysis

A cost savings analysis was performed for arrays of glazed and unglazed collectors. Assumed energy costs and equipment efficiencies for back-up heating, cooling and domestic hot water systems are presented in Table 23.

Table 23. *Auxiliary Heating and Cooling System Efficiencies*

Equipment	COP	Energy Cost
Heat Pump (Heating Mode)	2.75	$0.13 / kWh
Heat Pump (Cooling Mode)	4.0	$0.13 / kWh
Water Heater	1.0	$0.13 / kWh

Table 24 shows how the total solar fractions vary between glazed and unglazed collectors based on size. The unglazed collectors provide a substantially smaller energy cost savings per square meter. This same cost saving comparison is demonstrated in graphical form for each climate in Figure 55, Figure 56, and Figure 57.

Table 24. *Energy Cost Savings for Glazed and Unglazed Collectors at Different Array Sizes*

Area (m^2)	Raleigh Glazed	Raleigh Unglazed	Jacksonville Glazed	Jacksonville Unglazed	Albuquerque Glazed	Albuquerque Unglazed
3.8	$242.25	$124.59	$246.79	$143.68	$271.9	$144.34
7.6	$316.52	$177.43	$298.42	$187.46	$379.44	$211.41
11.4	$359.97	$208.34	$328.62	$213.06	$442.35	$250.64
15.2	$390.79	$230.28	$350.05	$231.23	$486.99	$278.48
19.0	$414.7	$247.29	$366.68	$245.32	$521.61	$300.07
22.8	$434.24	$261.19	$380.26	$256.83	$549.89	$317.71
45.6	$508.51	$314.03	$431.89	$300.6	$657.44	$384.78

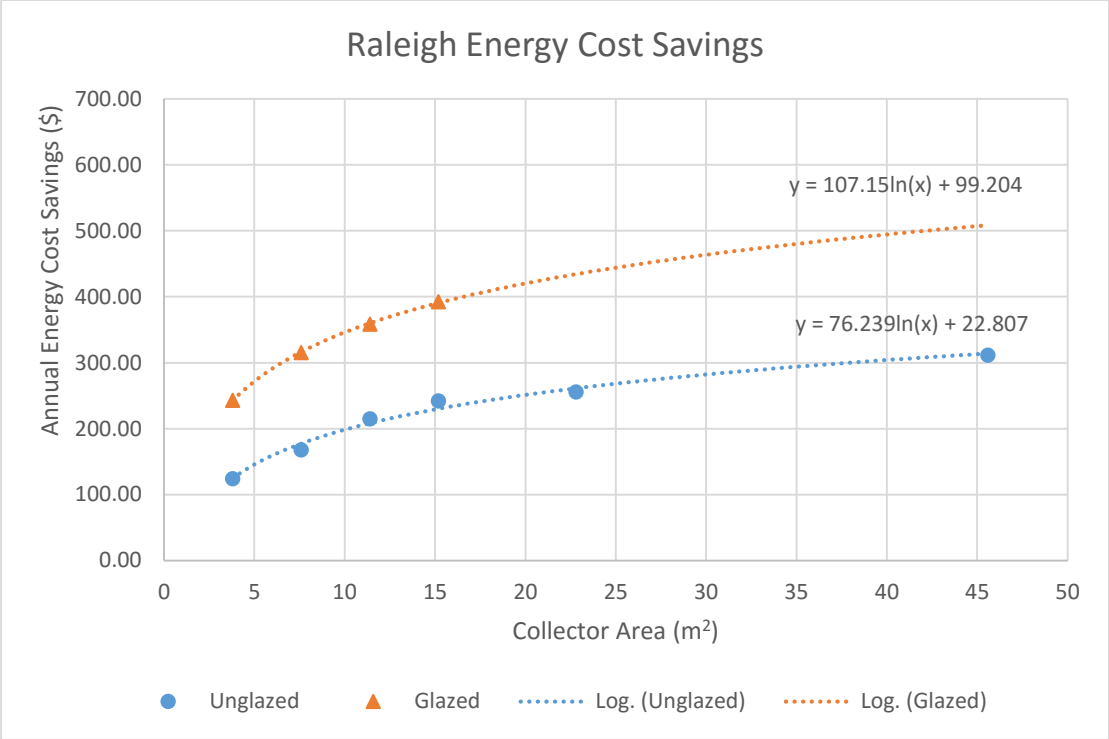

Figure 55. Energy cost savings for glazed and unglazed arrays in Raleigh.

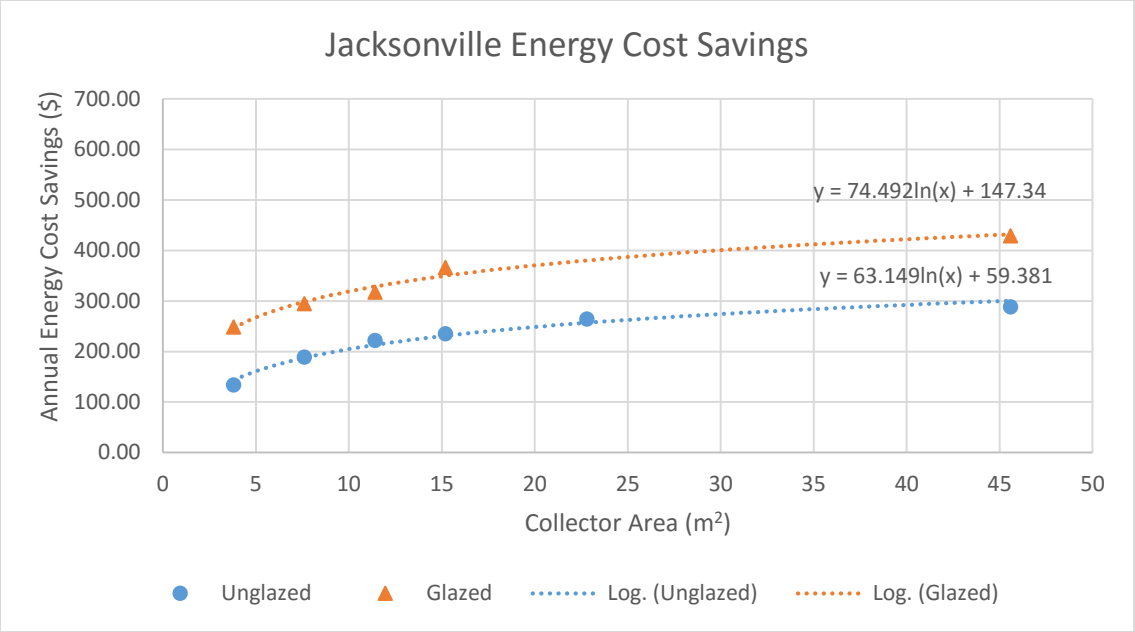

Figure 56. Energy cost savings for glazed and unglazed arrays in Jacksonville.

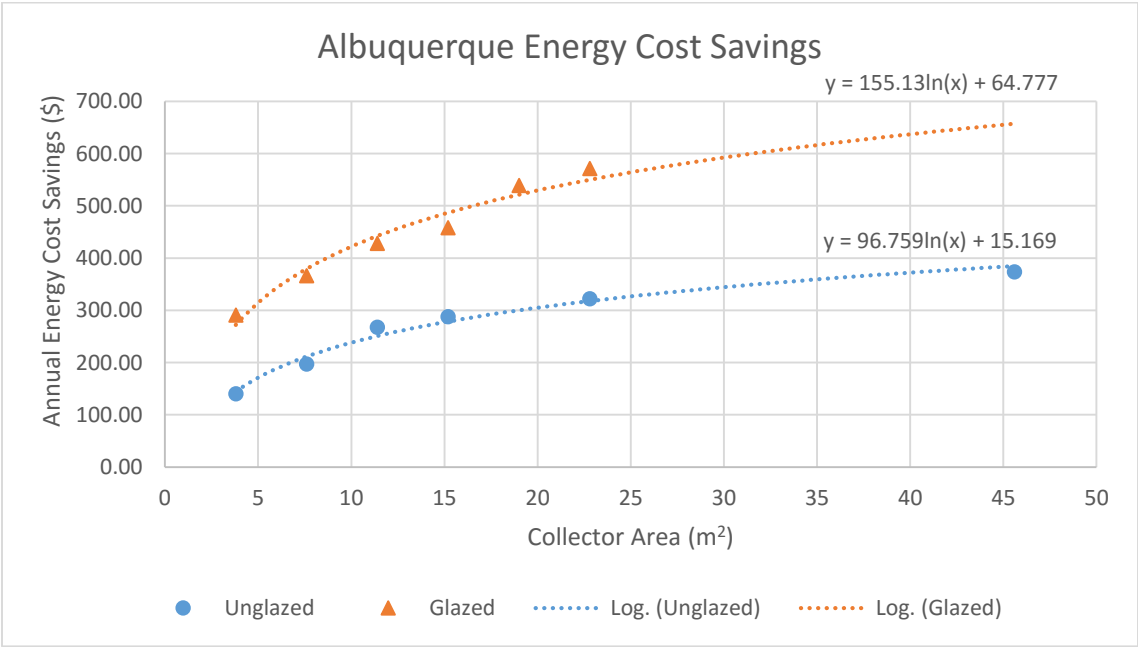

Figure 57. Energy cost savings for glazed and unglazed arrays in Albuquerque.

Table 25, Table 26, and Table 27 demonstrate the characterization of energy and cost savings for both types of collectors achieving similar solar fractions in the climates of Raleigh, Jacksonville, and Albuquerque, respectively.

Table 25. *Raleigh Annual Energy Cost Savings for Glazed and Unglazed Collectors at Similar Solar Fractions*

Collector Type		Space Heating Savings	DHW Savings	Space Cooling Savings	Overall Savings
Glazed (7.6 m^2)	Solar Fraction	0.42	0.43	0.05	0.26
	Energy Cost Savings	$148.36	$154.02	$13.13	$315.51
Unglazed (22.8 m^2)	Solar Fraction	0.16	0.39	0.24	0.23
	Energy Cost Savings	$56.81	$139.98	$58.86	$255.65

Table 26. *Jacksonville Annual Energy Cost Savings for Glazed and Unglazed Collectors at Similar Solar Fractions*

Collector Type		Space Heating Savings	DHW Savings	Space Cooling Savings	Overall Savings
Glazed (7.6 m^2)	Solar Fraction	0.62	0.61	0.05	0.28
	Energy Cost Savings	$78.64	$205.05	$11.22	$294.91
Unglazed (22.8 m^2)	Solar Fraction	0.33	0.54	0.17	0.28
	Energy Cost Savings	$42.41	$180.48	$41.48	$264.37

Table 27. *Albuquerque Annual Energy Cost Savings for Glazed and Unglazed Collectors at Similar Solar Fractions*

Collector Type		Space Heating Savings	DHW Savings	Space Cooling Savings	Overall Savings
Glazed (7.6 m^2)	Solar Fraction	0.45	0.44	0.10	0.36
	Energy Cost Savings	$197.16	$156.32	$12.62	$366.10
Unglazed (22.8 m^2)	Solar Fraction	0.25	0.44	0.44	0.33
	Energy Cost Savings	$108.74	$158.05	$55.25	$322.04

The solar fractions are approximately equal for glazed collector areas of 7.6 m^2 and unglazed collector areas of 22.8 m^2. The solar fractions at these areas range from about 25% to 35%, depending on climate. However, the savings on energy bills differ and are lower for the unglazed solar thermal system. The lower value results because a larger portion of the unglazed system's energy savings

comes from cooling, which is less expensive per kWh than heating. Looking only at the material cost of the collectors, the unglazed collectors would have to be lower than the cost fractions of glazed collectors specified in Table 28 in order to be cost competitive.

Table 28. *Ratios of System Cost per Unit Area of Collector ($/m^2) Required for Unglazed Collectors to Be Competitive with Glazed Collectors at Equal Energy Cost Savings*

Glazed Area	Raleigh Cost Ratio	Jacksonville Cost Ratio	Albuquerque Cost Ratio
3.8	0.21	0.2	0.27
7.6	0.16	0.17	0.18
11.4	0.14	0.16	0.14

Factors affecting equipment costs.

There is inherent uncertainty in determining the true representative costs of different types of collectors. The Energy Information Administration (EIA) provides year-by-year average costs of low and medium temperature collectors, but there is considerable variation between years (2012). Their medium-temperature category also includes evacuated tube, and presumably, flat plate collectors with selective coating, obscuring the cost comparison between the two types that only differ by the presence of glazing. The EIA's data show that the cost ratio between low-temperature and medium-temperature collectors is as low as 7% in 2009 to as high as 38% in 1990, with an average ratio of 15%. Taking into account the higher cost of evacuated tube collectors that were included in the EIA's medium-temperature category, the cost ratio of 20% referenced by Burch et al. (2005) seems like a reasonable rule of thumb.

Conclusions

The potential cost savings between glazed and unglazed collectors are a one-time reduction in expense of the installed solar thermal system. Because of the lower solar fractions achievable by the unglazed arrays, there is not a compelling financial reason to implement such a system on a residential scale when the same energy cost savings can be realized with a traditional glazed system.

Moreover, because the space cooling savings of the glazed system are minimal, better cost payback can probably be further achieved with glazed collectors by eliminating the cold water storage tank.

However, the characterization of the energy savings among space heating, DHW, and space cooling does reveal potential applications where unglazed collectors may be worthy of further investigation. The widest performance gap between glazed and unglazed collectors occurs in space heating. In climates and applications that require DHW heating and space cooling (but minimal space heating), unglazed collectors may approach or surpass the cost-performance of glazed collectors. In the chosen analysis, collectors make up a relatively small portion of the overall system cost—perhaps only 10% to 20% when all components, labor, and overhead costs are considered. But if implemented in a commercial or industrial application, the collector cost may be more significant.

There are also other considerations that may affect the choice of collector. Unglazed collectors do not pose much risk of boiling the glycol mixture, and may therefore require less maintenance and require less expensive quality of piping. The unglazed array typically must be larger, which will typically require more hours to install and greater expanses of piping. However, this could be partially offset in theory if the roof structure itself works as an unglazed collector, as in the experimental system of Anderson et al. (2013).

All aspects and limitations considered, the unglazed collectors did achieve more cost-effective energy savings in some cases compared to glazed collectors connected to an equal system. The system is probably not a practical means of saving energy for residences in the chosen climates, but the comparative performance of unglazed collectors makes a compelling case for research into their use in different climates or research into larger scale applications that require more substantial amounts of low-grade heating and cooling.

In summary, unglazed collector systems that are approximately three times the size of glazed collector systems can achieve equal energy savings of approximately 35% on combined heating, cooling, and water consumption. The cost per square meter for unglazed systems should be

substantially less than for glazed systems. However, the comparative rates of return on investment depend on total system costs, which were not fully analyzed.

Suggestions for Future Research

The simulation results create several interesting questions that could be addressed by future research. The unglazed collectors are clearly better for DHW heating and space cooling than for space heating, and would be expected to achieve a higher solar fraction when space heating is not needed. This would be particularly true for climates with clear skies (creating low night sky temperatures) and a high amount of insolation. Albuquerque fits this description best, and results show it had the greatest potential for savings. But the modeled house was still dominated far more by space heating (at 33.6 GJ per year) than space cooling (at 13.8 GJ per year) in this climate. A comparison to glazed collectors for buildings in hotter climates or with a higher relative amount of internal gains may reveal greater benefits.

The greatest weakness of unglazed collectors is their inability to capture heat in the medium to high temperature ranges. Their performance is highly sensitive to wind speed, but the magnitude of the effect is predicted differently by several different models. The uncertainty of wind's effect could be lessened by an experiment that measures local wind speed in conjunction with the performance of unglazed collectors mounted flush to a roof, which then compares the performance to ISO test results and different theoretical models of convective losses.

References

Anderson, T., Duke, M., & Carson, J. (April 2013). Performance of an unglazed solar collector for radiant cooling. *Australian Solar Cooling 2013 Conference.* Sydney, New South Wales. Retrieved from: http://aut.researchgateway.ac.nz/bitstream/handle/10292/5651/04a%20-%20Technical%20Session%20I%20-%20Components%20Stream%20-%20Anderson.pdf?sequence=2

Ayompe, L. D. (2011). Validated TRNSYS model for forced circulation solar water heating systems. *Applied Thermal Engineering*, *31*, 1536-1542.

Baer, S. (2001). Passive cooling and drainback heating with unglazed radiators/absorbers -- the architectural cool cell (TM). *In Proceedings of ASES National Solar Energy Conference* (pp. 637-640). Washington, DC: American Solar Energy Society.

Betz, F. (2014, November 14). *What are reasonable indoor air velocities?* Retrieved from http://www.researchgate.net/post/What_are_reasonable_indoor_air_velocities

Bonhôte, P. E. (2009). Unglazed coloured solar absorbers on facade: Modelling and performance evaluation. *Solar Energy*, *83*(6), 799-811. doi:10.1016/j.solener.2008.11.014

Brandemuehl, M. (2005). Predicting thermal comfort. Retrieved from http://ceae.colorado.edu/~brandem/aren3050/docs/ThermalComfort.pdf

Burch, D., Huggins, J., Wood, B., & Thornton, J. (April 1993). *Simulation based ratings for solar hot water systems*. Paper presented at the American Solar Energy Society Annual Conference, Washington, DC.

Burch, J., & Casey, R. (May 2009). *Wind issues in solar thermal performance ratings.* Paper presented at the American Solar Energy Society Annual Conference, Buffalo, NY. Retrieved from http://www.nrel.gov/docs/fy09osti/45466.pdf

Burch, J. C., Christensen, C., Salasovich, J., & Thornton, J. (2004). Simulation of an unglazed collector system for domestic hot water and space heating and cooling. *Solar Energy*, *77*(4), 399-406. doi:10.1016/j.solener.2003.12.014

Burch, J., Salasovich, J., & Hillman, T. (August 2005). *An assessment of unglazed solar domestic water heaters*. Paper presented at the ISES Solar World Congress, Orlando, FL. Retrieved from http://www.nrel.gov/docs/fy06osti/37759.pdf

Chuangchid, P., & Krarti, M. (2001). Foundation heat loss from heated concrete slab-on-grade floors. *Building and Environment 36*, 637-655. doi:10.1016/S0360-1323(00)00040-8

Conserval Engineering, Inc. (2015). *NightSolar solar cooling system*. Retrieved from http://solarwall.com/en/products/nightsolar-air-cooling.php

DOW Chemical Company. (2001). *Dowfrost: Inhibited propylene glycol-based heat transfer fluid.* Retrieved from http://msdssearch.dow.com/PublishedLiteratureDOWCOM/dh_0040/0901b80380040bcb.pdf?filepath=heattrans/pdfs/noreg/180-01314.pdf&fromPage=GetDoc

Duffie, J., & Beckman, W. (2006). *Solar engineering of thermal processes* (3rd ed.). Hoboken, NJ: John Wiley and Sons, Inc.

Edwards, S., Beausoleil-Morrison, I., & Laperrière, A. (2015). Representative hot water draw profiles at high temporal resolution for simulating the performance of solar thermal systems. *Solar Energy, 111*, 43-52.

Eicker, U., & Dalibard, A. (2011). Photovoltaic thermal collectors for night radiative cooling of buildings. *Solar Energy, 85*(7), 1322-1335. doi:10.1016/j.solener.2011.03.015

Elert, G. (2001). *Density of concrete*. Retrieved from http://hypertextbook.com/facts/1999/KatrinaJones.shtml

Elsland, R., Peksen, I., & Wietschel, M. (2014). Are internal heat gains underestimated in thermal performance evaluation of buildings? *Energy Procedia 62*, 32-41. doi: 10.1016/j.egypro.2014.12.364

Energy Information Administration (EIA). (2012). *Table 10.6 solar thermal collector shipments by type, price, and trade, 1974-2009*. Retrieved from http://www.eia.gov/totalenergy/data/annual/showtext.cfm?t=ptb1006

Energy Solaire. (2015). *Solar roof*. Retrieved from http://www.energie-solaire.com/wq_pages/de/site/page-163.php

Fafco, Inc. (2009). *Fafco solar pool heating owner's manual.* Retrieved from http://www.fafco.com/files/06836C_Pool%20Owners%20Manual_10-28-09.pdf

Firlag, S., & Zawada, B. (2013). Impacts of airflows, internal heat and moisture gains on accuracy of modeling energy consumption and indoor parameters in passive building. *Energy and Buildings 64*, 372-383. doi:10.1016/j.enbuild.2013.04.024

Florida Solar Energy Center. (2006). *Solar water heating and pool heating manual*. Coca, FL: Florida Solar Energy Center.

Frank, E., Mauthner, F., & Fischer, S. (2015). *Overheating prevention and stagnation handling in solar process heat applications.* International Energy Agency Solar Heating and Cooling Programme. Retrieved from http://www.nachhaltigwirtschaften.at/iea_pdf/reports/iea_shc_task49_overheatingstagnationreport.pdf

Furbo, S. (2004). *Hot water tanks for solar heating systems.* Kongens Lyngby: Department of Civil Engineering, Technical University of Denmark.

Goswami, D., Kreith, F., & Kreider, J. (2000). *Principles of solar engineering* (2nd ed.). Philadelphia, PA: Taylor and Francis.

Heisler, G. (1990). Mean wind speed below building height in residential neighborhoods with different tree densities. *ASHRAE Transactions, 96*(1), 1389-1396.

Helvaci, H., & Khan, Z. (2015). Mathematical modelling and simulation of multiphase flow in a flat plate solar energy collector. *Energy Conversion and Management, 106*, 139-150.

Hoyt, T., Schiavon, S., Piccioli, A., Dustin, M., & Steinfeld, K. (2013). *CBE thermal comfort tool*. Retrieved from Center for the Built Environment: http://comfort.cbe.berkeley.edu/

Huang, J., Hanford, J., & Fuqiang, Y. (1999). *Residential heating and cooling loads component analysis.* Berkeley: Lawrence Berkeley National Laboratory.

Intelligent Energy Europe. (2012). *A guide to the Standard EN12975.* From: SP Technical Research Institute of Sweden.

International Energy Agency (IEA). (1993). *The characterization and testing of solar collector thermal performance.* Kingston, Ontario: Solar Calorimetry Laboratory.

International Organization for Standardization (ISO). (2013). *ISO 9806: Solar energy -- solar thermal collectors -- test methods -- final draft*. Geneva, Switzerland. Retrieved from http://www.iccsafe.org/cs/standards/IS-STSC/Documents/SolarCollector/ISO9806-PublicCommentDraft.pdf

Marion, W., & Urban, K. (1995). *User's manual for TMY2s typical meteorological years.* Golden, CO: National Renewable Energy Laboratory.

Marion, W., & Wilcox, S. (n.d.). *Solar radiation data manual for flat plate and concentrating collectors.* Golden, CO: NREL. Retrieved from http://www.nrel.gov/docs/legosti/old/5607.pdf

Moore, T., Bauman, R., & Huizenga, C. (2006). *Radiant cooling research scoping study.* University of California, Berkeley: Center for the Built Environment. Retrieved from http://www.cbe.berkeley.edu/research/pdf_files/IR_RadCoolScoping_2006.pdf

Olesen, B.W. (2002). Radiant floor heating in theory and practice. *ASHRAE Journal*, *44*(7), 19-24.

Olesen, B.W. (2012). Thermo active building systems: Using building mass to heat and cool. *ASHRAE Journal*, *54*(2), 44-52.

International Code Council (ICC) (n.d.). *Residential prescriptive requirements 2009 international energy conservation code (IECC)*. Retrieved from https://energycode.pnl.gov/EnergyCodeReqs/index.jsp

Perers, B. (1987). *Performance testing of unglazed collectors: Wind and longwave radiation influence*. Unpublished manuscript.

Ragheb, M. (2014). *Solar thermal power and energy storage historical perspective.* Retrieved from http://www.solarthermalworld.org/sites/gstec/files/story/2015-04-18/solar_thermal_power_and_energy_storage_historical_perspective.pdf

Residential Energy Dynamics, LLC. (2013). *ASHRAE 62.2-2013 ventilation*. Retrieved from http://www.residentialenergydynamics.com/REDCalcFree/Tools/ASHRAE6222013

Siegenthaler, J. (2013). Renewable hydronic heating. *Home Power 152*. Retrieved from http://www.homepower.com/articles/solar-water-heating/space-heating/renewable-hydronic-heating?v=print

Sima, J., Sikula, O., Kosutova, K., & Plasek, J. (2013). Theoretical evaluation of night sky cooling in the Czech Republic. *Energy Procedia, 48*, 645-653. doi: 10.1016/j.egypro.2014.02.075

Solar Rating and Certification Corporation (SRCC). (2015a). *Solar facts - collector ratings*.Retrieved from: http://www.solar-rating.org/facts/collector_ratings.html#FlowRates

Solar Rating and Certification Corporation (SRCC). (2015b). *Solar facts - system ratings*.Retrieved from http://www.solar-rating.org/facts/system_ratings.html

Solar Rating and Certification Corporation (SRCC). (2015c). *Ratings*. Retrieved from http://www.solar-rating.org/ratings/index.html

Sousa, J. (2012). Energy simulation software for buildings: Review and comparison. *CEUR Workshop Proceedings.* Lisbon, Portugal: Carreira, P. & Amaral, V. Retrieved from http://ceur-ws.org/Vol-923/paper08.pdf

Solar Energy Laboratory (2009a). *TRNSYS 17 -- mathematical reference.* Madison, WI: Klein, S. et al. Retrieved from http://web.mit.edu/parmstr/Public/TRNSYS/04-MathematicalReference.pdf

Solar Energy Laboratory (2009b). *TRNSYS multizone slab model tutorial and example* [Computer software documentation]. Madison, WI: Klein, S. et al.

Thermal Energy System Specialists, LLC. (2009). *TESSLibs 17 solar library mathematical reference* [computer software documentation]. Madison, WI: Thornton, J. et al.

Thermal Energy System Specialists, LLC (2015). *What is TRNSYS?* Retrieved from http://trnsys.com/

Uponor. (2013). *Radiant cooling design manual.* Apple Valley, MN: Uponor, Inc. Retrieved from http://www.uponorpro.com/Technical-Support/Manuals.aspx

VanGeem, M., Fiorato, A., & Musser, D. (1982). Calibrated hot box tests of thermal performance of concrete walls. In American Society of Heating, Refrigeration, and Air-conditioning Engineers (ASHRAE), *Proceedings of the ASHRAE/DOE Conference on Thermal Performance of the Exterior Envelopes of Buildings II* (pp. 108-130). Las Vegas, NV: ASHRAE.

Appendix A: Overhang Design

The transmittance of beam radiation through the south-facing windows was analyzed during the summer and winter based on the angles shown Figure 58. The sun's angles in each climate were determined using a sun path charting program from the University of Oregon, shown in Figure 59, Figure 60, and Figure 61. A 2-foot overhang was used to block most of the beam radiation during the summer but allow most of it during the winter.

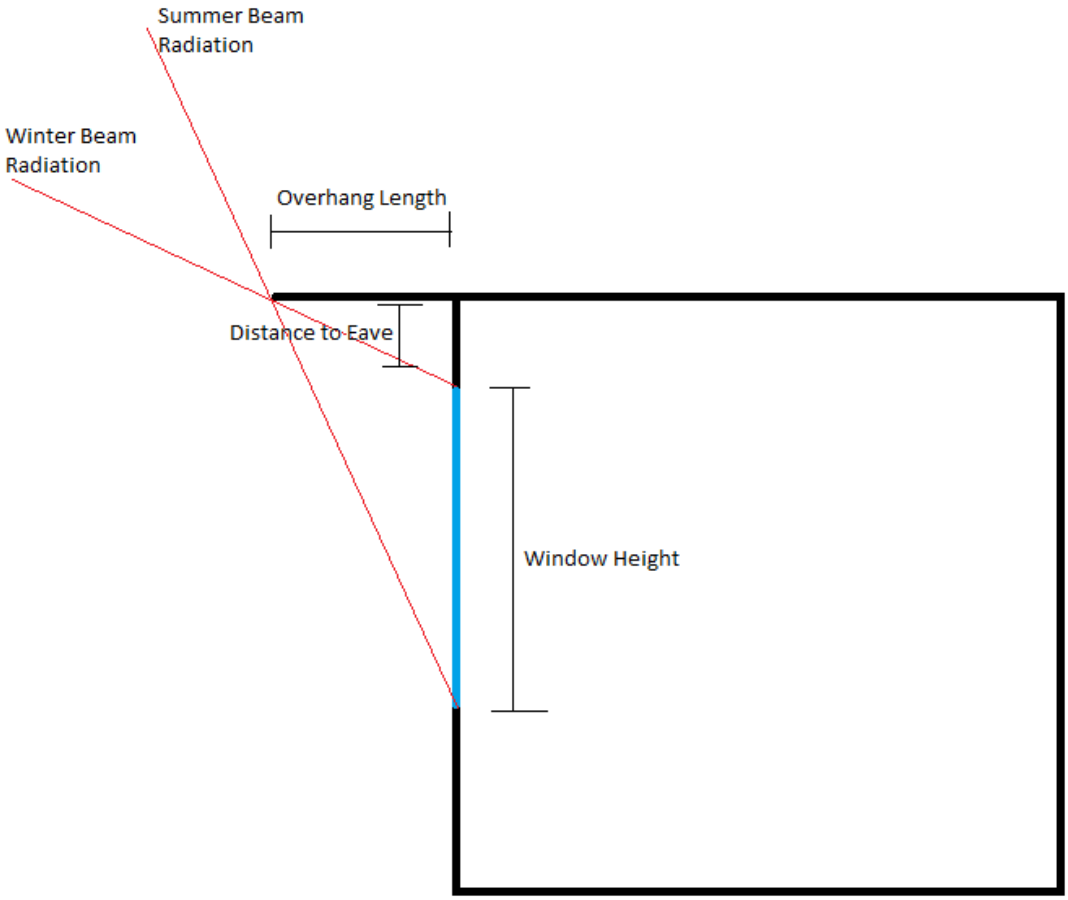

Figure 58. Schematic showing method of overhang analysis (using a 2-foot overhang).

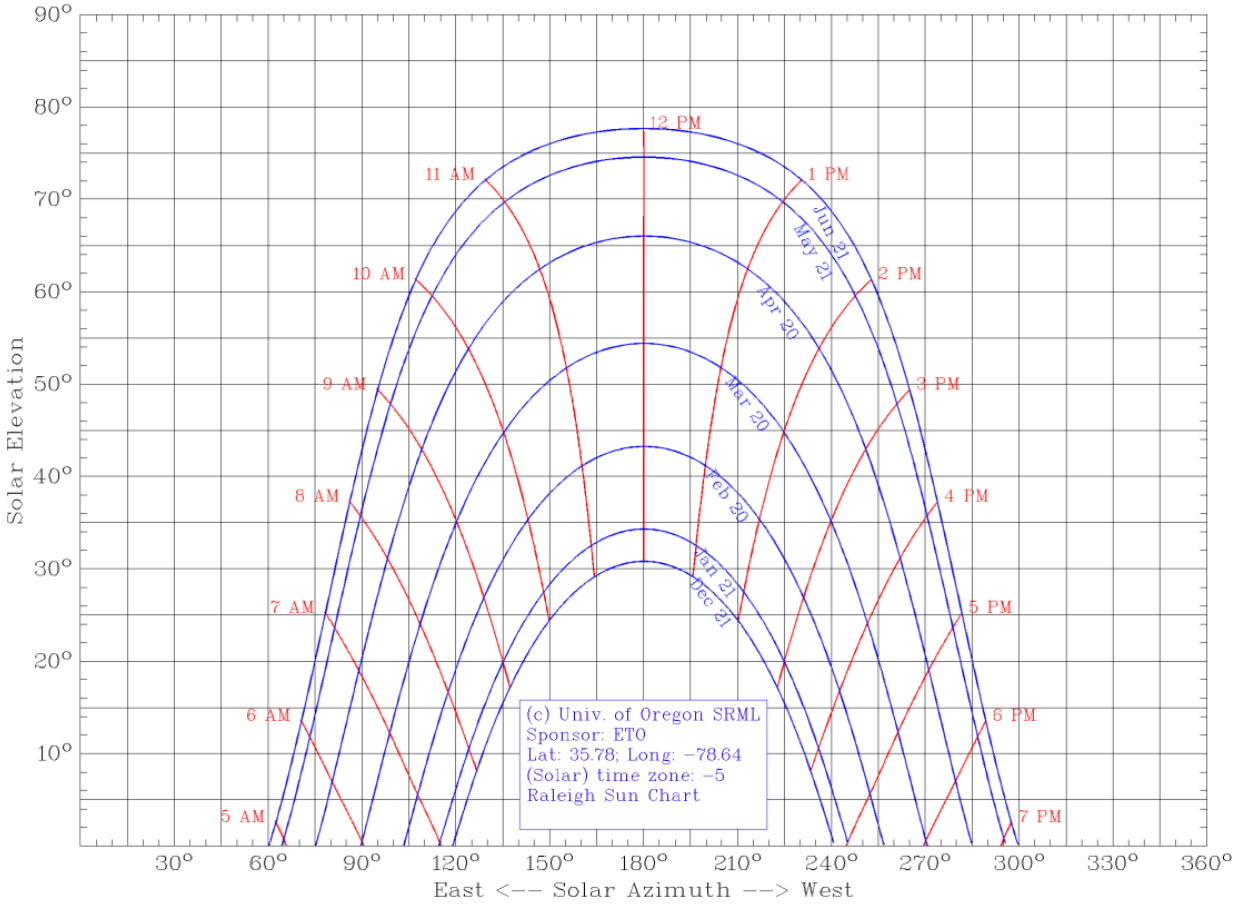

Figure 59. Sun chart for Raleigh. Generated from University of Oregon sun chart path program.

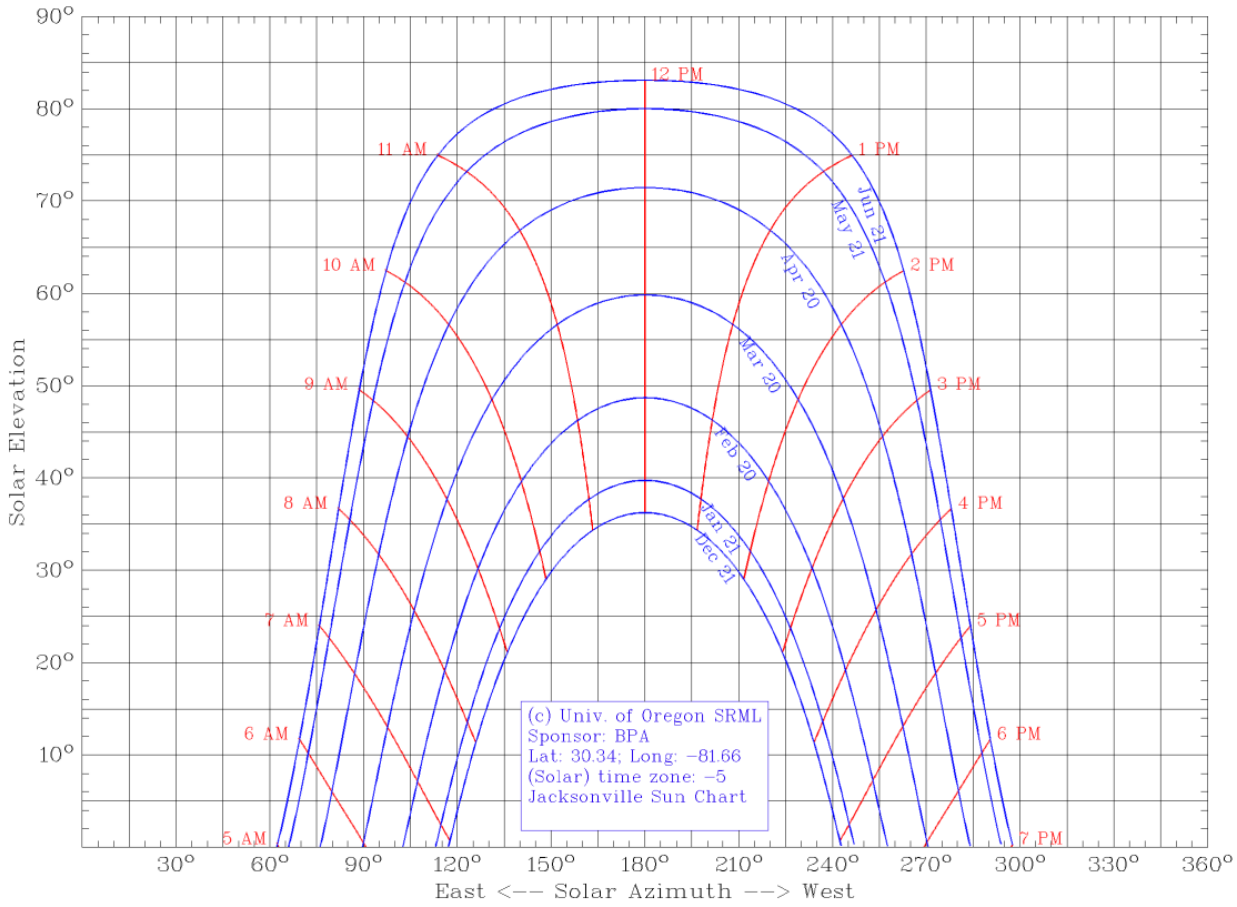

Figure 60. Sun chart for Jacksonville. Generated from University of Oregon sun path chart program.

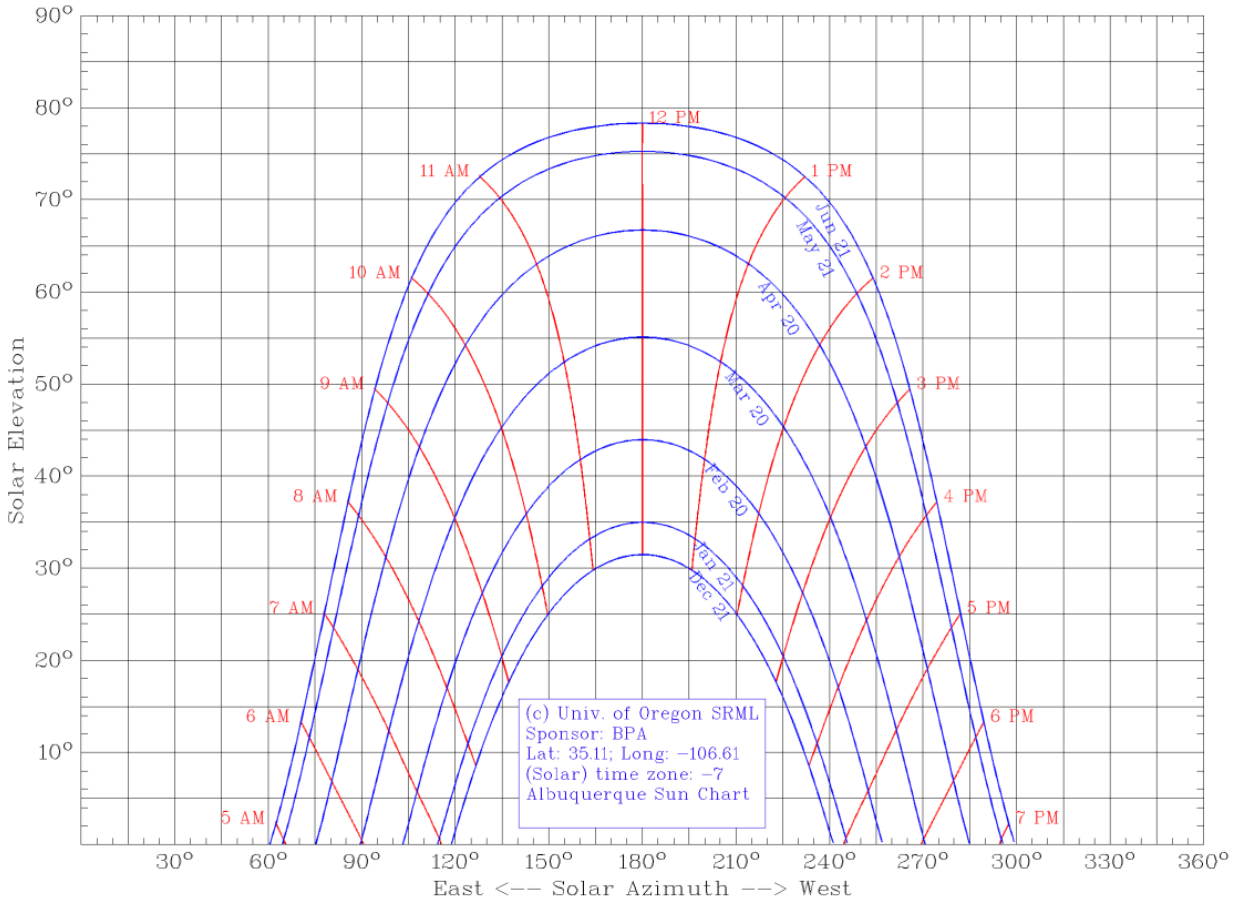

Figure 61. Sun chart for Albuquerque. Generated from University of Oregon sun chart path program.

Appendix B: TRNSYS Component Issues

Type 60c Tank Issue

The behavior of Type 60c varied based on the presence or absence of other components in Simulation Studio that were completely unconnected from it. These components were represented as a macro in Figure 62 (in the lower-left corner) for compactness. The Type 60c tank ran at a lower temperature when the macro was present, as shown in Figure 63, than when it was deleted, as shown in Figure 64.

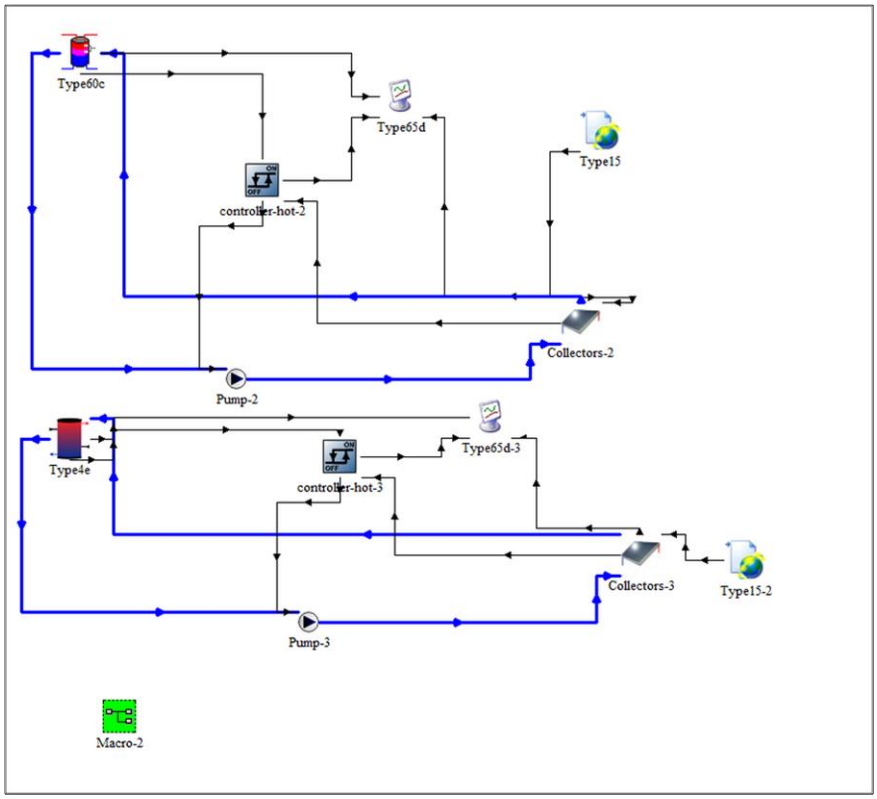

Figure 62. Simulation Studio schematic involving Type60c error.

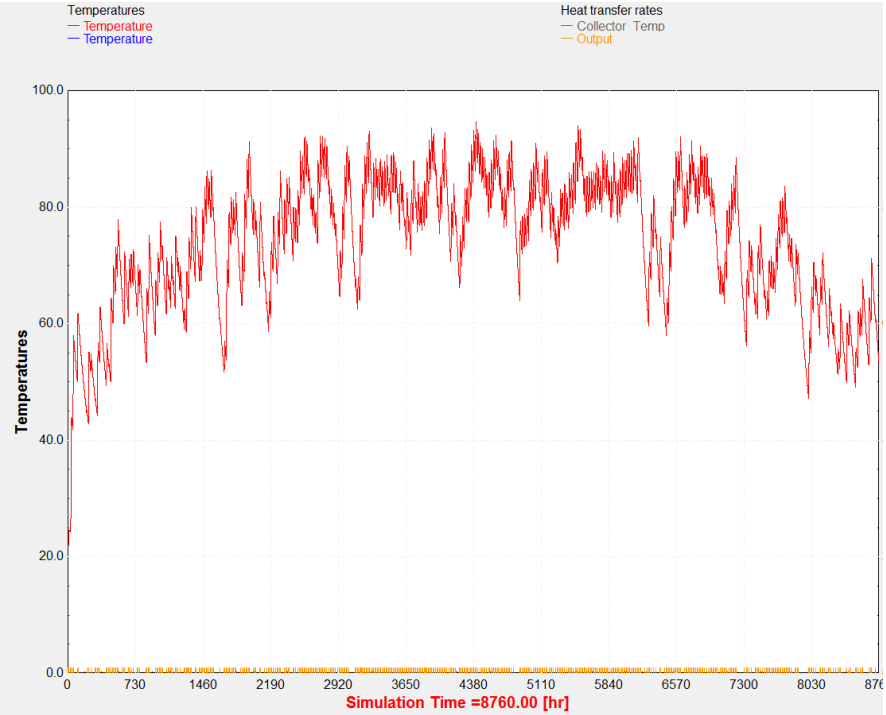

Figure 63. Type 60c with macro (representing third unconnected hydronic loop) present.

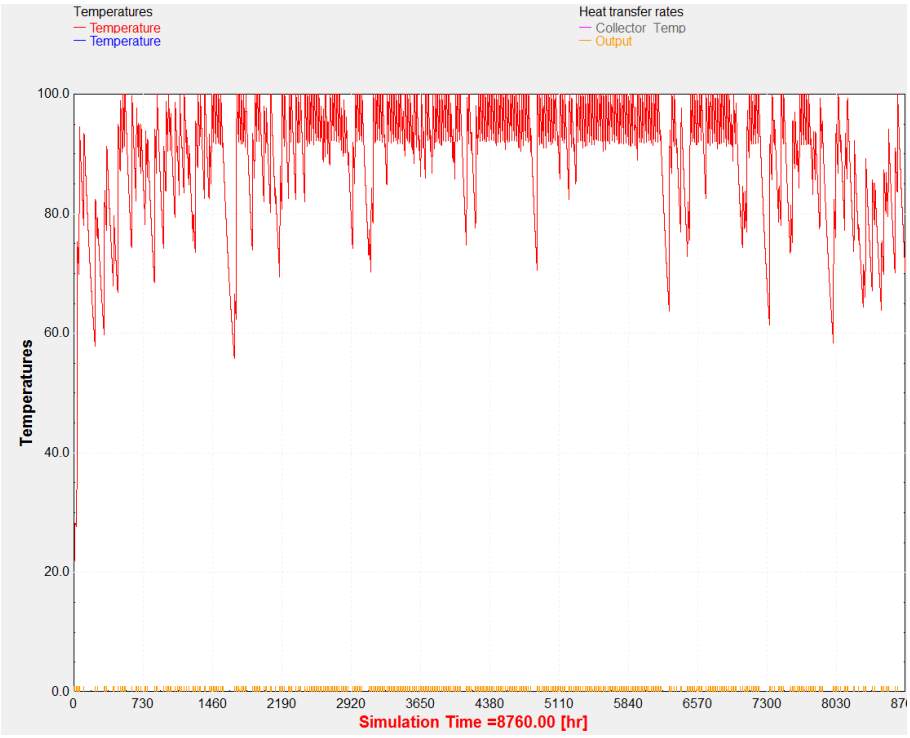

Figure 64. Type 60c tank performance with macro (representing third unconnected hydronic loop) deleted.

Type 559 Issue

A flaw was encountered in the Type 559 component, which the distributor attributed to a coding error. As sky temperature increased, the plate temperature decreased (Figure 65 and Figure 66).

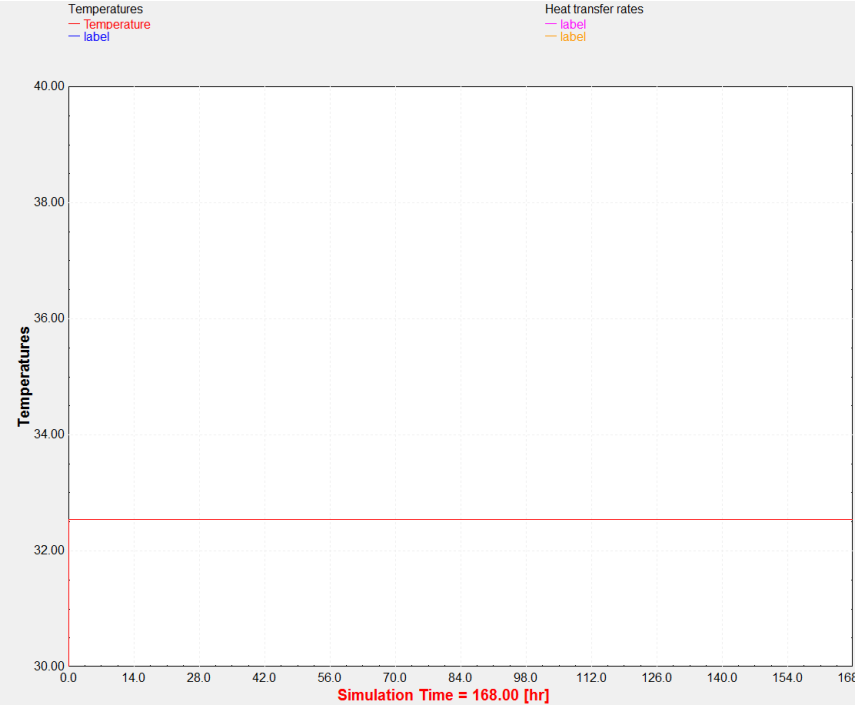

Figure 65. Type 559 plate temperature with 500 W irradiance, no wind, 20 degree ambient temperature and 0 degree sky temperature.

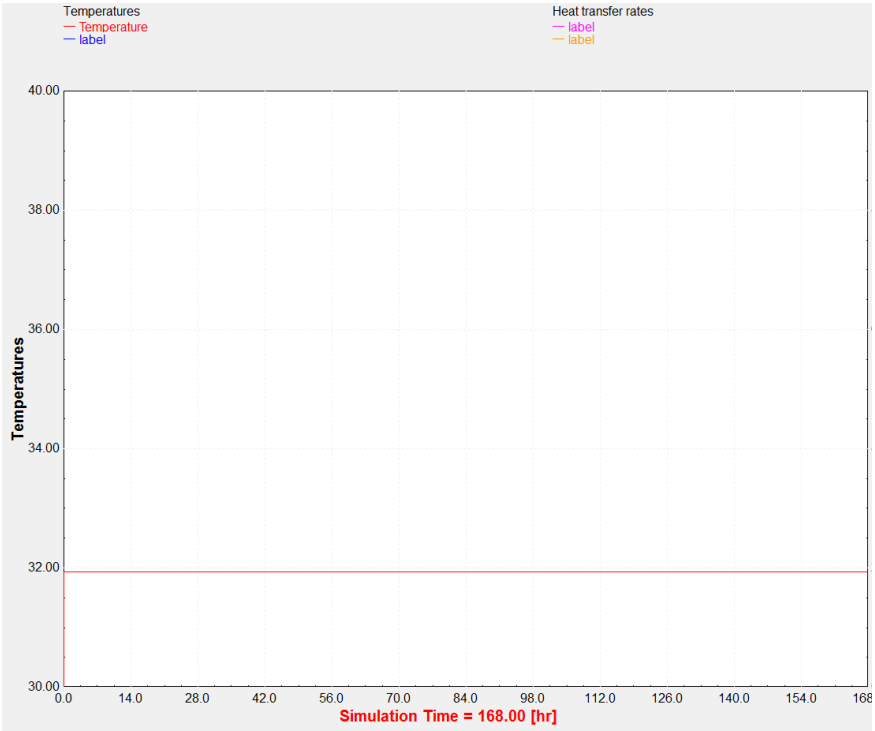

Figure 66. Type 559 plate temperature with 500 W irradiance, no wind, 20 degree ambient temperature and 20 degree sky temperature.

Appendix C: System Sketch

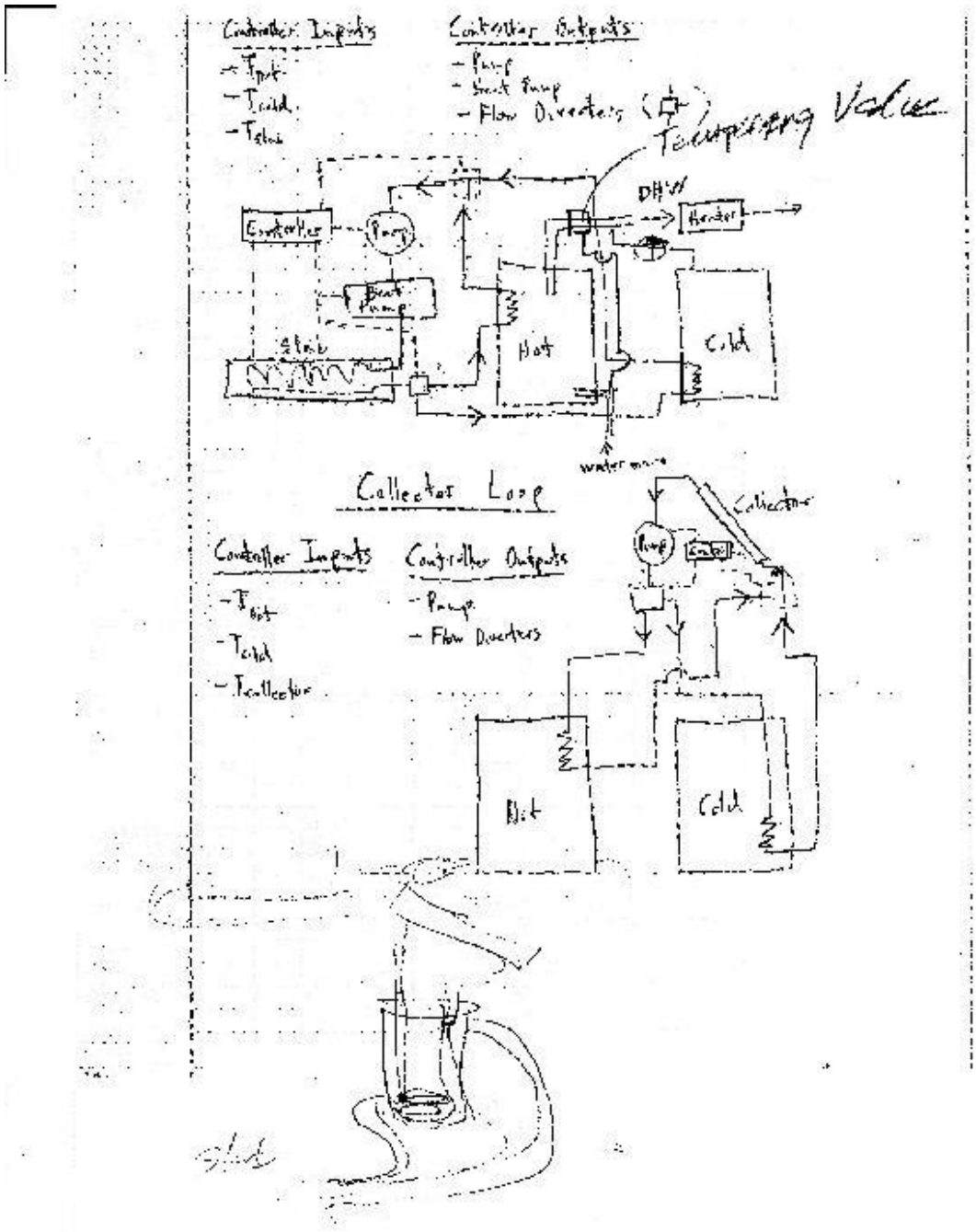

Figure 67. Hand sketch of solar thermal system.

Vita

Bradley Richard Painting was born in Fairlawn, Ohio. He attended public schools in Hudson, Ohio and graduated from Hudson High School in 2002. He then enrolled in Ohio University, where he was awarded a Bachelor of Science degree in Mechanical Engineering in 2007. Shortly after, he entered the field of sustainability by earning his LEED AP and working with consulting firms on sustainable building projects. He enrolled at Appalachian State University in 2013, pursuing an M.S. in Technology with a concentration in Renewable Energy Engineering. While at Appalachian State, he also collaborated on a HUD-funded study on the effects of home weatherization on indoor air quality, and was involved in the USDOE Race to Zero competition.